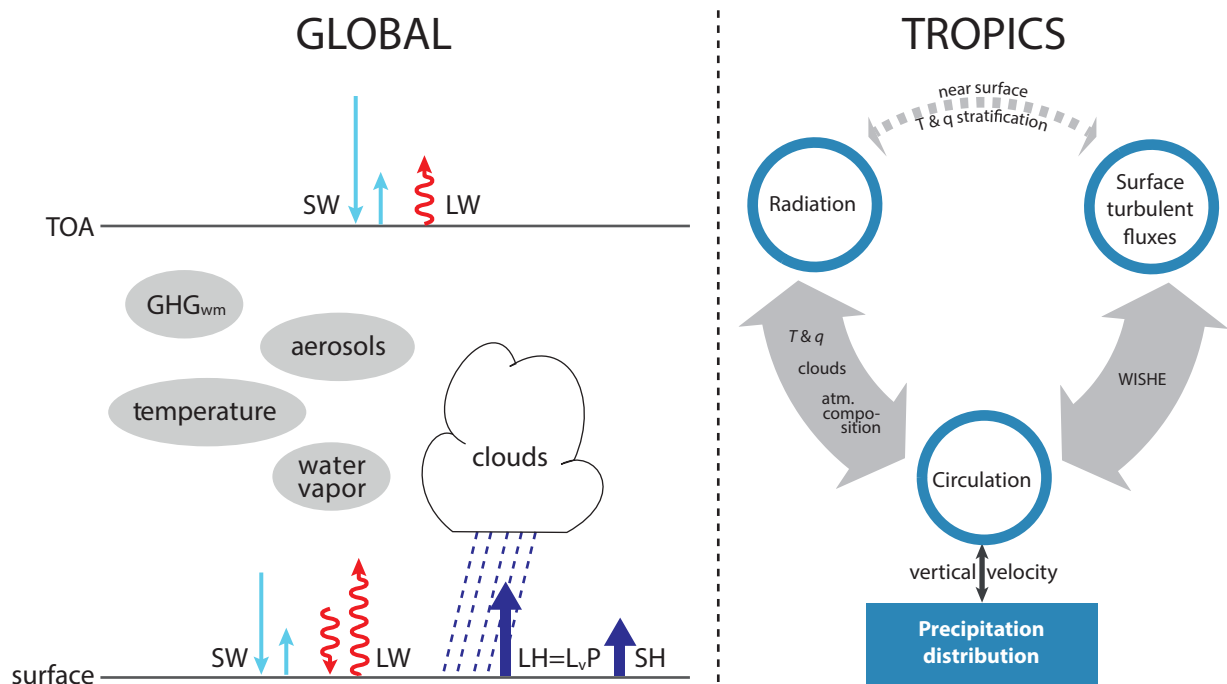


## Intermodel spread in global and tropical precipitation changes



Dagmar Fläschner (geb. Popke)

Hamburg 2016

## Hinweis

Die Berichte zur Erdsystemforschung werden vom Max-Planck-Institut für Meteorologie in Hamburg in unregelmäßiger Abfolge herausgegeben.

Sie enthalten wissenschaftliche und technische Beiträge, inklusive Dissertationen.

Die Beiträge geben nicht notwendigerweise die Auffassung des Instituts wieder.

Die "Berichte zur Erdsystemforschung" führen die vorherigen Reihen "Reports" und "Examensarbeiten" weiter.

## Anschrift / Address

Max-Planck-Institut für Meteorologie  
Bundesstrasse 53  
20146 Hamburg  
Deutschland

Tel./Phone: +49 (0)40 4 11 73 - 0

Fax: +49 (0)40 4 11 73 - 298

name.surname@mpimet.mpg.de

www.mpimet.mpg.de

## Notice

The Reports on Earth System Science are published by the Max Planck Institute for Meteorology in Hamburg. They appear in irregular intervals.

They contain scientific and technical contributions, including Ph. D. theses.

The Reports do not necessarily reflect the opinion of the Institute.

The "Reports on Earth System Science" continue the former "Reports" and "Examensarbeiten" of the Max Planck Institute.

## Layout

Bettina Diallo and Norbert P. Noreiks  
Communication

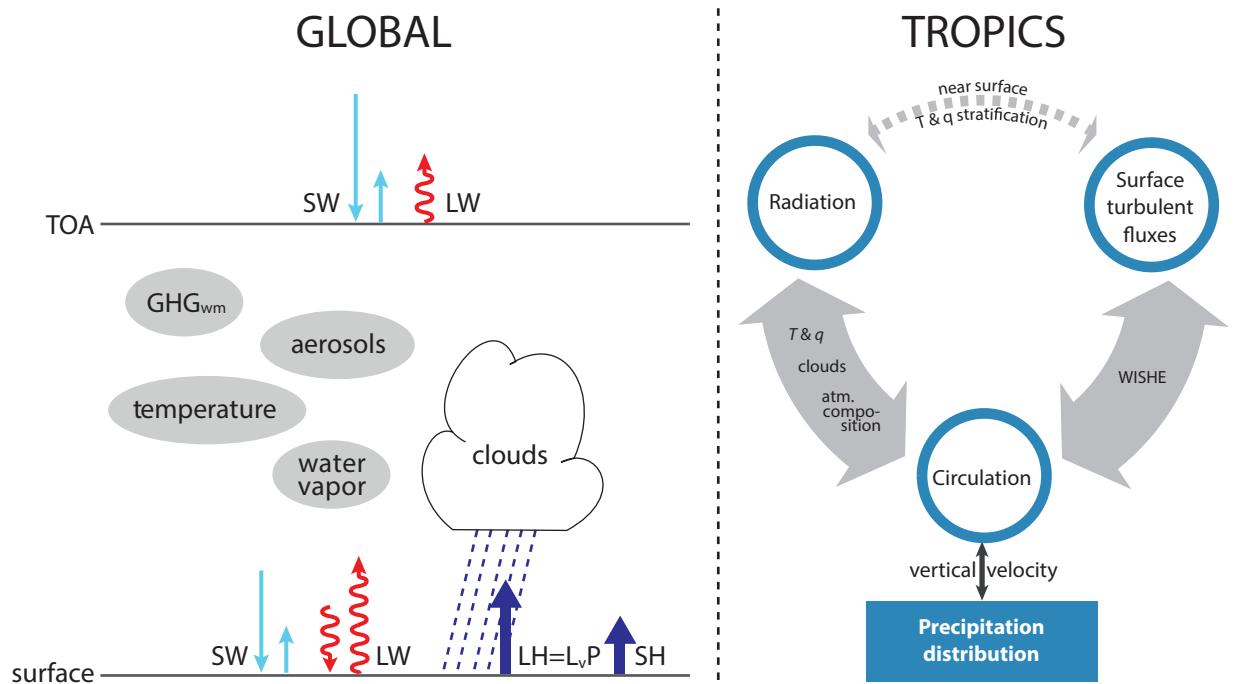
## Copyright

Photos below: ©MPI-M

Photos on the back from left to right:  
Christian Klepp, Jochem Marotzke,  
Christian Klepp, Clotilde Dubois,  
Christian Klepp, Katsumasa Tanaka



# Intermodel spread in global and tropical precipitation changes



Dagmar Fläschner (geb. Popke)

Hamburg 2016

# Dagmar Fläschner (geb. Popke)

Max-Planck-Institut für Meteorologie  
Bundesstrasse 53  
20146 Hamburg

Tag der Disputation: 1.7.2016

Folgende Gutachter empfehlen die Annahme der Dissertation:

Prof. Dr. Stefan Bühler  
Prof. Dr. Bjorn Stevens

---

## Abstract

Precipitation remains among the most poorly represented climate variables in state-of-the-art general circulation models. This thesis investigates reasons for intermodel spread in both global-mean precipitation as well as tropical precipitation patterns, and their change with warming. We examine the constraints on global-mean precipitation in experiments of different complexity provided by the Coupled Model Intercomparison Project phase 5 (CMIP5), and explore the intermodel spread in tropical precipitation patterns in idealized aquaplanet simulations from the Clouds On-Off Klimate Intercomparison Experiment (COOKIE).

Literature estimates of the rate of global-mean precipitation increase with surface warming disagree about the intermodel spread, reporting either a large or a small spread. Our analysis of this rate in the CMIP5 ensemble corroborates the estimates of a small intermodel spread. The spread is small if the temperature-mediated rate of precipitation increase is explicitly separated from the direct precipitation response to a change in the atmospheric composition; we respectively refer to these quantities as hydrological sensitivity parameter ( $\eta$ ) and adjustment ( $A$ ). The intermodel spread in  $\eta$  arises from disagreement in lower-tropospheric temperature and humidity changes in the tropics as well as diverse cloud radiative changes, as revealed by a radiative kernel analysis applied to the atmospheric heat budget. Three factors –  $\eta$ ,  $A$  and the surface warming – determine the total precipitation change with time. The intermodel disagreement in these three factors affects the spread in the precipitation response ( $\Delta P$ ) on different time scales. Upon changes in the atmospheric composition, in the short term the spread in  $\Delta P$  is dominated by  $A$ , while in the longterm the greatest spread arises from the surface temperature. From merely knowing  $A$  and  $\eta$ , the precipitation response in a transient forcing experiment can be replicated with a simple model.

Contrary to the recent suggestion that cloud radiative feedbacks are the key reason for intermodel differences in the tropical precipitation response to warming in aquaplanet simulations, we explore the hypothesis that the seed for intermodel spread is present also when the cloud-radiation interaction is inhibited. Indeed, the model spread is greater in the absence of atmospheric cloud radiative effects (ACREs), e.g. in the location of the intertropical convergence zone (ITCZ), or the organization of the tropical circulation. The ITCZ shifts polewards in all models when ACREs are absent, and the tropical distribution of precipitation, which is governed by the vertical velocity, becomes more diverse.

We develop a simple framework to diagnose the vertical velocity in the tropics. The framework is derived from the moist static energy (MSE) budget and assumes that the vertical velocity can be expressed by a specified vertical velocity structure associated with deep convection. Then the vertical mean vertical velocity is diagnosed as the ratio between column MSE heating terms and the gross moist stability, which is the vertical advection associated with the specified velocity structure. We find that the zonal-mean variation in the vertical velocity is governed by the column heating rather than the gross moist stability. Further, we employ the framework to understand the poleward shift of the ITCZ when ACREs are removed. The results suggest that the heterogeneity in cloud radiative heating with respect to the clear-sky column MSE heating terms is related to the shift in the ITCZ.



## Zusammenfassung

In den dem neuesten Forschungsstand entsprechenden allgemeinen Zirkulationsmodellen der Atmosphäre stellt der Niederschlag noch immer eine der am unzulänglichsten simulierten Variablen dar. In der vorliegenden Doktorarbeit werden Gründe für Modellunterschiede sowohl in dem simulierten globalen Niederschlag als auch in der tropischen Niederschlagsverteilung und deren Veränderungen mit der Erwärmung untersucht. Die globalen Niederschlagsänderungen werden in unterschiedlich komplexen Klimaexperimenten, die vom “Coupled Model Intercomparison Project phase 5” (CMIP5) zur Verfügung gestellt sind, evaluiert, während die Modellunterschiede der tropischen Niederschlagsverteilung in den Aquaplanetsimulationen vom “Clouds On-Off Climate Intercomparison Experiment” (COOKIE) untersucht werden.

Die in der Literatur veröffentlichten Modellunterschiede für die Anstiegsrate des globalen Niederschlags im Zuge einer Erwärmung weichen voneinander ab, wobei entweder geringe oder große Modellunterschiede angegeben werden. Unsere Analysen dieser Anstiegsrate in dem CMIP5 Modellensemble untermauern die Literaturangaben mit geringeren Modellunterschieden. Die Unterschiede werden geringer, wenn die direkte Niederschlagsveränderung als Reaktion auf Veränderungen in der atmosphärischen Zusammensetzung und die temperaturbeeinflussten Niederschlagsveränderungen explizit getrennt voneinander betrachtet werden. Wir nennen diese zwei Größen “Anpassung” ( $A$ ) und “hydrologischer Sensitivitätsparameter” ( $\eta$ ). Die Modellunterschiede von  $\eta$  können mit Hilfe einer Kernel-Analyse des atmosphärischen Strahlungsbudgets auf Unterschiede in den Änderungen der Temperatur und des Wasserdampfs in der unteren tropischen Troposphäre sowie auf unterschiedliche Wolkenveränderungen zurückgeführt werden. Die zeitliche totale Niederschlagsveränderung wird nicht nur von  $\eta$  und  $A$  bestimmt, sondern auch von der Oberflächenerwärmung. Die Diskrepanz zwischen den Modellen in diesen drei Größen beeinflusst die Modellunterschiede der totalen Niederschlagsveränderung ( $\Delta P$ ) auf verschiedenen Zeitskalen. Wenn die atmosphärische Komposition zum Beispiel durch Erhöhung von Kohlendioxid verändert wird, werden die Modellunterschiede in  $\Delta P$  auf kurzen Zeitskalen von  $A$  dominiert, während die Oberflächenerwärmung für die größten Niederschlagsunterschiede auf langen Zeitskalen sorgt. Die Kenntnis von  $A$  und  $\eta$  genügt um die Niederschlagsveränderung in einem transienten Antriebsexperiment mit einem einfachen Modell nachzubilden.

In Opposition zu dem vor kurzem veröffentlichten Vorschlag, dass Wolken-Strahlungsrückkopplungsprozesse die Hauptursache für die Streuung zwischen Modellergebnissen der tropischen Niederschlagsveränderung mit der Erwärmung in Aquaplanetsimulationen seien, untersuchen wir die gegensätzliche Hypothese, dass der Ursprung für die Streuung auch ohne das Vorhandensein von atmosphärischen Wolkenstrahlungseffekten (atmospheric cloud radiative effects, ACREs) gegeben ist. Wenn ACREs unterbunden sind, nimmt die Diskrepanz zwischen Modellergebnissen tatsächlich zu, wie zum Beispiel die Positionen der innertropischen Konvergenzzone (ITCZ) oder die Organisation der tropischen Zirkulation. Die ITCZ wird durch das Ausstellen der ACREs in allen Modellen polwärts verschoben. Dies sorgt für größere Modellunterschiede in der Verteilung des tropischen Niederschlags, der wiederum von der vertikalen Geschwindigkeit bestimmt wird.

Wir entwickeln ein theoretisches Konzept um die vertikale Geschwindigkeit in den Tropen zu diagnostizieren. Das theoretische Konzept wird aus dem Budget der feuchtstatischen Energie (moist static energy, MSE) hergeleitet und basiert auf der Annahme, dass die vertikale Geschwindigkeit aus dem Produkt der vertikal gemittelten vertikalen Geschwindigkeit und einer vorgegebenen Struktur der vertikalen Geschwindigkeit dargestellt werden kann, wobei die Struktur in Anlehnung an das Profil der Tiefenkonvektion gewählt ist. Damit kann die vertikale Geschwindigkeit aus dem Quotienten von MSE Wärmetermen und der Gesamt-Feuchtestabilität (gross moist stability,  $\Gamma_h$ ) diagnostiziert werden, wobei  $\Gamma_h$  die vertikale Advektion von MSE durch die angenommene Geschwindigkeitsstruktur darstellt. Mit Hilfe dieses Konzepts wird gezeigt, dass die zonal gemittelte Variation der vertikalen Geschwindigkeit von der Variation des MSE Wärmeterms bestimmt wird und nicht von  $\Gamma_h$ . Das Konzept wird weiterhin auf die Frage angewandt, warum die ITCZ in den Modellen unterschiedlich weit polwärts verschoben wird, wenn die Wolken-Strahlungs-Wechselwirkung verhindert ist. Die Ergebnisse lassen darauf schließen, dass das heterogene Heizen des Wolkenstrahlungseffekts im Vergleich zu dem wolkenfreien MSE Wärmeterm mit der Verschiebung der ITCZ in Verbindung steht.



# Contents

	Page
<b>1 Introduction</b>	<b>1</b>
1.1 The atmospheric heat budget as constraint on global-mean precipitation . . .	3
1.2 Constraints on tropical precipitation patterns . . . . .	6
<b>2 Understanding the intermodel spread in global-mean hydrological sensitivity</b>	<b>11</b>
2.1 Introduction . . . . .	11
2.2 Experiments and methods . . . . .	15
2.2.1 Experiments . . . . .	15
2.2.2 Calculation methods . . . . .	16
2.3 The slope of precipitation change with respect to surface temperature change	16
2.4 Applicability of the hydrological sensitivity parameter to transient experiments	20
2.5 Sources of intermodel spread in the global-mean precipitation response . . . .	21
2.5.1 Radiative decomposition of the spread in $\eta$ and $A$ . . . . .	24
2.5.2 Spread in the hydrological sensitivity parameter . . . . .	25
2.5.3 Spread in the adjustment . . . . .	28
2.6 Hydrological sensitivity parameter in coupled versus noncoupled experiments	29
2.7 Conclusions . . . . .	31
<b>3 Impact of ACRE on the intermodel spread in tropical precipitation</b>	<b>33</b>
3.1 Introduction . . . . .	33
3.2 COOKIE simulations . . . . .	35
3.3 Precipitation and circulation in COOKIE . . . . .	37
3.3.1 Tropical mean characterization . . . . .	37
3.3.2 Spatial characterization of the tropical precipitation and circulation .	41
3.4 Synthesis: Is the seed for intermodel spread present in the absence of ACREs?	47
<b>4 Diagnosing the zonal-mean precipitation via an MSE framework</b>	<b>49</b>
4.1 Introduction . . . . .	49
4.2 Simulations . . . . .	52
4.3 Diagnostic MSE framework for precipitation investigation . . . . .	52
4.3.1 Choice of generic vertical velocity profile influences gross moist stability	54
4.3.2 Validity of the MSE framework . . . . .	56
4.4 Employing the MSE framework . . . . .	57
4.4.1 Controls on the zonal-mean vertical velocity . . . . .	58
4.4.2 Influence of ACRE on the ITCZ shift . . . . .	63
4.5 Summary . . . . .	65
<b>5 Conclusions</b>	<b>67</b>

---

<b>A</b>	<b>Supplementary material to Chapter 2</b>	<b>71</b>
A.1	Temperature and water vapor kernels . . . . .	71
A.2	Testing for influences on the adjustment residual . . . . .	72
A.2.1	Non-linearity of $\Delta R_x$ with $\Delta T_s$ . . . . .	72
A.2.2	Internal variability . . . . .	72
<b>B</b>	<b>Hydrological sensitivity parameter estimates from PDRMIP</b>	<b>75</b>
	<b>List of Figures</b>	<b>77</b>
	<b>List of Tables</b>	<b>83</b>
	<b>Bibliography</b>	<b>85</b>

# 1 Introduction

This thesis presents advances in understanding physical reasons for the disagreement among state-of-the-art general circulation models (GCMs) in the representation of global-mean and regional precipitation as well as its change with warming. As part of the Coupled Model Intercomparison Project (CMIP) phase 5, these models have served as the basis for projections of the future climate in the latest Fifth Assessment Report of the Intergovernmental Panel on Climate Change.

Precipitation is the most important process for distributing freshwater over large areas. Apart from its importance for the ecosystem, the availability of freshwater through precipitation has been fundamental for the development of human populations in the past, their migrations as the climate changed, and directly affects billions of people in the present. Some 9000 to 6000 years ago, prehistoric settlements were abundant in the Sahara because the northward migrating African monsoonal rainfall provided freshwater to initiate a greening of the former desert (e.g. deMenocal and Tierney, 2012). As monsoonal rainfalls shifted back south, scarcity of freshwater in Northern Africa and the reduced risk of flooding triggered the reoccupation of the Nile river valley, marking the emergence of pharaonic civilizations (Kuper and Kröpelin, 2006). Despite today's advances in technology, human health and economic prosperity rely on replenishing freshwater resources by precipitation, e.g. in India (Sulochana Gadgil, 2006), or the Sahel zone (Barrios et al., 2010), but also industrialized countries, such as for example the United States of America (MacDonald, 2010). Future changes of the hydrological cycle, induced by rising greenhouse gas concentrations and global warming, are almost certain to increase global-mean precipitation but with substantial reductions in certain regions (e.g. Held and Soden, 2006; Bony et al., 2013; Hegerl et al., 2015). Precipitation extremes such as droughts, and floods associated with heavy rainfall are thought to increase in frequency and severity with global warming (e.g. Dai, 2013; Kharin et al., 2013). However, the representation of precipitation ranks among the most poorly simulated quantities in the general circulation models (Stephens et al., 2010; Hawkins and Sutton, 2011). The uncertainty of precipitation projections constitutes the key challenge for adapting water resource management to climate change (Jiménez Cisneros et al., 2014). A better physical understanding of the processes governing global-mean precipitation, precipitation patterns, and their changes with warming in GCMs as well as the causes for intermodel differences is imperative to prepare society with the knowledge base to cope with an uncertain future.

General circulation models differ in many regards. They are highly complex numerical representations of circulations in the atmosphere (AGCM), the coupled atmosphere-ocean system (AOGCM) including land, vegetation and sea ice, or of the Earth System (ESM) including for instance biogeochemical cycles like the carbon cycle, sulphur cycle and ozone.

At their basis, they numerically solve the well-known primitive equations, describing the atmospheric and oceanic circulations. These models solve the equations in time and in space on a three-dimensional grid. Due to limitations of computing resources, the horizontal grid sizes of the CMIP5 models used in this thesis are on average approximately 200 km, with the finest resolution at the equator being 120 km. Many atmospheric processes, such as for example convection, precipitation, and clouds, occur on much smaller scales and are thus not resolved. These processes have to be parameterized. Parameterizations are hypothetical relationships that represent the unresolved sub-grid scale variability in terms of resolved grid mean quantities. GCMs differ in many aspects: in the horizontal and vertical resolution, and accordingly the time step; in the parameterizations which vary in complexity; in the selection of represented processes, e.g. aerosols, atmospheric chemistry, dynamic vegetation, biogeochemical cycles; in the implementation of the aforementioned processes; and many more. Many of the parameters used in parameterizations are uncertain and often non-observable. In the final stages of model development, some of these non-constrained parameters are adjusted to tune the model to a known state of the climate system. The tuning process, though yielding an equally plausible model, can lead to different representations of the climate system, e.g. precipitation over land as expected from observations, or precipitation moving off the land to the ocean in the region of the maritime continent (Mauritsen et al., 2012). The models provided by different modeling centers in the CMIP5 archive are not necessarily independent from each other. Model components may have been shared in the development process which may lead to common biases (Knutti et al., 2013), the same model may have been submitted to the CMIP5 archive in different resolutions or with different selections of submodels. Nevertheless, the multi-model comparison to some extent samples structural uncertainty among the models.

Comparing the model response to changes in the external forcing is a powerful tool to test the understanding of how the forcing influences the climate state. The CMIP5 archive offers numerous simulations of different complexity, where external forcings are specified according to a protocol (for an overview see Taylor et al., 2012). External forcings – such as CO<sub>2</sub> and other greenhouse gas concentrations, aerosols, the solar constant, or others – are modified to represent e.g. the twentieth century, or are raised step-like in more idealized experiments. In addition, models are run in various configurations, ranging from the coupled AOGCMs, AGCMs with fixed sea surface temperatures, to very idealized water-covered aquaplanets. The intermodel comparison of the precipitation response to such controlled settings can help build confidence in the community’s understanding of certain processes, if their response to a forcing is consistent. If, however, their response differs, identifying the main processes leading to the intermodel spread may also help guide the model improvement.

Previous literature focusing on the intermodel spread in precipitation states that models disagree about both the global-mean changes of precipitation with warming as well as the regional changes, with particularly large spread in the tropical precipitation response. Because the physical constraints, and thus possible causes for intermodel spread, differ between the global-mean or tropical regional perspective, the subsequent introductory sections present an overview of the constraints on global-mean and the tropical spatial precipitation distribution. In addition, in the remainder of this introduction, the leading research objectives of this thesis are placed into the context of knowledge from the previous literature,

where **Chapter 2** focuses on the global-mean perspective, and **Chapters 3 and 4** on specific aspects of the spatial precipitation distribution in the tropics. Each chapter contains its own introduction and can thus be read independently.

## 1.1 The atmospheric heat budget as constraint on global-mean precipitation

Upon being evaporated from the Earth's surface, moisture is transported by atmospheric circulations. As air rises, water vapor condenses, releasing latent heat of condensation and forming clouds. Once precipitation again reaches the ground in liquid or solid form rather than re-evaporating, it has effectively heated the atmosphere. For the Earth's atmosphere to remain in balance, the amount of heat provided to the atmosphere from the ground by the latent and sensible heat fluxes has to equal the energy leaving the atmosphere. The atmosphere cools by emission of longwave radiation, and is heated by absorption of shortwave radiation by water vapor; but the longwave cooling dominates so that the net effect is a radiative cooling of the atmosphere. That the global-mean precipitation is constrained by energetics is by now broadly appreciated (e.g. Mitchell et al., 1987; Boer, 1993; Allen and Ingram, 2002; O'Gorman et al., 2012). From an atmospheric budget view, the global-mean precipitation ( $P$ ) is given as

$$L_v P = R - SH, \quad (1.1)$$

where multiplying by the latent heat of vaporization  $L_v$  transforms precipitation into energy units. The atmospheric net radiation,  $R$ , is given as the difference between top-of-atmosphere (TOA) and surface radiation, and  $SH$  is the surface sensible heat flux. As Figure 1.1 illustrates, the net atmospheric radiation is influenced by the atmospheric temperature and water vapor, clouds, the surface albedo, well-mixed greenhouse gases and aerosols. Global-mean precipitation can thus be understood from knowledge of the impacts of these constituents on the global-mean atmospheric radiation and the sensible heat flux.

Under global warming, the rising  $\text{CO}_2$  concentrations reduce the Earth's cooling to space, leading to a surplus of absorbed energy at the TOA. The system regains energy balance by increasing the surface temperature. The surface temperature change in response to a doubling of  $\text{CO}_2$  concentration is generally referred to as equilibrium climate sensitivity (ECS), following Charney et al. (1979). Initial increases in the surface temperature are amplified or reduced by positive or negative climate feedbacks, respectively. An increased water vapor concentration as well as a reduced surface albedo constitute positive feedbacks on the surface temperature; uniform increases of the tropospheric temperature (Planck response) and a reduced temperature lapse-rate constitute negative feedbacks; the sign of the cloud feedback is still uncertain but assessed to be likely positive (Vial et al., 2013; Boucher et al., 2013). Scientific consensus is that ECS likely ranges from 1.5 K to 4.5 K (Collins et al., 2013). Numerous intermodel comparison studies have identified the cloud feedback as root cause for intermodel spread in ECS estimates (e.g. Cess et al., 1990; Bony et al., 2006; Dufresne and Bony, 2008; Zelinka et al., 2012; Vial et al., 2013).

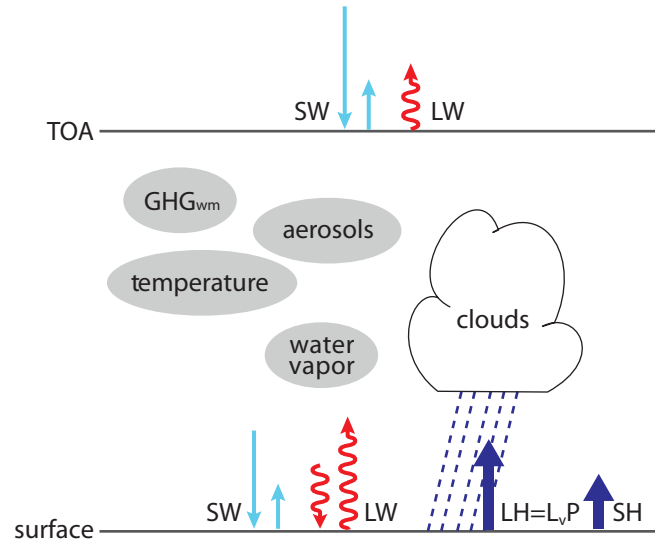


**Figure 1.1:** Illustration of the processes that influence the atmospheric heat budget. The net atmospheric radiation is given by the difference of top-of-atmosphere (TOA) and surface radiative fluxes. Longwave and shortwave radiative fluxes are abbreviated by LW and SW, respectively. Blue arrows denote the latent and sensible heat fluxes (LH and SH). Well-mixed greenhouse gases ( $\text{GHG}_{\text{wm}}$ ) are for example carbon dioxide or methane.

Because global-mean precipitation is tied to the energetics of the atmosphere, which in turn is linked to the surface temperature, it is not surprising that global-mean precipitation changes are related to surface temperature changes through the climate feedbacks' influences on the radiation. The rate of increase of global-mean precipitation with increasing surface temperature has conventionally been referred to as “hydrological sensitivity”. This quantity is estimated at the order of magnitude of  $2\% \text{ K}^{-1}$ , with considerable intermodel spread ranging from  $1\% \text{ K}^{-1}$  to  $3\% \text{ K}^{-1}$  (Held and Soden, 2006). This spread constitutes a factor of three difference between the lowest and highest model estimate, a spread as large as that of ECS. While Previdi (2010) finds an even larger spread of factor 3.3, Andrews et al. (2009) find a much smaller factor of 1.5 spread. Other factors of spread are scattered in between (Lambert and Webb, 2008; Takahashi, 2009; Lambert and Allen, 2009; Pendergrass and Hartmann, 2014).

An assessment of the literature shows, that the measure “hydrological sensitivity” has been defined ambiguously. Some studies take into account that the global-mean precipitation changes directly in response to changes in the atmospheric composition, e.g. abruptly increasing  $\text{CO}_2$  concentrations, while this direct precipitation response is neglected in other studies. When  $\text{CO}_2$  concentrations increase, the atmosphere cools less radiatively, resulting in less global-mean precipitation (Eq. 1.1). This direct precipitation response has previously been referred to as slow precipitation response (Bala et al., 2010), or as forcing (Andrews et al., 2009). It will be called adjustment hereafter, because the precipitation adjusts to the forcing induced by changes in the atmospheric composition, rather than representing a forcing in itself. In addition to different definitions, experiments forced with different

atmospheric composition changes were investigated in the studies. So far it had not been shown how the intermodel spread in the rate of global-mean increase in precipitation with warming depends on the definition and the investigated experiment.

There is some debate as to whether climate models show a muted precipitation response to warming compared to observations. Wentz et al. (2007) find a rate of increase of  $6\% \text{ K}^{-1}$  from satellite measurements, which is consistent to the rate of lower tropospheric moisture increase with warming expected from the Clausius-Clapeyron equation. However, their estimate is based only on a 20 year period, neglecting internal variability. GCMs can also predict precipitation increases of  $7\% \text{ K}^{-1}$  or even larger for 20 year periods (Previdi and Liepert, 2008; Liepert and Previdi, 2009), indicating that the modeled global-mean precipitation response to global warming is per se not inconsistent with observations. Due to poor data coverage, especially in the early twentieth century, observational records disagree on the trend of precipitation change in the twentieth century by a factor of three (Hartmann et al., 2013); though they all show that the global-mean precipitation has increased, coinciding with positive trends of global-mean surface temperatures in the twentieth century.

Among other possibilities for disagreement between observations and models in the twentieth century precipitation trend, the representation of twentieth century changes in the atmospheric forcing, e.g. volcanic forcings, well-mixed greenhouse gases, solar radiation or anthropogenic aerosols can lead to differences. Differences in the black carbon aerosol explains much of the intermodel spread in the CMIP3 simulations of twentieth century precipitation change (Pendergrass and Hartmann, 2012). Model simulations yield the possibility to separately study the impact of these forcings on the precipitation adjustment and the temperature-mediated precipitation response (Andrews et al., 2010; Kvalevåg et al., 2013), though only recently this became possible in a multi-model context (Samset et al., 2016).

Only few studies have attempted to attribute the intermodel spread of the precipitation rate of increase to the change in atmospheric variables such as the temperature, water vapor, or clouds induced by climate feedbacks. Previdi (2010) employed the radiative kernel technique (Soden et al., 2008) to the atmospheric heat budget. He found that the impact of clouds, water vapor and lapse-rate considered together, and the sensible heat flux caused similar intermodel deviations in how the atmospheric energy balance changed with warming. Extending this study with the same methodology, O’Gorman et al. (2012) emphasize that the spread caused by the cloud response dominates over that by lapse-rate and water vapor considered together. By redoing clear-sky radiative calculations from the models’ mean state changes, Pendergrass and Hartmann (2014) conclude that the intermodel scatter in the atmospheric heat budget change of lapse-rate plus water vapor changes is as large as that of cloud changes. However, none of the above studies have separated the atmospheric heat budget changes into those from rapid adjustments and temperature-mediated changes.

**Chapter 2** investigates the unresolved issues regarding the intermodel spread in the global-mean precipitation response to global warming as outlined above. To help reconcile the ambiguity of definitions concerning the rate of increase of precipitation with warming, I introduce a concise terminology in analogy to the ECS terminology. By making use of twenty-eight CMIP5 models and numerous experiments of different idealization, I assess how the

intermodel spread in the rate of increase of precipitation with warming depends on the employed definition. I discuss how the intermodel spread in adjustments, temperature-mediated precipitation increase and the surface warming impacts the spread in the precipitation response on different timescales. Finally, I estimate the influence of changing atmospheric variables due to climate feedbacks on the atmospheric heat budget change via the radiative kernel technique by specifically separating between adjustments and temperature-mediated response.

## 1.2 Constraints on tropical precipitation patterns

In contrast to the global-mean precipitation, the regional precipitation distribution is not simply constrained by the energetics of the atmosphere. The diabatic cooling by radiation only spatially correlates well with precipitation at hemispheric length scales or larger (Muller and O’Gorman, 2011). In the extra-tropics, precipitation is associated with cyclonic systems within the storm track regions. In the tropics, the strongest rain falls out of deep convective clouds forming within the intertropical convergence zone (ITCZ), while shallow cumulus clouds found in the trade wind zones produce intense but infrequent rain and stratocumulus drizzles. The storm tracks, ITCZ, and trade winds are tied to the atmospheric circulation – understanding what drives the intermodel spread in precipitation patterns and their changes with warming becomes a question of understanding what controls the circulation of the atmosphere.

In the tropics, defined as the region equatorward of  $\pm 30^\circ$  latitude, the model response in the regional precipitation to warming is less robust than in the extra-tropics (e.g. Knutti and Sedláček, 2013). Precipitation changes are often separated into changes induced by the thermodynamics and dynamics associated with changes in the circulation. As a consequence of the thermodynamic response, the general patterns of precipitation change in models exhibit increases or decreases in climatologically wet or dry areas, respectively. Observations of ocean salinity changes support this general pattern change (Durack et al., 2012). These pattern changes follow the “wet-get-wetter” and “dry-get-drier” paradigm (Held and Soden, 2006), which is based on the thermodynamically driven increases of lower tropospheric saturation vapor pressure. If the relative humidity and circulation remain constant, a surface warming by one Kelvin increases the lower tropospheric humidity by 6-7% according to Clausius-Clapeyron. In the case of a constant circulation, higher tropospheric humidity implies that the moisture convergence in convective areas increases, and moisture divergence in dry descending areas increases. The paradigm is sometimes referred to as “direct moisture effect” (Chou et al., 2006) or “rich-get-richer” (Chou et al., 2009). Because the thermodynamically induced precipitation changes rely on the precipitation climatology, the present-day biases in models will lead to biases in the projections of precipitation changes (Bony et al., 2013).

Common tropical model biases with respect to observations are related to the position of the ITCZ. The double ITCZ bias has been persistent throughout several model generations (Mechoso et al., 1995; Dai, 2006; Oueslati and Bellon, 2015; Zhang et al., 2015), where models simulate a secondary branch of the ITCZ south of the equator over the central



and eastern Pacific for more than half of the year. In nature, a weak southern ITCZ branch occurs over the eastern Pacific only during boreal spring. Over the Atlantic, models place the precipitation maximum associated with the ITCZ either too eastward or too westward with respect to observations (Siongco et al., 2015). These persistent biases have been related, for example, to errors in the simulated SST patterns in AOGCMs, to the horizontal resolution, and to the coupling between precipitation and the large-scale dynamics.

Dynamical precipitation changes are associated with changes in the vertical velocity. The tropical circulation slows down with warming in models (e.g. Held and Soden, 2006; Vecchi and Soden, 2007), which partially offsets the strength of the thermodynamic precipitation response. Part of the slowdown of the tropical circulation is induced by the direct effect of increased atmospheric CO<sub>2</sub> on timescales faster than one year (Bony et al., 2013). Xie et al. (2015) show that the intermodel spread in the tropical precipitation response is governed by the spread in the dynamical precipitation response associated with changes in the vertical velocity. Sea surface temperatures increase all over the tropics but not uniformly such that SST patterns change with warming (Xie et al., 2010). Because deep convection triggers more likely over the warmest SST (e.g. Graham and Barnett, 1987; Johnson and Xie, 2010), shifting SST patterns entail a shift in the overturning circulation. Indeed, precipitation pattern changes seem to be driven by SST pattern changes with warming (e.g. Ma and Xie, 2013; Chadwick et al., 2013; Chadwick et al., 2014), implying a “warmer-get-wetter” mechanism.

But the tropical precipitation also differs vastly among models, when sea surface temperatures are uniformly raised. In CMIP5 aquaplanet simulations with fixed SSTs, a simplified GCM configuration of a water-covered Earth, the tropical precipitation pattern change in response to uniformly increasing SST by 4 K differs strikingly among models (Stevens and Bony, 2013). One model’s ITCZ contracts towards the equator, another shifts the ITCZ polewards, in others precipitation increases all over the tropics. In the absence of erroneous SST patterns from ocean-atmosphere coupling, land-atmosphere interactions including orographic effects, aerosols or other chemical species in the idealized aquaplanet simulation, the problem of intermodel spread in the tropical precipitation response boils down to the question of how convection couples to the large-scale environment given by the tropospheric temperature, humidity and cloud distribution. Voigt and Shaw (2015) expand on this study by focusing on the two models that showed the most diverse precipitation response, with one showing a widening and the other a contraction of the ITCZ with warming. They decompose the precipitation and circulation response to warming into contributions from the isolated SST increase, the water vapor and the cloud changes by locking radiative feedbacks (e.g. Mauritsen et al., 2013). For both models, the zonal-mean precipitation change in response to the cloud radiative effect (CRE) change most closely resembles the total zonal-mean precipitation change. Consequently, Voigt and Shaw (2015) conclude that the diverse CRE change between the two models governs the diverse zonal-mean change in tropical precipitation and circulation. Their work indicates that not only are diverse CRE changes with warming the largest contributor to the intermodel spread in the equilibrium climate sensitivity, but they also appear to be the core problem for the intermodel spread in precipitation pattern changes.

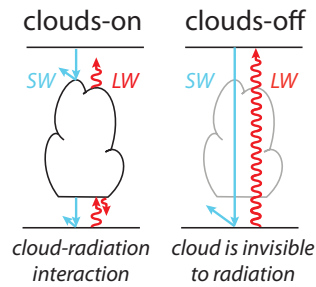


**Figure 1.2:** Illustration of how the cloud-radiation interaction is manipulated in the Clouds On-Off Climate Intercomparison Experiment. Longwave and shortwave radiative fluxes are abbreviated by LW and SW, respectively.

However, closer inspection of their results suggests that half of the difference in the equatorial precipitation change with warming can be attributed solely to the diverse precipitation response to increasing SST. This discrepancy between the apparent importance of CRE or SST changes on the precipitation response in two models motivates us to investigate the impact of CRE on the intermodel precipitation spread in a larger model ensemble. Six models performed aquaplanet Clouds On-Off Climate Intercomparison Experiment (COOKIE) simulations (Stevens et al., 2012), in which the cloud-radiation interaction is active like in the standard model configuration, or in which the cloud-radiative interaction is inhibited such that clouds become transparent to radiation (Figure 1.2). By exploring the difference between these “clouds-on” and “clouds-off” simulations, the impact of atmospheric cloud radiative effects (ACREs) on the tropical precipitation patterns and their change with warming can be determined. In **Chapter 3**, I explore the intermodel spread in tropical mean and spatial precipitation distribution in the COOKIE aquaplanet simulations. In particular, I discuss the hypothesis that the seed for intermodel spread may exist already in the absence of cloud-radiation interaction, opposing the conclusion of Voigt and Shaw (2015).

The paragraphs above highlight that the controls on the spatial distribution of precipitation are complex. The nature of the problem of simulating tropical precipitation is the coupling between the circulation, radiation and surface heat fluxes (Figure 1.3). The ratio between radiative cooling and the static stability determines the vertical velocity. Radiative cooling builds up convective instability, which eases the triggering of convection. In turn, convection transports moisture and upon condensation heats the column through release of latent heat. The latent heating and formation of clouds again modify the stratification and radiation. Apart from clouds, water vapor and temperature stratification, the radiative cooling is influenced by the atmospheric composition, e.g. greenhouse gases or aerosols. The large-scale circulation between regions of ascending and descending motion also impacts the surface turbulent fluxes through surface winds. The surface turbulent fluxes heat and moisten the boundary layer, affecting the boundary layer moist static energy. The moist static energy (MSE), a conserved quantity in moist adiabatic ascent, is the sum of latent, internal and potential energy. Convection occurs where the boundary layer MSE maximizes (e.g. Möbis and Stevens, 2012). The stronger the surface winds, the stronger is the heat input into the boundary layer, which further enforces the convection, constituting a positive feedback of wind induced surface heat-exchange (WISHE). Where convection, and with that precipita-

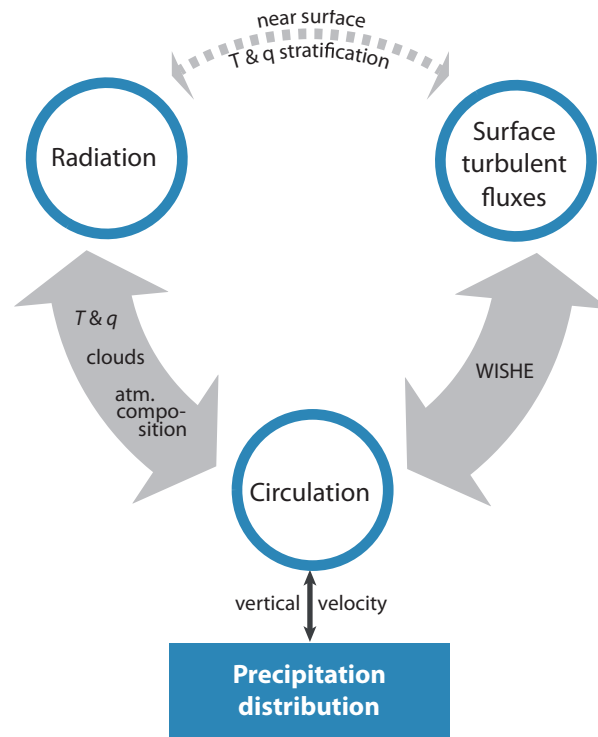


**Figure 1.3:** Illustration of the constraints on the tropical precipitation. The radiation and circulation are strongly coupled in that they both depend on and influence the temperature ( $T$ ) and humidity ( $q$ ) structure, the clouds, and the atmospheric composition (e.g. by transporting chemical species). The radiation and surface turbulent fluxes both influence and depend on the near-surface vertical temperature and humidity gradients. The circulation and surface fluxes are coupled by the wind-induced surface heat exchange (WISHE), which constitutes a positive feedback. A stronger circulation enhances the transport of heat from the surface to the atmosphere through stronger surface winds. A stronger heat input from the surface in turn enhances convection and strengthens the circulation. Because the vertical velocity determines the precipitation, understanding the coupling between radiation, surface turbulent fluxes and the circulation is a prerequisite to advance understanding of the tropical precipitation distribution.

tion, occurs, is thus set by the coupling between radiation, circulation and surface turbulent fluxes.

These three components are collectively represented in the column-integrated MSE budget. The budget contains sources and sinks to the column MSE such as the surface turbulent fluxes, the atmospheric radiative flux divergence, and horizontal as well as vertical advection of MSE. Because it couples the impact of the horizontal winds, radiation and surface fluxes to the vertical velocity, it has found many applications in conceptual models of the tropical dynamics (e.g. Neelin and Held, 1987; Neelin and Zeng, 2000). These models are usually built upon the assumption that the vertical velocity can be expressed by one vertical mode associated with deep convection, which gives rise to the definition of the gross moist stability. The gross moist stability can be thought of as a normalized vertical advection that represents the efficiency with which MSE is exported from the column. The conceptual models vary in complexity from a two-layer model that predicts surface moisture convergence (Neelin

and Held, 1987) to sophisticated self-sufficient models of intermediate complexity coupled to radiation, cloud and land surface schemes (e.g. Neelin and Zeng, 2000; Zeng et al., 2000). A diagnostic tool to study how heating and the gross moist stability influence the vertical velocity in different GCMs would be desirable to close the gap in the complexity of conceptual models for the tropical dynamics.

Even in the simplified aquaplanet configuration with fixed SSTs peaking at the equator, details of the coupling between radiation, circulation and surface turbulent fluxes can influence the distribution of tropical precipitation. The aquaplanet configuration has been widely used to study the persistent model double ITCZ bias mentioned above. In some cases the ITCZ appears as one single band of convection right at the equator, and in other cases a double ITCZ occurs with two bands of convection located off the equator on either hemisphere. Many different factors have been shown to influence the ITCZ position: the latitudinal SST gradient, the dynamical core and horizontal resolution, the feedback between surface wind and evaporation, the parameterization of convection, and even the solar constant (e.g. Dahms et al., 2011; Williamson et al., 2013; Oueslati and Bellon, 2013b; Liu et al., 2010; Möbis and Stevens, 2012; Oueslati and Bellon, 2013a; Numaguti, 1993; Chou and Neelin, 2004; Kirtman and Schneider, 2000; Barsugli et al., 2005). Only very recently, the impact of ACREs on the position of the ITCZ on aquaplanets has received in depth attention. By analyzing the COOKIE aquaplanet simulations, Harrop and Hartmann (2016) find a consistent poleward shift when cloud-radiation interaction is inhibited. They argue that the reduced atmospheric stability owing to the absence of ACRE modifies the convective available potential energy, such that convection can be triggered more easily further off the equator. However, this suggested mechanism lacks insight into why the ITCZ shifts more strongly in some models than in others.

To understand the zonal-mean precipitation distribution in the COOKIE simulations, in **Chapter 4** a simple framework is developed that diagnoses the vertical velocity, which in turn is closely related to precipitation. The framework is derived from the moist static energy budget. It assumes one vertical mode for the vertical velocity associated with deep convection. Testing the framework shows that the diagnosed vertical velocity reproduces the actual one well. The framework is employed to the COOKIE aquaplanet simulations with the goal to understand the zonal-mean precipitation distribution as well as ITCZ shifts induced by inhibiting cloud-radiation interactions.

## 2 Understanding the intermodel spread in global-mean hydrological sensitivity<sup>1</sup>

### Abstract

This chapter assesses intermodel spread in the slope of global-mean precipitation change ( $\Delta P$ ) with respect to surface temperature change. The ambiguous estimates in the literature for this slope are reconciled by analyzing four experiments from phase 5 of CMIP (CMIP5) and considering different definitions of the slope. The smallest intermodel spread (a factor of 1.5 between the highest and lowest estimate) is found when using a definition that disentangles temperature-independent precipitation changes (the adjustments) from the slope of the temperature-dependent precipitation response; here this slope is referred to as the hydrological sensitivity parameter ( $\eta$ ). The estimates herein show that  $\eta$  is more robust than stated in most previous work. The authors demonstrate that adjustments and  $\eta$  estimated from a steplike quadrupling CO<sub>2</sub> experiment serve well to predict  $\Delta P$  in a transient CO<sub>2</sub> experiment. The magnitude of  $\eta$  is smaller in the coupled ocean–atmosphere quadrupling CO<sub>2</sub> experiment than in the noncoupled atmosphere-only experiment. The offset in magnitude due to coupling suggests that intermodel spread may undersample uncertainty.

Also assessed are the relative contribution of  $\eta$ , the surface warming, and the adjustment on the spread in  $\Delta P$  on different time scales. Intermodel variation of both  $\eta$  and the adjustment govern the spread in  $\Delta P$  in the years immediately after the abrupt forcing change. In equilibrium, the uncertainty in  $\Delta P$  is dominated by uncertainty in the equilibrium surface temperature response. A kernel analysis reveals that intermodel spread in  $\eta$  is dominated by intermodel spread in tropical lower tropospheric temperature and humidity changes and cloud changes.

### 2.1 Introduction

The intermodel spread in global-mean precipitation response appears to be substantial in simulations of global warming. To narrow this spread, it may be helpful to understand the slope of global-mean precipitation changes with respect to global-mean temperature. However, estimates of the intermodel spread in this slope vary from one study to another. To discern the origin of these differences, we reassess intermodel spread and the magnitude of

---

<sup>1</sup> This chapter has been published with minor modifications as: Fläschner, D., T. Mauritsen, and B. Stevens (2016). “Understanding the Intermodel Spread in Global-Mean Hydrological Sensitivity”. *Journal of Climate*, **29**, no. 2, pp. 801–817. doi: 10.1175/JCLI-D-15-0351.1.

the slope of global-mean precipitation change with global-mean surface warming in climate change experiments carried out as part of phase 5 of the Coupled Model Intercomparison Project (CMIP5). We further investigate the relative contributions of different processes to the spread in the simulated global-mean precipitation response. We only investigate global-mean precipitation changes in this study. For simplicity hereafter, when we mention precipitation or surface temperature, we refer to the global-mean quantities.

That changes in global-mean precipitation are constrained by the energetics of the atmosphere is well understood (e.g. Newell et al., 1975; Mitchell et al., 1987; Boer, 1993; Allen and Ingram, 2002; Held and Soden, 2006; O’Gorman et al., 2012). Given this energetic constraint, it could be assumed that estimates of the slope of precipitation change with surface temperature change would be likewise constrained. However, the estimates of intermodel spread vary among studies, from the smallest spread of 1.82-2.70  $\text{W m}^{-2} \text{K}^{-1}$  (factor of 1.5 between lowest and highest model estimate) in Andrews et al. (2009) to studies suggesting much larger intermodel spreads up to a factor of 3.3 for models participating in CMIP3 and CMIP5 (Table 2.1). In addition to different estimates of intermodel spread, the ensemble-mean magnitude of the ratio of precipitation change with warming also differs across these model-based studies.

**Table 2.1:** Comparison between the literature and this study for estimates of the slope of precipitation change with respect to surface temperature change.  $\eta$  denotes the hydrological sensitivity parameter and  $\eta_a$  the apparent hydrological sensitivity parameter. The absolute spread shows the lowest and highest model estimate ( $\text{W m}^{-2} \text{K}^{-1}$ , values in parantheses have the unit  $\% \text{K}^{-1}$ ). The factor of spread is the approximate ratio between the lowest and highest model estimate. The dispersion (%) is the ensemble standard deviation divided by the ensemble mean.

Study	Definition of slope	Absolute spread	Factor of spread	Dispersion
Held and Soden (2006)	$\eta_a$	(1-3)	3	–
Lambert and Webb (2008)	$\eta$	1.3-3.2 (1.4-3.4)	2.4 2.4	– –
Andrews et al. (2009)	$\eta$	1.82-2.70	1.5	11
Takahashi (2009)	$\eta$	1.50-3.13	2.1	19
Lambert and Allen (2009)	$\eta$	0.84-1.97	2.3	27
Frieler et al. (2011)	$\eta$	–	–	24
Previdi (2010)	$\eta_a$	(0.71-2.37)	3.3	31
Pendergrass and Hartmann (2014)	$\eta_a$	0.7-1.9	2.7	27
<b>This study</b> (from abrupt4xCO2)	$\eta$	1.85-2.73 (2.1-3.3)	1.5 1.6	11 11

General circulation models are an indispensable tool for studying and predicting precipitation changes. However, the different estimates of the slope of global-mean precipitation change may raise doubts as to the models’ ability to correctly predict global-mean precipitation changes with global warming. Understanding the reasons for the different model-based

estimates in the literature is important to judge how confident one can be in the predictions of precipitation change. This insight may eventually help to improve the representation of physical processes in the models and eventually the prediction of precipitation change with global warming.

Physical and methodological issues complicate the interpretation of estimates of the precipitation response to warming in the literature. First, climate change experiments with different degrees of idealization, from very idealized CO<sub>2</sub>-step configurations to transient scenarios including multiple forcing agents, were analyzed. Second, authors define the slope of precipitation change with respect to surface temperature change in different ways, but describe it using the same term: “hydrological sensitivity”.

In some studies the term hydrological sensitivity is used to denote the ratio of global-mean precipitation change to the corresponding global-mean surface temperature change, where the changes were estimated as the differences between the perturbed and control mean states (e.g. Held and Soden, 2006; Bala et al., 2008; Previdi, 2010; Pendergrass and Hartmann, 2014). Other studies incorporate the expectation that precipitation not only changes proportionally with surface temperature, but also adjusts directly to forcing agents. For instance, Allen and Ingram (2002) and other studies (e.g. Lambert and Webb, 2008; Andrews et al., 2009) express the global-mean precipitation changes ( $\Delta P$ ) as a linear function of the surface temperature changes ( $\Delta T_s$ ) following

$$\Delta P = \eta \cdot \Delta T_s + A, \quad (2.1)$$

where  $\eta$  is the proportionality factor between  $\Delta P$  and  $\Delta T_s$ , and  $A$  is an adjustment term which measures the direct response of precipitation to forcing, independent of any eventual surface temperature change. If, for example, the CO<sub>2</sub> concentration in the atmosphere is abruptly increased, the atmosphere is directly cooled less via the increased absorption of longwave radiation from CO<sub>2</sub> (Ramanathan, 1981). To balance this reduction in radiative cooling, the atmosphere reacts rapidly by reducing a heating source, the precipitation (e.g. Allen and Ingram, 2002; Andrews et al., 2009). Rising temperatures due to the forcing then lead to more atmospheric cooling. Precipitation is thus initially suppressed by abruptly increasing levels of CO<sub>2</sub>, but increases proportionally to surface temperature warming when the forcing is held constant. The proportionality factor  $\eta$  of precipitation change with surface temperature change has formerly been referred to as “differential hydrological sensitivity” but also ambiguously as “hydrological sensitivity”.

A more precise terminology for precipitation changes with temperature changes would be helpful. For the remainder of this work we will adopt a terminology (illustrated in Figure 2.1) that is analogous to the well-defined framework of equilibrium climate sensitivity (ECS).

In the ECS framework (e.g. Sherwood et al., 2015), an external forcing  $F$  causes a radiative imbalance at the top-of-atmosphere ( $\Delta R^{\text{TOA}}$ ) which arises from the direct radiative forcing as well as adjustments of atmospheric properties without any change in the global-mean surface temperature, e.g. clouds. The surface temperature responds to the radiative imbalance according to  $\Delta R^{\text{TOA}} = \lambda \Delta T_s + F$  (e.g. Gregory et al., 2004) until a new equilibrium is reached. The slope  $\lambda$  is called “climate feedback parameter” and the surface warming in equilibrium due to a doubling of CO<sub>2</sub> is called “equilibrium climate sensitivity”.

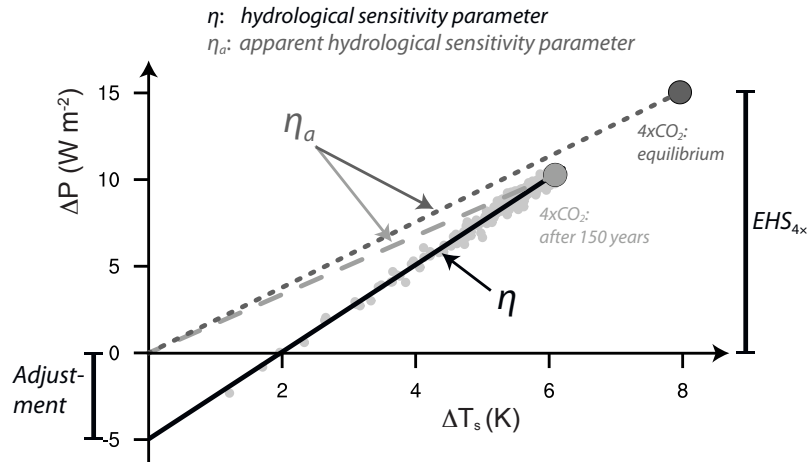


**Figure 2.1:** Illustration of the terminology for precipitation change with surface temperature change adopted in this work, by the example of abrupt4xCO<sub>2</sub> data from IPSL-CM5A-LR. The “hydrological sensitivity parameter” ( $\eta$ ) is the slope of the global-mean precipitation response with respect to surface temperature change when explicitly taking into account the rapid “Adjustment” of precipitation due to forcing agents. The “apparent hydrological sensitivity parameter” ( $\eta_a$ ) is given by the slope of global time-mean responses without accounting for rapid precipitation adjustments. The equilibrium precipitation change due to a quadrupling of CO<sub>2</sub> is denoted as “equilibrium hydrological sensitivity” at 4×CO<sub>2</sub> ( $EHS_{4x}$ ). Small circles signify annual global-means, and large circles the endpoint and equilibrium mean.

In analogy, for precipitation changes we will hereafter refer to the amount of global-mean precipitation change in equilibrium due to a doubling of CO<sub>2</sub> as “equilibrium hydrological sensitivity” (EHS) and to  $\eta$ , the slope of temperature-dependent precipitation change, as “hydrological sensitivity parameter”. In contrast to  $\lambda$ ,  $\eta$  is not a feedback parameter, because  $\Delta P$  does not feed back on  $\Delta T_s$ . The slope of total precipitation change to total surface temperature change will be referred to as the “apparent hydrological sensitivity parameter” ( $\eta_a$ ), where “apparent” alludes to the fact that  $\eta_a$  is what one might observe, but is sensitive to the nature of the forcing. On the contrary, we prefer to think of  $\eta$  as a more characteristic quantity that does not depend on the specifics of the forcing agent or the details of the surface warming (Andrews et al., 2009; Bala et al., 2010; Andrews et al., 2010; Kvalevåg et al., 2013). However, if  $A$  is not known a priori, then  $\eta$  can only be estimated in steplike forcing experiments.

The aim of this work is to gain more insight into reasons for the intermodel spread in the hydrological sensitivity. In light of the terminological ambiguity discussed above, we aim to investigate the term “hydrological sensitivity” for both the previous definition and our current terminology. First, we reassess the intermodel spread in the slope of precipitation change with surface temperature change ( $\eta$  and  $\eta_a$ ) in four CMIP5 experiments, compare our estimates with the literature, and provide physical explanations for differences among estimates. We discuss how the value and intermodel spread depend on the definition and on the analyzed climate change experiment in a set of CMIP5 models (Section 2.3) as well as the applicability of  $\eta$  and  $A$  derived from idealized steplike CO<sub>2</sub> forcing experiment to a transient CO<sub>2</sub> experiment (Section 2.4).



In the second part of this study, we discuss the intermodel spread in global-mean precipitation response among the different CMIP5 models in an idealized experiment with abruptly quadrupled CO<sub>2</sub> concentration (Section 2.5). We assess how the three factors from Eq. 2.1 ( $\eta$ ,  $\Delta T_s$ , and  $A$ ) contribute to the spread in the equilibrium precipitation response, following the illustrative approach of Hawkins and Sutton (2009). Previdi (2010) and O’Gorman et al. (2012) investigated reasons for intermodel spread in the slope of precipitation change with the radiative kernel method (Soden et al., 2008), finding that the spread from clouds dominates over the spread from temperature and water vapor changes. Takahashi (2009) proposes that the intermodel spread in the slope is caused by scatter in the shortwave absorption among models. Pendergrass and Hartmann (2014) show that temperature and water vapor profiles change differently and thus cause differences in the atmospheric heat budget. To gain more insight into causes for intermodel spread in  $\eta$  and  $A$ , we employ the methodology as in Previdi (2010), but use newer radiative kernels (radiative flux perturbations due to a unit change in atmospheric state variable) to decompose the atmospheric heat budget into contributions from CO<sub>2</sub>, temperature, water vapor and clouds.

## 2.2 Experiments and methods

### 2.2.1 Experiments

We investigate four CMIP5 experiments (Taylor et al., 2012), in which the atmospheric heat budgets are perturbed in distinct ways. Coupled ocean-atmosphere (piControl, historical, 1pctCO2, and abrupt4xCO2) and noncoupled atmosphere-only experiments (amip and amip4K) are analyzed. To interpret our findings we also analyze some more specialized experiments (amipFuture; see also sstClim and sstClim4xCO2 in Appendix A).

The historical simulation starts from preindustrial control conditions (piControl experiment) but with prescribed transient historical forcings. Transient forcings include well-mixed greenhouse gases, natural and anthropogenic aerosols as well as land-use, solar and orbital forcings. Although recommended input for most of these forcings was provided, modeling groups were free to specify e.g. the aerosol forcing.

The radiative forcing is less ambiguously defined in the more idealized CMIP5 experiments. In the 1pctCO2 experiment the forcing consists of a gradual 1% per year increase of the CO<sub>2</sub> concentration, yielding a near-linear increase in radiative forcing. The CO<sub>2</sub> concentration doubles after 70 years and quadruples after 140 years. In the abrupt4xCO2 experiment, the preindustrial CO<sub>2</sub> concentration is abruptly quadrupled with respect to piControl and then held constant for the remainder of the simulation. The CMIP5 experiment protocol calls for at least 150 years of simulation length for experiments with coupled models. If modeling centers provided longer time series, all available monthly mean values were included in the analysis. We selected models for which the abrupt4xCO2 experiment was available. Only the r1i1p1 ensemble member of each model is included in the analysis. The noncoupled amip and amip4K experiments are part of the Cloud Feedback Model Intercomparison Project (Bony et al., 2011) where models are driven by prescribed sea-surface temperatures for

the period 1979-2008 and the corresponding forcing agents. In amip4K, the sea-surface temperatures are uniformly raised by 4K but all other boundary conditions remain as in the amip experiment.

### 2.2.2 Calculation methods

Two common methods exist to calculate the hydrological sensitivity parameter  $\eta$ : the regression method (e.g. Gregory et al., 2004; Andrews et al., 2009; Lambert and Webb, 2008) and the fixed-SST method (Hansen et al., 2005; Bala et al., 2010; Andrews et al., 2010; Kvalevåg et al., 2013). For the abrupt4xCO2 experiment we perform an ordinary least squares regression between annual global-mean  $\Delta T_s$  and  $\Delta P$ , where  $\eta$  is given by the slope, and  $A$  by the  $y$ -intercept. For the amip4K experiment, we compute  $\Delta P$  and  $\Delta T_s$  as the global and time-mean differences over the period of 1979-2008 between amip4K and amip. Because the adjustment,  $A$ , is zero in amip4K,  $\eta$  is given directly as the ratio  $\Delta P/\Delta T_s$ .

The apparent hydrological sensitivity parameter  $\eta_a$  has usually been calculated by subtracting global time-averages over the last years of the perturbed experiment from a climatological mean of the control state or alternatively of the beginning years of the perturbed climate change experiment. We follow this approach for the abrupt4xCO2 experiment, and estimate  $\eta_a$  for two different time-means. The endpoint-mean refers to the global time-average over the last ten years of a model’s simulation. The equilibrium-mean is discussed here, because the endpoint-mean is not representative of equilibrium conditions, as the equilibration timescale in coupled models is much greater than the typical 150 year simulation length. To estimate the equilibrium hydrological sensitivity for a quadrupling of CO<sub>2</sub> (EHS<sub>4x</sub>), we follow the Gregory method (Gregory et al., 2004) and extrapolate the top-of-atmosphere radiative flux imbalance towards equilibrium, finding the equilibrium climate sensitivity for a 4×CO<sub>2</sub> forcing (ECS<sub>4x</sub>). Together with  $\eta$  and  $A$ , the EHS<sub>4x</sub> is determined by Eq. 2.1. Unless otherwise noted, we calculate  $\eta_a$  for both the historical and 1pctCO2 experiments as the slope from the regression of annual mean  $\Delta T_s$  and  $\Delta P$ . We choose this method because it yields the general trend of precipitation evolution with surface temperature for the transient forcing experiment. This method is shown to be superior to the method of differencing time-averages for estimating linear trends (Barnes and Barnes, 2015). Note, transient forcing simulations do not readily allow one to separate the adjustment.

## 2.3 The slope of precipitation change with respect to surface temperature change in CMIP5 simulations

Here we compare the slope of global-mean precipitation increase with respect to surface warming as found in four CMIP5 experiments and estimated according to the definitions in Section 2.1. The ensemble-mean values and their intermodel spread of the hydrological sensitivity parameter ( $\eta$ ) and the apparent hydrological sensitivity parameter ( $\eta_a$ ) are portrayed by Gaussian distributions (Figure 2.2a). Individual model values are given in Table 2.2. The spread is shown as the standard deviation across the ensemble (Figure 2.2a) or in terms of

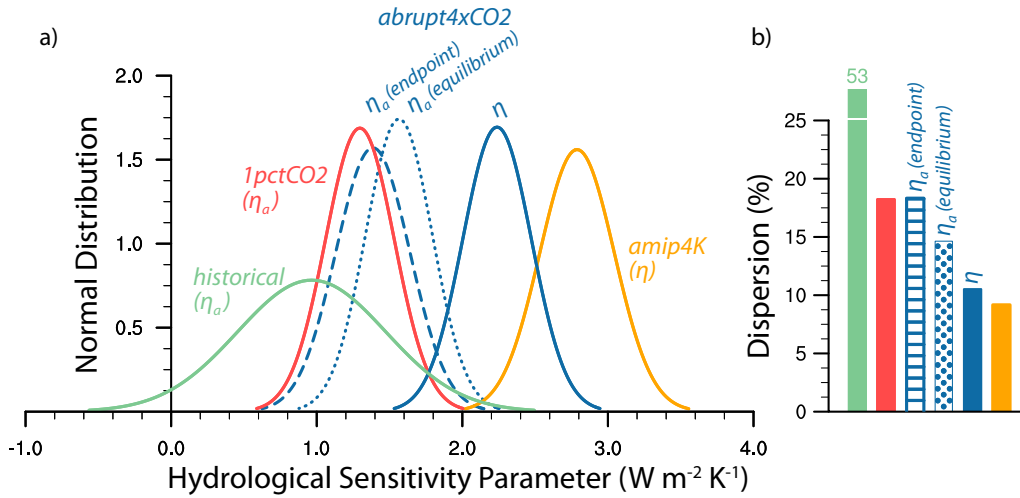


**Figure 2.2:** Comparison of the slope of precipitation change with respect to surface temperature change for different definitions of the slope and different CMIP5 experiments. a) The spread is shown as Gaussian curves, as given by the ensemble mean and standard deviation of the hydrological sensitivity parameter ( $\eta$ ) and the apparent hydrological sensitivity parameter ( $\eta_a$ ). b) The ensemble standard deviation is scaled by the ensemble mean to yield the dispersion. Table 2.2 lists the parameter values for all models.

the dispersion (Figure 2.2b), which is the standard deviation normalized by the ensemble mean. Because the dispersion provides a measure of the relative spread among models, it is more indicative of the inter-experiment spread than the standard deviation. The smaller the dispersion, the smaller is the relative intermodel spread.

First we examine how the magnitude and spread depend on the definition of the slope. The dependence on the definition can only be tested with the abrupt4xCO2 experiment. It is well understood that  $\eta$  is greater than  $\eta_a$  because the fast precipitation adjustment to an increase in CO<sub>2</sub> is negative (e.g. Allen and Ingram, 2002; Andrews et al., 2009; Bala et al., 2010). We show that the choice of  $\eta$  or  $\eta_a$  to characterize the “hydrological sensitivity” also strongly influences the spread of the slope (Figure 2.2b). The dispersion, and thus the relative intermodel spread, is smallest for  $\eta$  (10.7%) and larger for the two  $\eta_a$  estimates. The smaller spread in  $\eta$  is simply explained by the fact that the spread of the slope is explicitly separated from the spread of the adjustment. Estimating the slope via the definition of  $\eta_a$  reveals that its magnitude and spread are sensitive to the surface warming, and thus time. When  $\eta_a$  is computed at equilibrium conditions (greater surface warming), the spread from the adjustment loses its impact on the spread of the slope relative to endpoint conditions (smaller dispersion of 14.6% versus 18.2%). Not being influenced by the adjustment, the definition of  $\eta$  yields a more precise estimate for the increase of precipitation with surface warming ( $2.24 \pm 0.24 \text{ W m}^{-2} \text{ K}^{-1}$ , error is given as one intermodel standard deviation).

The inter-experiment differences in magnitude and spread of the slope depend on the experiment configuration. For the idealized steplike warming experiment (amip4K), the spread in  $\eta$  is similarly small (dispersion of 9.3%) as for abrupt4xCO2. That the magnitude of  $\eta$  is higher in amip4K ( $2.79 \pm 0.26 \text{ W m}^{-2} \text{ K}^{-1}$ ) as compared to abrupt4xCO2 is unexpected;

**Table 2.2:** Values of the hydrological sensitivity parameter ( $\eta$ ) and the apparent hydrological sensitivity parameter ( $\eta_a$ ) from different CMIP5 experiments. All values are in  $\text{W m}^{-2} \text{K}^{-1}$  or for abrupt4xCO2 additionally in parantheses in  $\% \text{K}^{-1}$ . Error estimates are given as plus or minus one standard error from the ordinary least squares regression. Ensemble error is plus or minus one ensemble standard deviation. The models are ordered such that their  $\eta$  value in the abrupt4xCO2 simulation increases. Data has been horizontally interpolated to a common Gaussian T63 grid prior to analysis.

Model	historical ( $\eta_a$ )	1pctCO2 ( $\eta_a$ )	abrupt4xCO2 ( $\eta$ )	amip4K ( $\eta$ )	Reference
ACCESS1-0	$0.47 \pm 0.15$	$0.82 \pm 0.01$	$1.85 \pm 0.02$ ( $2.06 \pm 0.02$ )	–	Bi et al. (2013)
BNU-ESM	$0.93 \pm 0.07$	$1.22 \pm 0.02$	$1.87 \pm 0.03$ ( $2.14 \pm 0.04$ )	–	Ji et al. (2014)
HadGEM2-A	–	–	–	2.32	Collins et al. (2011)
HadGEM2-ES	$0.70 \pm 0.20$	$0.98 \pm 0.01$	$1.90 \pm 0.02$ ( $2.13 \pm 0.02$ )	–	”
FGOALS-s2	–	$1.45 \pm 0.02$	$1.92 \pm 0.04$ ( $2.49 \pm 0.05$ )	–	Bao et al. (2013)
CanESM2	$0.84 \pm 0.07$	$1.10 \pm 0.02$	$1.97 \pm 0.03$ ( $2.48 \pm 0.03$ )	–	Arora et al. (2011)
CanAM4	–	–	–	2.55	Salzen et al. (2013)
FGOALS-g2	$1.44 \pm 0.09$	$1.29 \pm 0.01$	$1.99 \pm 0.02$ ( $2.44 \pm 0.02$ )	2.59	Li et al. (2013)
GFDL-ESM2G	$1.26 \pm 0.10$	$0.82 \pm 0.05$	$2.01 \pm 0.03$ ( $2.34 \pm 0.04$ )	–	Dunne et al. (2012)
MIROC-ESM	$0.08 \pm 0.09$	$1.37 \pm 0.01$	$2.08 \pm 0.03$ ( $2.56 \pm 0.03$ )	–	Watanabe et al. (2011)
MPI-ESM-LR	$1.19 \pm 0.07$	$1.42 \pm 0.01$	$2.15 \pm 0.03$ ( $2.54 \pm 0.04$ )	2.74	Stevens et al. (2013)
GFDL-ESM2M	$1.50 \pm 0.12$	$1.12 \pm 0.04$	$2.17 \pm 0.03$ ( $2.53 \pm 0.04$ )	–	Dunne et al. (2012)
BCC-CSM1-1	$1.26 \pm 0.04$	$1.33 \pm 0.01$	$2.18 \pm 0.03$ ( $2.69 \pm 0.04$ )	2.74	Wu et al. (2014)
MPI-ESM-MR	$1.29 \pm 0.09$	$1.53 \pm 0.02$	$2.23 \pm 0.04$ ( $2.59 \pm 0.04$ )	2.93	Giorgetta et al. (2013)
ACCESS1-3	$0.76 \pm 0.16$	$1.46 \pm 0.02$	$2.24 \pm 0.03$ ( $2.44 \pm 0.03$ )	–	Bi et al. (2013)
CNRM-CM5	$0.42 \pm 0.17$	$1.27 \pm 0.02$	$2.24 \pm 0.03$ ( $2.52 \pm 0.03$ )	2.77	Voltaire et al. (2012)
IPSL-CM5B-LR	$1.51 \pm 0.06$	$1.06 \pm 0.02$	$2.24 \pm 0.04$ ( $2.79 \pm 0.05$ )	2.89	Hourdin et al. (2013)
CSIRO-Mk3-6-0	$0.29 \pm 0.14$	$1.47 \pm 0.02$	$2.25 \pm 0.02$ ( $2.68 \pm 0.03$ )	–	Rotstayn et al. (2012)
MPI-ESM-P	$1.03 \pm 0.07$	$1.42 \pm 0.01$	$2.25 \pm 0.03$ ( $2.66 \pm 0.04$ )	–	Giorgetta et al. (2013)
GFDL-CM3	$0.82 \pm 0.20$	$1.37 \pm 0.02$	$2.26 \pm 0.03$ ( $2.56 \pm 0.03$ )	–	Donner et al. (2011)
NorESM1-M	$0.84 \pm 0.12$	$1.05 \pm 0.02$	$2.32 \pm 0.03$ ( $2.86 \pm 0.04$ )	–	Bentsen et al. (2013)
CCSM4	$1.43 \pm 0.06$	$1.22 \pm 0.01$	$2.39 \pm 0.03$ ( $2.82 \pm 0.04$ )	3.10	Meehl et al. (2011)
BCC-CSM1-1-m	$1.55 \pm 0.05$	$1.58 \pm 0.02$	$2.40 \pm 0.03$ ( $2.97 \pm 0.04$ )	–	Wu et al. (2014)
MIROC5	$0.72 \pm 0.12$	$1.15 \pm 0.02$	$2.42 \pm 0.06$ ( $2.61 \pm 0.06$ )	2.71	Watanabe et al. (2010)
INMCM4	$1.38 \pm 0.08$	$1.26 \pm 0.02$	$2.43 \pm 0.06$ ( $2.69 \pm 0.06$ )	–	Volodin et al. (2010)
GISS-E2-H	$0.74 \pm 0.08$	$1.36 \pm 0.01$	$2.49 \pm 0.03$ ( $2.68 \pm 0.03$ )	–	Schmidt et al. (2014)
IPSL-CM5A-LR	$1.60 \pm 0.05$	$1.50 \pm 0.01$	$2.51 \pm 0.02$ ( $3.27 \pm 0.03$ )	2.83	Dufresne et al. (2013)
IPSL-CM5A-MR	$1.81 \pm 0.07$	$1.49 \pm 0.01$	$2.57 \pm 0.03$ ( $3.24 \pm 0.03$ )	–	Dufresne et al. (2013)
GISS-E2-R	$0.38 \pm 0.14$	$1.27 \pm 0.02$	$2.63 \pm 0.05$ ( $2.86 \pm 0.06$ )	–	Schmidt et al. (2014)
MRI-CGCM3	$-0.19 \pm 0.22$	$1.92 \pm 0.02$	$2.73 \pm 0.05$ ( $3.22 \pm 0.06$ )	3.30	Yukimoto et al. (2012)
<b>Ensemble</b>	$0.97 \pm 0.51$	$1.30 \pm 0.24$	$2.24 \pm 0.24$ ( $2.64 \pm 0.30$ )	$2.79 \pm 0.26$	

the usage of the same definition should yield similar values if  $\eta$  is a characteristic quantity for the evolution of the temperature-dependent  $\Delta P$ . Possible reasons for differences are discussed in more detail in Section 2.6.

For the transient experiments (1pctCO2 and historical), the slope is, as explained above, suppressed by the effect of the adjustments. Here only  $\eta_a$  can be estimated because the exact forcings for the individual models are unknown. The suppression is stronger in the historical simulation ( $0.91 \pm 0.51 \text{ W m}^{-2} \text{K}^{-1}$ ). In addition to greenhouse gas forcings, absorbing aerosols (e.g. biomass burning and black carbon) reduce the precipitation increase (e.g. Andrews et al., 2010; Kvalevåg et al., 2013). Among the considered experiments, the spread is largest in the historical simulation (dispersion of 53%), although it is calculated by the regression method, thereby yielding the trend of historical  $\Delta P$  evolution with  $\Delta T_s$ . Esti-

**Table 2.3:** Comparison of the regression and the endpoint method. The regression method applied to abrupt4xCO<sub>2</sub> yields  $\eta$ , all other estimates yield  $\eta_a$ . Values shown are the ensemble mean plus or minus one ensemble standard deviation and in parantheses are the minimum-maximum range of model values. Units are  $\text{W m}^{-2} \text{K}^{-1}$ .

Experiment	Regression	Endpoint
historical	$0.97 \pm 0.51$ (-0.19- 1.81)	$0.44 \pm 0.94$ (-1.64-1.76) <sup>1</sup>
1pctCO <sub>2</sub>	$1.30 \pm 0.24$ ( 0.82- 1.92)	$1.28 \pm 0.23$ ( 0.72-1.88)
abrupt4xCO <sub>2</sub>	$2.24 \pm 0.24$ ( 1.85- 2.73)	$1.39 \pm 0.25$ ( 0.91-1.97)

<sup>1</sup> Endpoint ensemble estimates for the historical experiment exclude GFDL-CM3 for which  $\eta_a = -16.4 \text{ W m}^{-2} \text{K}^{-1}$ .

mates of  $\eta_a$  have even greater spread when calculated using the endpoint method (Table 2.3) because endpoint-means strongly depend on the forcing and thus time. The spread in the historical experiment cannot be expected to be as small as in the idealized experiments, because a large diversity in aerosol load and distribution (e.g. Stevens, 2015) causes a variable forcing on the respective model’s atmospheric heat budget. Aerosols have been shown to exert a great impact on the intermodel spread of  $\eta_a$  in the CMIP3 ensemble (e.g. Previdi, 2010; Pendergrass and Hartmann, 2012). In addition, the natural variability is high compared to the signal from the forcing, which increases the intermodel spread of the estimated slope. The effect of natural variability is also apparent in Hegerl et al. (2015), where the spread in the representative concentration pathways (RCPs) reduces with increasing forcing (their Figure 1b).

The merit of estimating  $\eta_a$  for a transient experiment with such variable forcings on the atmospheric heat budget remains questionable because physical reasons for intermodel spread in  $\eta_a$  are difficult to disentangle. On the contrary, the concept of the hydrological sensitivity parameter  $\eta$  reveals that models in fact agree well on the magnitude of  $\eta$ .

We consider the estimate in  $\eta$  from abrupt4xCO<sub>2</sub> as the most appropriate estimate for the CMIP5 model ensemble for the rate of increase in precipitation with surface warming. The estimate, with absolute model spread of  $1.85\text{-}2.73 \text{ W m}^{-2} \text{K}^{-1}$  (with a factor of 1.5 between the highest and lowest model estimate) and a dispersion of 10.7%, supports the results in Andrews et al. (2009) who also find a factor of 1.5 spread among models. Why is the intermodel spread in  $\eta$  larger in the remaining studies (Table 2.1)?

The analysis above demonstrates that the spread in the slope of precipitation increase is larger when  $\eta_a$  is calculated (Held and Soden, 2006; Previdi, 2010; Pendergrass and Hartmann, 2014). Studies that estimate  $\eta$  from transient multi-experiment model ensembles via a multiple regression analysis must make assumptions as to the magnitude of forcings, finding larger spreads (Lambert and Allen, 2009; Frieler et al., 2011). Takahashi (2009) finds the best estimate from a muti-model multi-run ensemble by looking at two transient and one steplike CO<sub>2</sub> and accounting for adjustments. The larger dispersion (19%) in that study may arise from a different application of the regression method. Lambert and Webb (2008) calculate  $\eta$  from the  $2 \times \text{CO}_2$  CMIP3 experiment and from a large ensemble of models with physically perturbed atmospheric sub-grid scale parameters. Probably the analysis of models with physically perturbed parameters initiated the larger spread in Lambert and

Webb (2008) (factor of 2.4 difference), but such experiments are less constrained estimates of the present climate. The large number of CMIP5 models analyzed here may therefore be considered as a representative sample to infer that intermodel differences resulting in a factor of 1.5 spread in  $\eta$  among models which is comparably small to what has been estimated in most previous work.

## 2.4 Applicability of the hydrological sensitivity parameter to transient experiments

We have shown that the hydrological sensitivity parameter is a robust measure in the idealized abrupt  $4\times\text{CO}_2$  experiment, but  $\eta_a$  found in transient forcing simulations is sensitive to the experimental configuration. Transient forcings, however, are more realistic, as an abrupt quadrupling of  $\text{CO}_2$  concentration is not expected to happen in reality.

Of what use is then a measure estimated from the abrupt4xCO2 simulations to understand precipitation change in the more complex reality? Thorpe and Andrews (2014) demonstrated that  $\eta$  estimated from abrupt4xCO2 serves well for predicting the overall precipitation response in the historical and different Representative Concentration Pathway (RCP) experiments, simply by considering fast precipitation adjustments to aerosols, ozone,  $\text{CO}_2$ , solar changes and other greenhouse gases. For this analysis, TOA forcing estimates for the different forcing agents had to be converted into atmospheric forcings, but the conversion ratios were known for only two models and thus had to be applied to the rest of the models. Consequently, the total spread of  $\Delta P$  could not be exactly predicted.

Here we ask how well precipitation changes in the transient 1pctCO2 can be predicted by only knowing the temperature-dependent precipitation response ( $\eta$ ) and the fast precipitation adjustment ( $A$ ) from abrupt4xCO2. To do so, we scale  $A$  (the adjustment for a four-fold  $\text{CO}_2$  increase) by the relative change in forcing in year  $n$  to predict  $\Delta P$

$$\Delta P_{\text{pred.}}^n = \eta \cdot \Delta T_s^n + A \cdot \frac{n}{2} \log_2 1.01. \quad (2.2)$$

The scaling factor multiplying  $A$  has been estimated by assuming that the forcing increases linearly with the logarithm of the  $\text{CO}_2$  concentration, which increases at 1% per year. It is thus identically one at the time of  $\text{CO}_2$  quadrupling, i.e.,  $n = 139.32$  years. This approach is similar to the one adopted by Good et al. (2012).

The predicted evolution of precipitation changes with surface temperature changes coincides with the overall model precipitation change (Figure 2.3a). Apart from the two GISS models, the absolute difference between predicted and model  $\Delta P$  is smaller than ca.  $\pm 0.9 \text{ W m}^{-2}$  (or  $\pm 0.03 \text{ mm day}^{-1}$ ) as shown by the gray shading (Figure 2.3b). Precipitation increases non-linearly with surface warming in the GISS models in the abrupt4xCO2 experiment which leads to ambiguity in the estimates of  $\eta$  and  $A$ , resulting in a biased  $\Delta P_{\text{pred.}}^n$ . The good agreement in the other models, however, suggests that idealized climate change experiments may serve well in projecting the global-mean precipitation response.

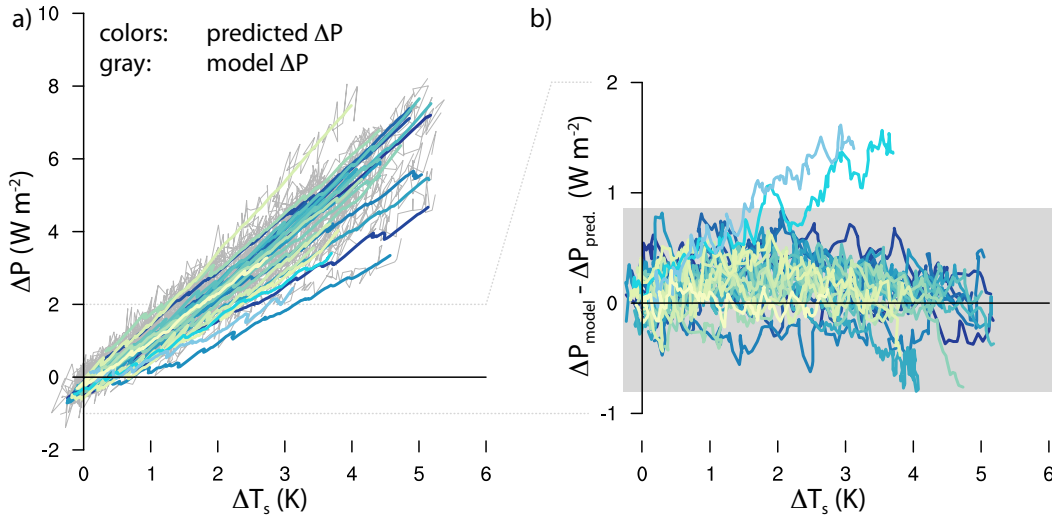


**Figure 2.3:** a) Evolution of annual mean precipitation change ( $\Delta P$ ) with corresponding surface temperature change ( $\Delta T_s$ ) in the 1pctCO<sub>2</sub> experiment, with respect to the climatological mean in piControl. Gray thin lines show actual model results, and colored thick lines the predicted precipitation change following Eq. 2.2. b) Absolute deviation of predicted and model  $\Delta P$ . All colored lines are smoothed by a 5-year running average. The gray shading ranges from  $-0.80$  to  $0.86 \text{ W m}^{-2}$ . All 1pctCO<sub>2</sub> experiments from Table 2.2 are shown, except GFDL-ESM2M and GFDL-ESM2G as our analysis suggests that their CO<sub>2</sub> increase stopped after 70 years.

From this we deduce that the difficulties to exactly project  $\Delta P$  in Thorpe and Andrews (2014) arose from uncertainties in forcing estimates other than from CO<sub>2</sub>. For here it is shown that  $\eta$  and  $A$ , estimated from abrupt  $4\times\text{CO}_2$  experiments, can predict the precipitation change in a transient CO<sub>2</sub> experiment reasonably well.

## 2.5 Sources of intermodel spread in the global-mean precipitation response on different timescales

In this section we address the causes of intermodel spread in the precipitation response on different timescales whereas the previous sections investigated the degree of difference among models in the slope of precipitation change with surface temperature change. As we have shown that the intermodel spread in the slope ( $\eta$ ) corresponds to the smallest estimate of spread in the literature, one might think that global-mean precipitation predictions from models would converge towards the same value. Nevertheless, the global-mean equilibrium precipitation response to an abrupt  $4\times\text{CO}_2$  forcing – hereafter Equilibrium Hydrological Sensitivity at  $4\times\text{CO}_2$  (EHS<sub>4×</sub>) – exhibits a factor of 3 spread among CMIP5 models, even though  $\eta$  has a twofold smaller factor of spread (1.5) in the same experiment (Section 2.3).

Which factors, then, determine the larger spread in EHS<sub>4×</sub>? Assuming that  $\Delta P$  linearly increases with  $\Delta T_s$ , the spread in EHS<sub>4×</sub> is affected by the spread in Equilibrium Climate Sensitivity for a quadrupling of CO<sub>2</sub> (ECS<sub>4×</sub>), the hydrological sensitivity parameter and the adjustment (Figure 2.4a).

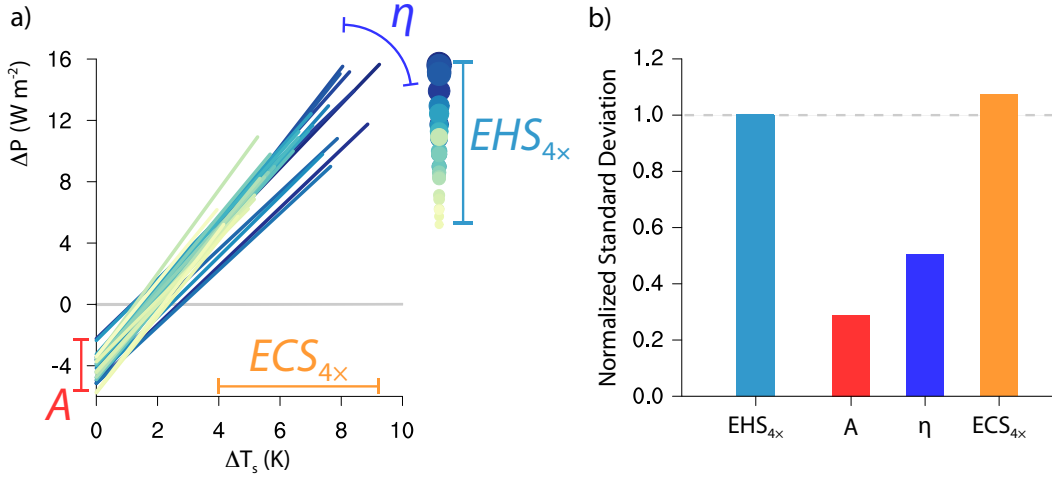


**Figure 2.4:** a) Adjustment ( $A$ ), hydrological sensitivity parameter ( $\eta$ ), and Equilibrium Climate Sensitivity for a quadrupling of  $\text{CO}_2$  ( $\text{ECS}_{4\times}$ ) in the 28 abrupt4xCO2 models. Dots denote the Equilibrium Hydrological Sensitivity for a quadrupling of  $\text{CO}_2$  ( $\text{EHS}_{4\times}$ ), where dot size increases for larger  $\text{EHS}_{4\times}$ . Colors darken for increasing  $\text{ECS}_{4\times}$ . b) Contributions to spread in  $\text{EHS}_{4\times}$  from  $A$ ,  $\eta$  and  $\text{ECS}_{4\times}$ ; estimated via Eq. 2.1, by setting 2 of the three factors to their corresponding ensemble-mean values. The standard deviations of  $\Delta P$  due to variation of the free factors are normalized by the actual standard deviation in equilibrium  $\Delta P$ . Note that normalized standard deviations do not add to unity.

At equilibrium, it is the spread in  $\text{ECS}_{4\times}$  which primarily impacts the large range of  $\text{EHS}_{4\times}$  (Figure 2.4b). Here the respective standard deviations  $\sigma_i$ , with  $i$  being  $A$ ,  $\eta$  or  $\text{ECS}_{4\times}$ , are normalized by the standard deviation of  $\text{EHS}_{4\times}$ , yielding  $\hat{\sigma}_i$ . When comparing the respective contributions to  $\sum_i \hat{\sigma}_i$ , then  $\text{ECS}_{4\times}$  on its own makes up 57% of the spread, whereas  $A$  and  $\eta$  contribute with only 16 and 27% respectively. Thus,  $\text{ECS}_{4\times}$  conditions the spread of the  $\text{EHS}_{4\times}$ . In fact, if only the spread in  $\text{ECS}_{4\times}$  were to determine the spread in  $\text{EHS}_{4\times}$ , the spread in  $\text{EHS}_{4\times}$  would be slightly larger ( $\hat{\sigma}_{\text{ECS}_{4\times}}=1.07$ ). An anticorrelation between  $\eta$  and  $\text{ECS}_{4\times}$  leads to smaller  $\Delta P$  for models with high surface temperature warming and vice versa; the spread of  $\text{EHS}_{4\times}$  is thus smaller when  $\eta$  and  $A$  can vary than if only  $\text{ECS}_{4\times}$  caused the spread. Our conclusion, that the spread in  $\text{ECS}_{4\times}$  dominates the spread in  $\text{EHS}_{4\times}$  is consistent with other analysis (Thorpe and Andrews, 2014).

The spread in adjustment is important in the early stages of warming, where the spread in adjustment dominates over the influence of differing surface warming among models, with ca. 45% contribution to the sum of  $\hat{\sigma}_i$  (Figure 2.5). The importance of  $\eta$  rises with warming, surpassing the adjustment's contribution to  $\sum_i \hat{\sigma}_i$  after about 20 years. The residual, given as offset between model  $\Delta P$  and that of the regression line following Eq. 2.1, amounts to about 20% in the very beginning but reduces with time. The residual is both due to errors in the prediction and internal variability. Uncertainty due to surface warming only overwhelms the combined effect of  $\hat{\sigma}_\eta + \hat{\sigma}_A$  after year 70 of the abrupt4xCO2 simulation (Figure 2.5).

To understand the spread in precipitation response over all timescales, it is thus necessary to better understand separate sources of spread for equilibrium surface warming,  $\eta$  and  $A$ . All three spread-causing factors are determined by how the energy fluxes of the system change



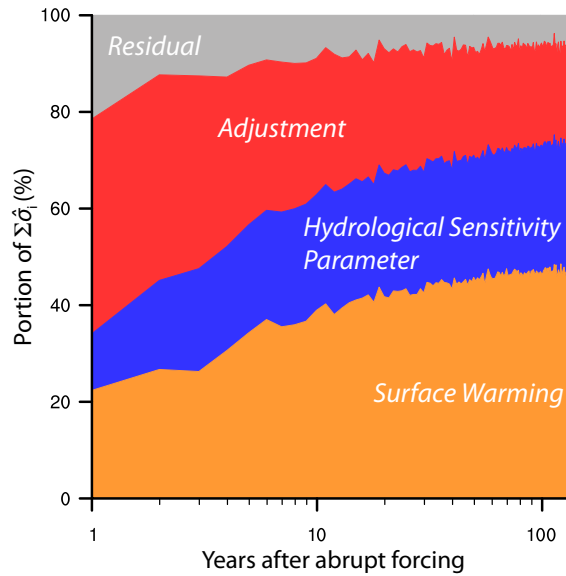


**Figure 2.5:** Contributions of surface warming, hydrological sensitivity parameter, adjustment and residual to the sum of their respective normalized standard deviation ( $\hat{\sigma}_i$ ) as a function of years after the  $4 \times \text{CO}_2$  forcing. Note the logarithmic timescale. The  $\hat{\sigma}_i$  are estimated as in Figure 2.4b but for annual mean standard deviations of  $\Delta P$ . The residual contribution is given by the portion of normalized standard deviation of differences between model and calculated  $\Delta P$  following Eq. 2.1.

in response to the  $\text{CO}_2$  forcing in the abrupt4x $\text{CO}_2$  models. The analysis of spread-causing factors in the energetics of the atmosphere thus serves as a straightforward approach for better understanding the variation in precipitation response.

Since the 1970s when General Circulation Models were first established, extensive effort has been placed on developing a framework for understanding contributions to the spread in ECS (Charney et al., 1979). This framework has made it possible to decompose the temperature response into radiative contributions from climate change feedbacks: temperature, cloud, water vapor and surface albedo feedback. The uncertainty in ECS estimates originates foremost from the uncertainty in simulated cloud feedback (e.g. Cess et al., 1990; Dufresne and Bony, 2008), and in particular in the shortwave component of the low-cloud feedback (e.g. Bony and Dufresne, 2005; Zelinka et al., 2012; Vial et al., 2013). The path towards better constraining the spread in climate sensitivity has thus been comprehensively laid out.

Less attention has been focused on understanding intermodel spread in the slope of precipitation change with surface temperature change and in the rapid adjustment. Previdi (2010), one of the pioneers in this undertaking, diagnosed the radiative impact of changing atmospheric variables on the atmospheric heat budget. In so doing, the respective contributions of these radiative effects could be attributed to  $\eta_a$ . That study, however, was based on an experiment which was simultaneously forced by  $\text{CO}_2$  and aerosols, where the latter has subsequently been found to dominate the intermodel spread in  $\eta_a$  (Pendergrass and Hartmann, 2012). O’Gorman et al. (2012), extending the analysis of Previdi (2010) for the same experiment, emphasized that different changes of clouds in the models cause larger intermodel scatter than lapse-rate plus water vapor changes. Using a different methodology,

Pendergrass and Hartmann (2014) found that both clear-sky radiative cooling spread, resulting from differing changes in lapse-rate plus moistening, and cloudy-sky radiative cooling spread contribute to intermodel scatter in  $\eta_a$ .

None of the above studies, however, addressed intermodel spread in  $\eta$  and  $A$  due to radiative effects from changing atmospheric variables, for instance by separating between the fast and temperature-dependent atmospheric heat budget changes resulting from abruptly increased CO<sub>2</sub> levels. This knowledge would seem helpful, though, to gain insight into the sources of spread in precipitation response resulting from the spread in the adjustment and the hydrological sensitivity parameter, especially for early years of warming (Figure 2.5). To this end, we perform radiative decompositions of the spread in  $\eta$  and  $A$  in the abrupt4xCO<sub>2</sub> experiment.

### 2.5.1 Radiative decomposition of the spread in $\eta$ and $A$

We decompose the changes of the atmospheric radiative imbalance ( $\Delta R = \Delta R^{\text{TOA}} - \Delta R^{\text{surface}}$ ) in the abrupt4xCO<sub>2</sub> by the kernel method (Soden et al., 2008). The decomposition is performed such that

$$L_v \Delta P \approx \sum \Delta R_x - \Delta SH, \quad (2.3)$$

with the sensible heat flux  $SH$ , the latent heat of vaporization  $L_v = 2500 \text{ kJ kg}^{-1}$ , and the index  $x$  denotes: contributions from CO<sub>2</sub> plus stratospheric temperature changes (CO<sub>2</sub> + Strat), changes in the tropospheric temperature lapse-rate (LR), changes due to uniform tropospheric warming arising from surface temperature increase (Planck), changes in water vapor (WV), changes in surface albedo, and changes in clouds. The investigation of the decomposed slope from the regression of  $\Delta R_x$  against  $\Delta T_s$  provides information as to sources of spread in the hydrological sensitivity parameter ( $\eta_x$ ), and the  $y$ -intercept of the regression as to sources of spread in the rapid precipitation adjustment ( $A_x$ ).

To isolate  $\Delta R_x$  from changes in the atmospheric heat budget for individual changes in atmospheric state variables ( $\Delta x$ ), we follow the technique described by Previdi (2010), but employ a newer kernel (Block and Mauritsen, 2013) calculated with the MPI-ESM-LR model (Stevens et al., 2013) which is then used for every model in this analysis. The kernels are vertically interpolated to the CMIP5 pressure levels and mass-weighted by the pressure thickness of each vertical layer. Any  $\Delta x$  is derived as a monthly mean deviation in abrupt4xCO<sub>2</sub> from the climatological mean of all available piControl months in the given model, preserving the monthly, regional and vertical structure. Afterwards  $\Delta x$  is interpolated to the same horizontal resolution as the applied kernel (Gaussian grid with T63) before performing the radiative decomposition. We choose to interpolate the model variables to the kernel grid, because the temperature and water vapor kernels have sharp gradients in orographic areas, where grid points below the surface are defined as missing values. Interpolation of fields with stronger gradients introduces more errors. Detailed information about the MPI-ESM-LR kernels is given in Block and Mauritsen (2013).

We illustrate the practicalities of our calculations by the example of the lapse-rate component of the hydrological sensitivity parameter (see Previdi (2010) for more details on the kernel method applied to the atmospheric heat budget). The lapse-rate change ( $\Delta LR$ ) is defined as the change in deviation of tropospheric temperature from a uniform tropospheric warming equal to the change in surface temperature. The change in atmospheric radiative fluxes due to a lapse rate change ( $\Delta R_{LR}$ ) is then given by the vertical integral from the surface to the tropopause  $\Delta R_{LR} \approx \int_{p_s}^{p_t} k_T \cdot \Delta LR dp$ , where  $p$  denotes pressure and the subscripts  $s$  and  $t$  surface and tropopause. The temperature kernel ( $k_T$ ) is the change of atmospheric radiative fluxes due to a unit temperature change at a given grid point and vertical level. Deducing from  $k_T$  (Figure S1), a temperature increase by 1 K leads to increases of atmospheric cooling at any vertical level, but this effect is stronger in the lower troposphere. Similarly to Soden et al. (2008), the tropopause is approximated to be at 100 hPa in the tropics (30°N to 30°S) and linearly drops in height with increasing latitude towards 300 hPa at the poles. The stratospheric temperature changes are considered in the  $x = CO_2 + \text{Strat}$  term, where the contributions are first calculated separately using a  $CO_2$  kernel and by multiplying stratospheric temperature changes with the temperature kernel before summing both terms.

Then  $\eta_{LR}$  arises from the slope found by ordinary least squares regression of annual global-mean  $\Delta R_{LR}$  vs.  $\Delta T_s$ ; the  $y$ -intercept gives  $A_{LR}$ . Almost all abrupt4xCO2 models from Table 2.2 are included in the following results, except FGOALS-g2 and CSIRO-Mk3-6-0 as they did not provide all necessary variables for this analysis. Signs are chosen in terms of atmospheric heating; negative contributions lead to stronger cooling which is balanced by increases in  $\eta$  or a less strong adjustment. The other  $\eta_x$  and  $A_x$  are estimated with the standard kernel technique, but for atmospheric radiative convergence instead of TOA radiative fluxes.

### 2.5.2 Spread in the hydrological sensitivity parameter

Intermodel spread of atmospheric heating changes with warming in the abrupt4xCO2 experiment is dominated by large absolute and interquartile ranges of lapse-rate and cloud-induced radiative changes with warming (Figure 2.6a), whereas models agree well on the magnitude of radiative contributions coming from surface albedo changes, Planck effect, water vapor and sensible heat flux changes.

To better assess the spread due to changes in the thermodynamic structure of the troposphere, contributions to  $\Delta P$  from lapse-rate and water vapor changes are considered together ( $\eta_{LR+WV}$ ), as the water vapor concentration increases with temperature approximately following the Clausius-Clapeyron equation (e.g. Trenberth et al., 2005; Held and Soden, 2006). The separation of  $\eta_{LR+WV}$  into three vertical layers reveals that models disagree most in the lower tropospheric changes (Figure 2.6b). Although intermodel spreads of  $\eta_{LR}$  and  $\eta_{WV}$  in the middle and upper troposphere are individually as large or even larger than in the lower troposphere (not shown), they cancel almost perfectly in the middle and upper troposphere because  $\eta_{LR}$  and  $\eta_{WV}$  are anti-correlated (with  $r = -0.89$  and  $r = -0.92$ ). In the lower troposphere, however,  $\eta_{LR}$  and  $\eta_{WV}$  correlate positively ( $r = 0.61$ ). The opposite correlation between the lower and upper troposphere can be understood by considering how increases in

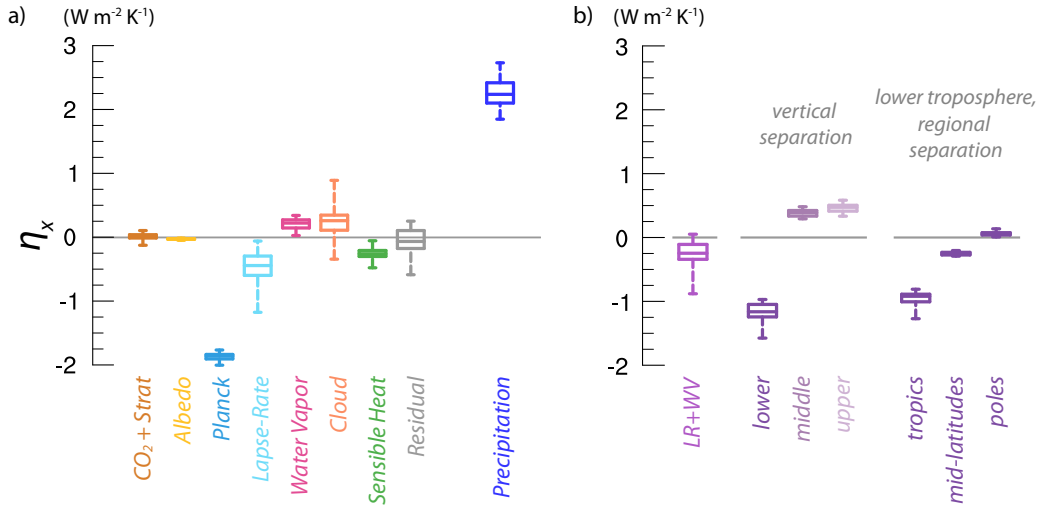


**Figure 2.6:** a) Decomposition of the hydrological sensitivity parameter ( $\eta$ ) for 26 abrupt4xCO2 models. Box-whisker-plots show the minimum and maximum as the whiskers; the box shows the 1st quartile, the median and the 3rd quartile as horizontal lines. The residual is the difference between model  $\Delta R/\Delta T_s$  and  $\sum_x \eta_x$ . b) Vertical separation of  $\eta_{\text{LR+WV}}$  into the lower (pressure  $p > 700$  hPa), middle ( $700 \text{ hPa} \geq p > 400$  hPa) and upper ( $400 \text{ hPa} \geq p \geq 100$  hPa) troposphere. The lower tropospheric  $\eta_{\text{LR+WV}}$  is further separated into regions and shown here for the tropics (equatorward of  $\pm 30^\circ$ ), the mid-latitudes ( $\pm 30^\circ$  to  $\pm 60^\circ$ ) and the poles (poleward of  $\pm 60^\circ$ ). For any separation, first  $\Delta R_x$  is vertically integrated at each grid point and month, then if applicable, regionally averaged and last regressed against global annual-mean  $\Delta T_s$ .

water vapor and temperature modify the radiative budget at the surface and TOA (Pendergrass and Hartmann, 2014). In the upper troposphere, increases of water vapor lead to less radiative cooling at the TOA, while increased surface temperatures lead to more cooling; the uncertainties cancel approximately. Increased water vapor and temperature in the lower troposphere both lead to more cooling of the atmosphere to the surface; hence uncertainties due to the models' lower tropospheric temperature and humidity structure amplify the lower tropospheric spread in  $\eta_{\text{LR+WV}}$ . Further separation of the lower tropospheric changes into three regions – tropics, mid-latitudes, and poles – indicates that the spread in the lower troposphere mainly emerges from differing model responses of the lower tropospheric structure in tropical areas (Figure 2.6b).

That intermodel spread does not reduce strongly by summing up lapse-rate and water vapor changes may appear surprising as these are usually thought to offset each other to a large degree (e.g. Bony et al., 2006). This thought, however, arises from considering how lapse-rate and water vapor changes affect the TOA fluxes and not the surface. For the spread of  $\eta_{\text{LR+WV}}$  and  $\eta_{\text{LR}}$  to be commensurate (Figure 2.6), this implies that the spread originates in the surface contribution to the atmospheric heating. Our results agree well with Pendergrass and Hartmann (2014) who also conclude that the radiative effects of lapse-rate and water vapor changes do not compensate each other in the atmosphere. These results differ, however, from the findings of O’Gorman et al. (2012) who report a smaller intermodel spread in  $\eta_{\text{LR+WV}}$  than in the respective  $\eta_{\text{LR}}$  or  $\eta_{\text{WV}}$ .

In terms of precipitation magnitude, warming of the troposphere (with medians of  $\eta_{\text{Planck}} = -1.86 \text{ W m}^{-2} \text{ K}^{-1}$  and  $\eta_{\text{LR}} = -0.44 \text{ W m}^{-2} \text{ K}^{-1}$ ) is the single most important determinant for the increase in precipitation with surface warming ( $\eta = 2.24 \text{ W m}^{-2} \text{ K}^{-1}$ ) by increasing the longwave atmospheric cooling on a global-mean basis (Figure 2.6a). A less important source of precipitation increase is the sensible heat flux ( $\eta_{\text{SH}} = -0.26 \text{ W m}^{-2} \text{ K}^{-1}$ ); the magnitude of the sensible heat flux decreases with warming in all models, which must be offset by more precipitation. The precipitation increase is dampened by changes in water vapor ( $\eta_{\text{WV}} = 0.22 \text{ W m}^{-2} \text{ K}^{-1}$ ) and clouds ( $\eta_{\text{Cloud}} = 0.26 \text{ W m}^{-2} \text{ K}^{-1}$ ) in most models. Although increases of water vapor concentration enhance the longwave cooling of the atmosphere ( $\eta_{\text{WV, LW}} = -0.66 \text{ W m}^{-2} \text{ K}^{-1}$ ), this cooling is overcompensated by the additional absorption of shortwave radiation by the water vapor ( $\eta_{\text{WV, SW}} = 0.87 \text{ W m}^{-2} \text{ K}^{-1}$ ). Contrary to our study, Previdi (2010) and O’Gorman et al. (2012) find that  $\eta_{\text{WV, LW}} > 0$ , although both studies use a very similar methodology to ours. Qualitative comparison suggests that probably the opposing results are caused by differences in the longwave water vapor kernel (see the discussion of Figure A1 in Appendix A.1), particularly in the lower troposphere. However, our calculations concerning  $\eta_{\text{WV, LW}}$  are in line with the findings of other studies (Mitchell et al., 1987; Pendergrass and Hartmann, 2014).

Noteworthy challenges remain in better separating contributions of radiative effects on  $\eta$  with the kernel method, as there exists a considerable spread in the residual between  $\sum_x \Delta R_x$  and the model atmospheric heat budget change (Figure 2.6a). Because only one set of kernels derived from a single model in a preindustrial state was employed to perform the decomposition in the individual models, a residual may reflect differences in host model treatments of radiative transfer particularly in the shortwave spectrum (Takahashi, 2009; Pendergrass and Hartmann, 2014). Though more shortcomings of the kernel method exist, a better method that addresses these issues and is as computationally and practically feasible has yet to be developed.

Presenting the residual of the kernel decomposition is important for validating the kernel calculations and to gain confidence in the results. We test whether the scatter of the residual arises from systematic offsets in any of the  $\eta_x$ . No single  $\eta_x$  is responsible for the residual, as the correlation coefficients between the residual and the individual  $\eta_x$  are small ( $|r| \leq 0.26$ ). The spread in the residual can thus be understood as a combined effect of small errors arising from each of the  $\eta_x$ . As such, the spread in the residual does not contradict the main result that models disagree most concerning how their cloud and lower tropical tropospheric temperature and moisture structure changes affect the atmospheric heat budget changes.

The lower tropospheric warming response and its impact on the surface energy budget thus is crucial to better understand how the atmospheric heat budget and therefore precipitation will change on slow timescales. Moreover, this understanding seems to also be important to interpret the offset in ensemble-mean  $\eta$  between the coupled and noncoupled simulations (Section 2.6).

### 2.5.3 Spread in the adjustment

Better understanding of the precipitation adjustments  $A$  has received less attention than  $\eta$ . Recently Richardson et al. (2016) have explored regional precipitation adjustments to different forcing agents, where precipitation increases rapidly over land in the tropics but reduces over land in the mid-latitudes and over the ocean in response to increased  $\text{CO}_2$ . Here we investigate how the global precipitation adjustment is composed of the separate contributions from the typical factors considered in kernel analyses of radiative effects.

It is straightforward to employ the kernel method to attain these contributions to fast changes of the atmospheric energy budget. Here the radiative contributions to the adjustment are given by the  $y$ -intercept of the regression. Global-mean precipitation initially decreases (with a median of  $A = -4.26 \text{ W m}^{-2}$ ) when  $\text{CO}_2$  increases. This precipitation decrease is sustained by the combined radiative heating of  $\text{CO}_2$  and the fast cooling of the stratosphere ( $A_{\text{CO}_2+\text{Strat}} = 3.67 \text{ W m}^{-2}$ ) which induces additional atmospheric heating (Figure 2.7).

The decomposition shows that precipitation adjustments are not influenced by the surface albedo or by the Planck effect (medians of  $A_{\text{Albedo}} = 0.01 \text{ W m}^{-2}$  and  $A_{\text{Planck}} = 0.01 \text{ W m}^{-2}$ ), nor does water vapor have a discernible effect ( $A_{\text{WV}} = 0.13 \text{ W m}^{-2}$ ). The only other term systematically influencing the fast changes of the atmospheric heat budget appears to be the lapse-rate adjustment ( $A_{\text{LR}} = -1.34 \text{ W m}^{-2}$ ). The lapse-rate adjustment influences the hydrological cycle through stabilizing the atmosphere (Kamae et al., 2015). The stabilization of the atmosphere with higher  $\text{CO}_2$  levels increases atmospheric cooling and thus counteracts the direct effect of  $\text{CO}_2$  on the precipitation adjustment. Our analysis reveals a considerable intermodel spread in the lapse-rate and cloud adjustment.

It is somewhat discouraging that not only does the residual exhibit a large spread, but the residual is also large with a median of  $2.50 \text{ W m}^{-2}$ . The reason for this offset in the

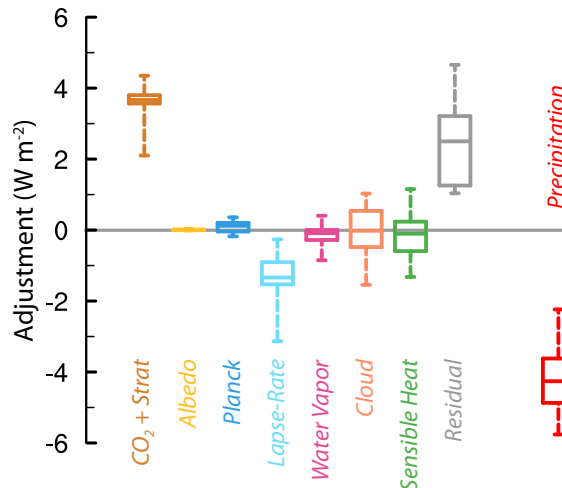


**Figure 2.7:** Decomposition of the atmospheric heat budget adjustment derived from 26 models performing the abrupt4x $\text{CO}_2$  experiment. More details are provided in the caption of Figure 2.6.

radiative decomposition of the adjustment is difficult to trace down; we tested for two possible errors arising from estimating the adjustment via the regression method. Residuals in the adjustment may result from non-linearities in any of the  $\Delta R_x$  with  $\Delta T_s$ , or from the fact that the regression-based adjustment does not capture internal variability. However, neither of these two possible errors can account for the offset in the adjustment residual from the radiative decomposition (see detailed discussion in the Appendix A.2 including  $A_x$  estimated with the fixed-SST method).

Studies investigating the CO<sub>2</sub> plant physiological effect find differing (about a factor of 4) estimates of rapid precipitation reduction over land due to reduced transpiration in two models (Abe et al. (2015) find ca.  $-0.75 \text{ W m}^{-2}$  in MIROC3 and Andrews et al. (2011) ca.  $-2.89 \text{ W m}^{-2}$  in HadCM3), which may also be a source for intermodel spread of  $A_x$  and  $A_{\text{SH}}$ . The kernel decomposition cannot identify the role of plant physiological effects in the intermodel spread in adjustment; this deficiency cannot explain the residual, however, because the radiative fluxes have to balance with or without a plant physiological effect.

Notwithstanding the difficulties in attributing the residual, the sensible heat flux is unaffected by the radiative decomposition, evolves quite linearly with  $\Delta T_s$ , and its adjustment is consistently diagnosed with both calculation methods (Figure A2, lower left panel). Half of the models predict that the sensible heat flux increases on fast timescales, while the other half predicts the opposite (Figure 2.7). Considering that the spread in sensible heat flux adjustment correlates strongly with the spread in fast precipitation adjustment ( $r=0.76$ ), for future work it would be useful to improve understanding of fast sensible heat flux changes to get a deeper insight in fast precipitation changes.

In summary, to represent precipitation changes on fast timescales more consistently among models, more understanding about the spread in fast adjustment to a CO<sub>2</sub> forcing is required. In particular, our results have shown that more attention is needed to better separate radiative contributions to the adjustment from vertical temperature structure changes and sensible heat flux changes immediately after CO<sub>2</sub> levels have been raised.

## 2.6 Hydrological sensitivity parameter in coupled versus noncoupled experiments

The magnitude of the estimated hydrological sensitivity parameter ( $\eta$ ) between coupled ocean-atmosphere and noncoupled atmosphere-only models differs surprisingly by ca. 12-30% (Section 2.3), although intermodel spread in  $\eta$  is similarly small (dispersion of 10.7% and 9.3%) for the coupled abrupt4xCO<sub>2</sub> experiment and for the noncoupled amip4K experiment. As a first assumption we expected the same magnitude of  $\eta$  in both the coupled and noncoupled experiment. If  $\eta$  is a consistent descriptive quantity of the climate system, constrained by the atmospheric heat budget,  $\eta$  should be of the same magnitude independent of the model configuration. Although the noncoupled amip experiments do not account for changes in ocean temperatures in response to surface flux imbalances, they have the advantage of being driven by observed sea-surface temperature distributions and thus more

adequately represent the pattern of precipitation. Here we discuss possible reasons for a larger  $\eta$  in the noncoupled model configuration.

Differing magnitudes in  $\eta$  can easily be achieved by employing either the endpoint or regression method (Table 2.3). This reasoning does not apply here because the hydrological sensitivity parameter is concisely defined as the slope of precipitation change with surface temperature change when accounting for the fast precipitation adjustment. The expectation of similar multi-model mean  $\eta$  in different experiments relies on the assumption, though, that the atmospheric heat budgets will change in the same way with warming. In the following we test several hypotheses why the atmospheric radiative cooling may increase more strongly in the noncoupled models.

The warming patterns differ between the coupled and the amip4K experiments. The coupled abrupt4xCO2 experiment exhibits stronger polar than tropical warming, whereas the sea-surface in amip4K per definition warms globally uniformly. We test for the influence of warming patterns by estimating  $\eta$  in patterned warming AMIP experiments (amipFuture), which are scaled to also warm by 4 K in the global-mean. Analysis is performed for a subset of eight available amip4K and amipFuture models. If patterned warming was responsible for the greater  $\eta$  in amip4K than in abrupt4xCO2, then  $\eta$  would have to be smaller in amipFuture. This is, however, not the case as in seven of eight models  $\eta$  is even slightly larger (not shown). Patterned warming is thus not the reason for higher mean  $\eta$  in the noncoupled model configuration.

The hydrological sensitivity parameter may be lower in a higher CO<sub>2</sub> loading world (Good et al., 2012). Is the lower CO<sub>2</sub> concentration in amip4K causing the higher  $\eta$ ? We address this suggestion by performing AMIP and AMIP+4K at 4×CO<sub>2</sub> concentrations in the ECHAM6 model (Stevens et al., 2013). Indeed, we find that  $\eta$  is smaller by 6% compared to the corresponding ECHAM amip4K experiment at 1×CO<sub>2</sub> concentration (2.63 W m<sup>-2</sup> K<sup>-1</sup> vs. 2.79 W m<sup>-2</sup> K<sup>-1</sup>). This finding, however, accounts for less than a third of the difference in  $\eta$  between the coupled (2.15 W m<sup>-2</sup> K<sup>-1</sup>) and noncoupled (2.74 W m<sup>-2</sup> K<sup>-1</sup>) MPI-ESM-LR model.

Finally, we investigate how the atmospheric heat budget is influenced by differently changing state variables like temperature, humidity or clouds between the coupled and noncoupled models. For this, we perform the same kernel methodology as in Section 2.5.2 to the time-mean differences of amip4K and amipFuture respectively. Only six models are included in this analysis, as not all necessary variables were available for BCC-CSM1-1 and IPSL-CM5B-LR.

The greatest offset between coupled and noncoupled models is found in how the thermodynamic structure changes (Figure 2.8). A systematic difference in radiative impact of cloud changes between coupled and noncoupled experiments is apparent, but this difference actually counteracts the signal of higher  $\eta$  in noncoupled models. The offset in changes in the thermodynamic structure is again dominated by the lower troposphere (pressure  $p > 700$  hPa), as it warms more strongly in the noncoupled experiments (not shown). A stronger warming implies enhanced atmospheric cooling, and thus a larger hydrological sensitivity parameter. It is as of yet unclear how coupling leads to weaker warming in the lower troposphere in abrupt4xCO2. Possibly different land-sea contrasts or the fact that the surface



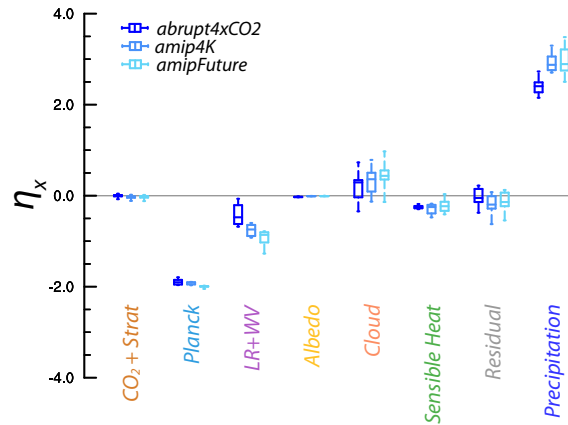


**Figure 2.8:** Comparison of the decomposed hydrological sensitivity parameter ( $\eta$ ) between coupled (abrupt4xCO2) and noncoupled (amip4K & amipFuture) experiments. Analysis is performed analogously to Figure 2.6a, but for a common set of 8 available coupled and noncoupled models.

temperature cannot respond to precipitation in the noncoupled experiments could offset  $\eta$ . In any case, the budget analysis suggests that quantifying the effect of coupling on the lower tropospheric thermodynamic structure may provide insights to how precipitation is simulated to change with warming.

Considering that coupling varies the mean values of  $\eta$  by 12-30 %, it is questionable whether models fully represent the whole scope of the real world hydrological sensitivity parameter. Although the intermodel spread of  $\eta$  is small for either the coupled or the noncoupled experiments, the model configuration dictates with which magnitude the atmospheric heat budget adapts to surface warming.

## 2.7 Conclusions

The majority of previous literature states that models disagree about the slope of precipitation change with respect to surface temperature change with up to a factor of three difference between the lowest and highest estimate (Held and Soden, 2006; Previdi, 2010; O’Gorman et al., 2012). However, the very definition of the slope varies among the studies. To facilitate the comparison of estimates, we introduce a more formal terminology analogous to that of the equilibrium climate sensitivity framework. The slope of temperature-dependent precipitation change, when accounting for rapid precipitation changes (adjustment) of the atmosphere to radiative forcings, is referred to as “hydrological sensitivity parameter” ( $\eta$ ) and the slope of total precipitation response to surface warming as “apparent hydrological sensitivity parameter” ( $\eta_a$ ). The word “apparent” encompasses that  $\eta_a$  depends on atmospheric forcing and surface warming. We introduce the term “equilibrium hydrological sensitivity” as the equilibrium change of precipitation due to a doubling of CO<sub>2</sub>.

We compare the intermodel spread and magnitude of  $\eta$  and  $\eta_a$  in four different forcing experiments among current CMIP5 models. We show that intermodel spread in  $\eta$  is

small in the abrupt4xCO2 experiment relative to most previous work. Our estimate of  $\eta=2.24 \pm 0.24 \text{ W m}^{-2} \text{ K}^{-1}$ , with a total range of 1.85-2.73  $\text{W m}^{-2} \text{ K}^{-1}$  correspond to the estimates in Andrews et al. (2009). The spread is larger in part of the other studies because for the definition of  $\eta_a$  the spread in the adjustment projects onto that of the temperature-dependent precipitation response (Held and Soden, 2006; Previdi, 2010; Pendergrass and Hartmann, 2014). In other studies (Takahashi (2009); Lambert and Allen (2009); Frieler et al. (2011)) the multi-regression approach to estimate  $\eta$  from transient experiments yielded larger spread than the direct calculation from idealized steplike climate change experiments as in this study. We further demonstrate that  $\eta$  and  $A$  estimated from the idealized abrupt4xCO2 experiment reproduce the simulated precipitation in the transient 1pctCO2 simulation well.

The comparison of the similarly idealized coupled ocean-atmosphere abrupt4xCO2 and the noncoupled atmosphere-only amip4K simulations reveals that the experimental configuration modifies the magnitude of  $\eta$ . In both configurations the atmospheric heat budget changes robustly. However, the choice, whether or not the atmosphere is coupled to the ocean, offsets the magnitude of  $\eta$  estimates by 12-30% towards higher  $\eta$  in the noncoupled amip4K. This offset suggests that the intermodel spread for a given climate change experiment may underestimate the real model spread of the hydrological sensitivity parameter arising from different experiment configurations. To put this in perspective, the difference in multi-model mean  $\eta$  between the amip4K and abrupt4xCO2 experiments is nearly as large as the intermodel spread within one of the experiments.

Although the hydrological sensitivity parameter is more robust than assumed from a literature review, the simulated global-mean precipitation response at the end of the abrupt4xCO2 simulation remains uncertain. In equilibrium conditions we attribute this spread in equilibrium hydrological sensitivity due to a quadrupling of CO<sub>2</sub> foremost to the uncertainty in the corresponding equilibrium climate sensitivity. In contrast, in the first half of the simulation ( $\sim 70$  years) the largest contributor to the spread is uncertainty in the adjustment, followed by the uncertainty in the hydrological sensitivity parameter.

We perform a radiative decomposition of the atmospheric heat budget changes via the kernel method to attribute how radiative effects influence the hydrological sensitivity parameter and the adjustment. The spread in  $\eta$  mainly arises from the spread in cloud radiative effects and lapse-rate plus water vapor. The spread in lapse-rate and water vapor radiative effects across the model ensemble can be attributed to different lower tropospheric temperature and water vapor changes, foremost in the tropics. In terms of spread in the adjustment, a non-negligible residual from the decomposition hinders a firm conclusion. The analysis reveals, however, that the spread in the fast response of the sensible heat flux, where half of the models reduce and half increase the sensible heat flux on fast timescales, may be a strong suspect for causing uncertain fast precipitation changes.

---

## 3 Impact of ACRE on the intermodel spread in tropical precipitation

### 3.1 Introduction

State-of-the art general circulation models disagree about the projected changes in regional precipitation with warming, especially in the tropics (Xie et al., 2015). The ability to consistently project regional precipitation change has not improved between the earlier phase 3 of the Coupled Model Intercomparison Project (CMIP) and the newer model generations of phase 5 (Knutti and Sedláček, 2013). This chapter will explore possible reasons for the intermodel spread in tropical precipitation patterns and their changes. Particularly we investigate the influence of atmospheric cloud radiative effects on the intermodel spread in precipitation in idealized aquaplanet simulations.

The intermodel spread in tropical precipitation change is linked to uncertainty in how the tropical circulation will change with warming (e.g. Shepherd, 2014; Xie et al., 2015). The tropical circulation, in turn, depends on the interaction between surface fluxes, atmospheric radiation, and moist convective processes. Whereas uncertainty in precipitation predictions may also arise from scenario uncertainty and internal variability, the model uncertainty dominates the difficulty in predicting precipitation (Hawkins and Sutton, 2011). Models differ e.g. in the formulation of their dynamical cores, in the parameterization of sub-scale processes such as moist convection, clouds, land surface, treatment of sea ice and vegetation, horizontal and vertical resolution and many other factors. Even when the model configuration is simplified to only compare models in aquaplanet configuration with fixed sea surface temperatures (SSTs) – thus removing e.g. intermodel differences in SST patterns, land-sea contrasts, atmosphere-vegetation interactions, and ocean circulations – the tropical precipitation change to a uniform warming by 4 K diverges strongly among models (Stevens and Bony, 2013). In some models the band associated with the strongest tropical precipitation, the intertropical convergence zone (ITCZ), contracts towards the equator; in others it shifts polewards. The response of cloud radiative effects is just as diverse among models, resembling the precipitation changes.

Many studies have identified the importance of cloud radiative effects on the tropical circulation (e.g. Ramanathan, 1987; Slingo and Slingo, 1988; Slingo and Slingo, 1991; Randall et al., 1989; Sherwood et al., 1994; Bergman and Hendon, 2000; Fermepin and Bony, 2014; Li et al., 2015). One possibility by which clouds impact the circulation is by modulating the spatiotemporal pattern of atmospheric diabatic heating of the atmosphere. Different cloud types induce different atmospheric cloud radiative effects (ACREs), which are determined by the difference in cloud radiative effects between the top of the atmosphere (TOA) and

the surface. Deep clouds found in the tropical convergence zones exert a heating on the atmosphere, and low clouds found primarily over low SST regions induce a diabatic cooling, especially in the lower troposphere (Tian and Ramanathan, 2002).

Cloud radiative effects have long been known to be the root cause for intermodel spread in the temperature response to a doubling of the atmospheric  $\text{CO}_2$  concentration (e.g. Cess et al., 1990; Bony and Dufresne, 2005; Vial et al., 2013), the equilibrium climate sensitivity (ECS). Lately, ACREs have been hypothesized to also constitute the root cause for intermodel spread in the precipitation response to surface warming (e.g. Voigt et al., 2014; Voigt and Shaw, 2015). Voigt and Shaw (2015) focus on the two CMIP5 aquaplanet models (MPI-ESM-LR and IPSL-CM5A-LR) showing the most diverse tropical precipitation change with warming. Whereas the intertropical convergence zone (ITCZ) contracts in the MPI model such that precipitation increases strongly at the equator and decreases in the remaining tropics, the IPSL model weakly enhances precipitation in the entire tropics (Figure 3.1, top row). Voigt and Shaw (2015) employ the feedback locking technique (e.g. Mauritsen et al., 2013) that allows decomposing the circulation response with warming between the radiative effects of changing SSTs, clouds and water vapor. They conclude that the circulation response to warming – and with that the precipitation response – is most strongly shaped by how the cloud radiative heating changes with warming. Upon closer inspection of their results, however, the precipitation response to uniformly raising SST by 4 K strongly differs between the two models, explaining about half of the difference in total precipitation response at the equator. This different precipitation response to warming occurs although water vapor and cloud radiative effects are fixed to the control state.

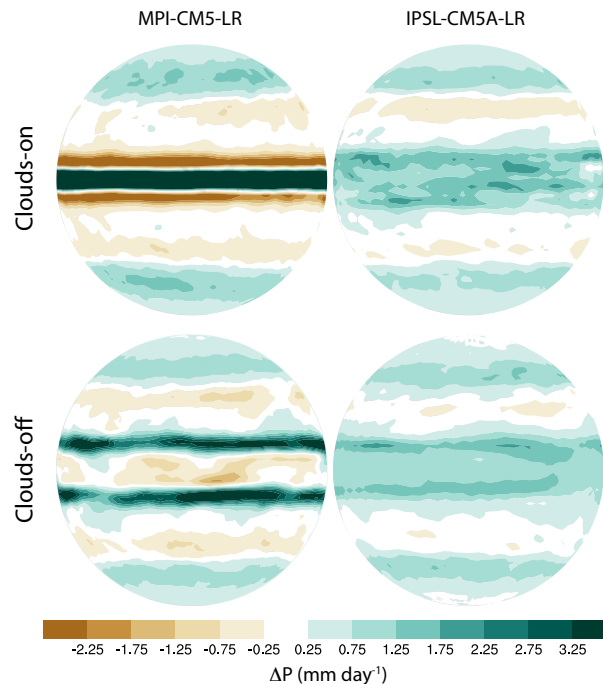


**Figure 3.1:** Precipitation change ( $\Delta P$ ) in response to a 4 K uniform warming for the MPI-CM5-LR and IPSL-CM5A-LR models (left and right column). The response is shown for the clouds-on and clouds-off simulations (top and bottom row).

Is it then possible that the seed of intermodel differences is present in the absence of atmospheric cloud radiative effects, and only gets accentuated by ACREs? This question motivates us to investigate the impact of ACREs on the intermodel spread of variables related to the tropical precipitation and circulation in a larger model ensemble. We will analyze model simulations from the Clouds On-Off Klimate Intercomparison Experiment (Stevens et al., 2012, COOKIE), which provides simulations where the cloud-radiation interaction is inhibited, and simulations where ACREs are active. To investigate our hypothesis, like Voigt and Shaw (2015) we will focus on the aquaplanet configuration as it has been shown to be a useful, idealized testbed for studying processes related to climate change (Medeiros et al., 2015). The atmospheric cloud radiative effect certainly impacts the precipitation change in response to warming SSTs by 4 K, as portrayed by the different response in the clouds-on versus clouds-off simulations (Figure 3.1). But even in the absence of cloud-radiation interaction, the precipitation responds quite differently between the MPI and the IPSL model; with drying between the double ITCZs in MPI-CM5-LR and wettening in the entire tropics in IPSL-CM5-LR.

After describing the COOKIE simulations in more detail (Section 3.2), we will characterize the precipitation and circulation in the COOKIE simulations. In particular we focus on the question whether the seed for intermodel spread in tropical precipitation is present also in the absence of cloud-radiation interaction (Section 3.3). We provide a synthesis of the analysis in Section 3.4.

## 3.2 COOKIE simulations

We investigate simulations from the Clouds On-Off Klimate Intercomparison Experiment (COOKIE; Stevens et al., 2012) in the aquaplanet configuration, which have been performed by six atmospheric general circulation models.

COOKIE consists of two main sets of experiments: 1) the “clouds-on” simulations where clouds interact with the radiation as normal, and 2) the “clouds-off” simulations where clouds are artificially made transparent to radiation by setting their cloud liquid and cloud ice to zero in the calculation of radiative transfer. Note that clouds can still develop in the “clouds-off” experiment – they just do not influence radiation. Besides the different radiative settings, the two sets of experiments are identical. The comparison between both sets of experiments allows assessing how the atmospheric cloud radiative effect (ACRE) impacts the mean state of the models, for example their precipitation patterns and circulation.

To better identify intermodel differences, we limit our analysis to the idealized aquaplanet model configuration. In this configuration, the planet’s surface is assumed to be saturated with a fixed sea surface temperature (SST). The SSTs vary zonally uniformly with latitude following the ‘Qobs’ profile, which is closest to the observed zonal-mean temperature distribution compared to other idealized aquaplanet SST profiles (Neale and Hoskins, 2001). Following ‘Qobs’, the surface temperatures peak at 27 °C at the equator, decline throughout the tropics and mid-latitudes, and are held constant poleward of 60° latitude at 0 °C. Besides the modifications to the calculation of radiative transfer in the clouds-off experiment, the

**Table 3.1:** Aquaplanet COOKIE models used in this study.

Model	Reference
CNRM-CM5	Voldoire et al. (2012)
MPI-CM5-LR <sup>1</sup>	Stevens et al. (2013)
IPSL-CM5A-LR	Dufresne et al. (2013)
MIROC5	Watanabe et al. (2010)
MRI-CGCM3	Yukimoto et al. (2012)
HadGEM2-A	Collins et al. (2011)

<sup>1</sup> Although the COOKIE version of the MPI model is essentially similar to the MPI-ESM-LR used in CMIP5, we refer to it with the name under which it is provided in the COOKIE project.

COOKIE aquaplanet configuration follows that of the aquaplanets in the Coupled Model Intercomparison Project phase 5 (CMIP5). The solar radiation is specified as perpetual equinox conditions, removing the seasonal cycle but the diurnal cycle is retained. Sea ice, orography and aerosols are set to zero.

We analyze aquaplanet simulations with the ‘Qobs’ SST, hereafter referred to as “control”, and simulations where ‘Qobs’ SSTs are uniformly raised by 4 K, hereafter referred to simply as “4K”. Thus four experiments, two warming states and two different specifications of clouds, are available for the investigation of intermodel spread in precipitation patterns and their changes with warming. Six modeling centers performed the COOKIE simulations for both warming states (Table 3.1). All modeling centers were using the model version corresponding to what they used in CMIP5 for the simulations, except for the MPI model. A slightly newer version than in CMIP5 was used (ECHAM6.1.05) with added bug fixes, but the newer version does not influence the mean climate to any significant extent.

Though the surface temperatures should be identical to the ‘Qobs’ profile in all models according to the COOKIE protocol, this is not the case for all models (Figure 3.2). The MRI-CGCM3 model has higher peak SSTs than the remaining models. Especially near the equator, SST gradients are steeper, which complicates the direct comparison to the other models. The differing SST profile arises because a skin sea surface temperature scheme is employed in the MRI model and the ‘Qobs’ profile is used to fix the sub-skin layer temperature. In the MRI model, SSTs thus can vary zonally and are offset from the other models. The IPSL-CM5A-LR model has slightly lower SSTs than ‘Qobs’. However, as the SST gradients are similar to ‘Qobs’, the intermodel comparison should not be hindered. Though the MIROC5 model uses the ‘Qobs’ profile in both clouds-off simulations, a different SST profile is used in the clouds-on simulations (not shown) with steeper SST gradients close to the equator (named ‘Control’ in Neale and Hoskins (2001)). Models tend to place the ITCZ more equatorward when the SST are steeper (Williamson et al., 2013). In MIROC5, assessing the impact of atmospheric cloud radiative effects on climate variables is thus not feasible because differences between the clouds-on and clouds-off simulations might also arise from differing SST profiles. We focus our analysis on the tropics, which are defined as areas equatorward of  $\pm 30^\circ$  latitude.

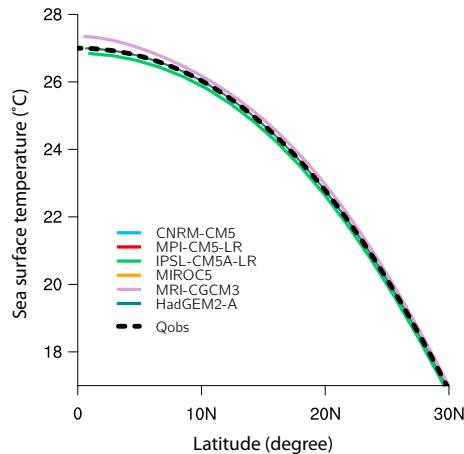


**Figure 3.2:** Sea surface temperature in the control clouds-off simulation in the tropics. The thick dashed line corresponds to the ‘Qobs’ profile.

### 3.3 Precipitation and circulation in COOKIE

In this section we characterize the precipitation and circulation in the COOKIE simulations. In particular, we explore the hypothesis stated in the introduction – that the seed of intermodel spread is present in the absence of cloud radiative effects. For this, we first focus on intermodel spread in tropical mean quantities and subsequently on regional aspects of precipitation and circulation in the clouds-on versus clouds-off simulations. We include circulation quantities in this characterization, because, as discussed in the introduction, the regional tropical precipitation is primarily controlled by the circulation. This point is emphasized by the close intermodel agreement of how the mean precipitation, binned into different circulation regimes, relates to the strength of the vertical mean vertical velocity  $\omega^*$  (Figure 3.3). Strong convection (negative  $\omega^*$ ) leads to strong precipitation, whereas precipitation amounts are independent of the subsidence velocity for  $\omega^*$  approximately greater than  $15 \text{ hPa day}^{-1}$ . This relationship is independent of whether ACREs are active or inactive.

#### 3.3.1 Tropical mean characterization

The absence of ACREs leads to larger tropical mean precipitation ( $P$ ) in all models (Figure 3.4). The tropical mean precipitation scales positively between the clouds-on and clouds-off simulation, such that models with smaller  $P$  in the standard clouds-on configuration tend to have smaller precipitation values also in the absence of ACREs, and vice versa. In terms of intermodel spread, the range between minimum and maximum  $P$  is smaller in the clouds-off ( $0.64 \text{ mm day}^{-1}$ ) than in clouds-on ( $0.91 \text{ mm day}^{-1}$ ) experiment; clouds amplify the intermodel spread. Both higher  $P$ , as well as smaller spread in the clouds-off simulation are also found in the 4K state (not shown). However, the estimated range of  $P$  sensitively relies on the MIROC5 model, in which different SST profiles are specified in the clouds-on and clouds-off configurations. It is unclear whether the larger intermodel spread in the clouds-on

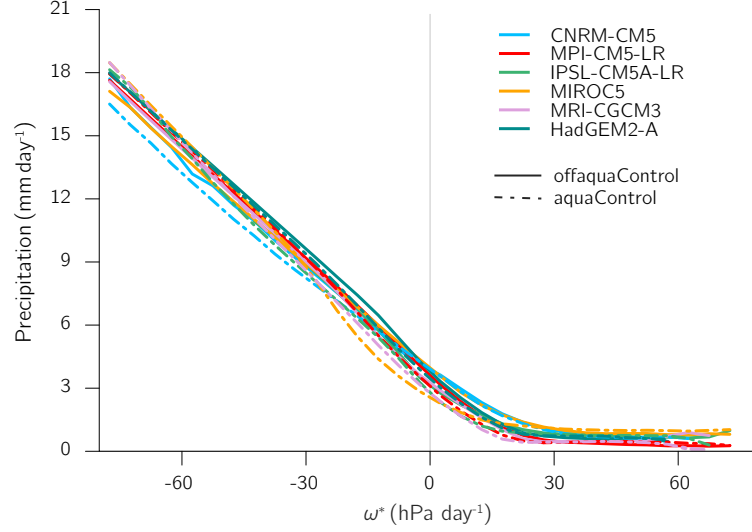


**Figure 3.3:** Relationship of tropical precipitation with the vertical mean vertical velocity ( $\omega^*$ ). The precipitation is averaged in bins of  $\omega^*$  of  $5 \text{ hPa day}^{-1}$ . Negative  $\omega^*$  denote convective regimes, and positive  $\omega^*$  denote subsidence regimes.

configuration arises solely from ACREs or also from the effect of differing SST profiles in MIROC5.

To determine for which reasons the tropical mean precipitation is larger in the absence of ACREs, we explore the atmospheric heat budget. Globally, the cooling by atmospheric radiation ( $R = R^{\text{TOA}} - R^{\text{surface}}$ ) is balanced by latent heating from precipitation ( $L_v P$ ) and the surface sensible heat flux (SH) as discussed in Chapter 2 (Eq. 2.3). For the tropical mean, this budget includes a residual term associated with moisture and heat export out of the tropics

$$0 = R + L_v P + \text{SH} + \text{Residual}, \quad (3.1)$$

with  $L_v = 2500 \text{ kJ kg}^{-1}$  denoting the latent heat of vaporization. The atmospheric radiation can further be separated into the sum of atmospheric clear-sky radiation ( $R_{\text{clr}}$ ) and the ACRE. Positive signs correspond to heating of the atmosphere. Note that three models (MPI-CM5-LR, MIROC5, MRI-CGCM3) diagnose ACRE also in the clouds-off experiment. Nevertheless, the clouds are transparent in the radiative transfer calculations such that ACRE is set to zero in the following analysis.

Differences in the tropical heat budget terms between the clouds-on/off simulations provide insight into reasons for the differing  $P$ . The cloud-radiation interaction makes it rain less in all models in the tropical mean mainly because of atmospheric cloud radiative heating in the control state (Figure 3.5) as well as in 4K (not shown). That ACRE is positive indicates that the heating from deep clouds outweighs the radiative cooling from low clouds. Additionally to the removed heating by clouds in the clouds-off experiment (multi-model mean  $\Delta \text{ACRE} = 16.34 \pm 4.54 \text{ W m}^{-2}$  with the spread being one ensemble standard deviation), the atmosphere is cooled less by clear-sky radiation in the clouds-off case ( $\Delta R_{\text{clr}} = -6.57 \pm 2.90 \text{ W m}^{-2}$ ). The smaller clear-sky radiative cooling in clouds-off is probably associated



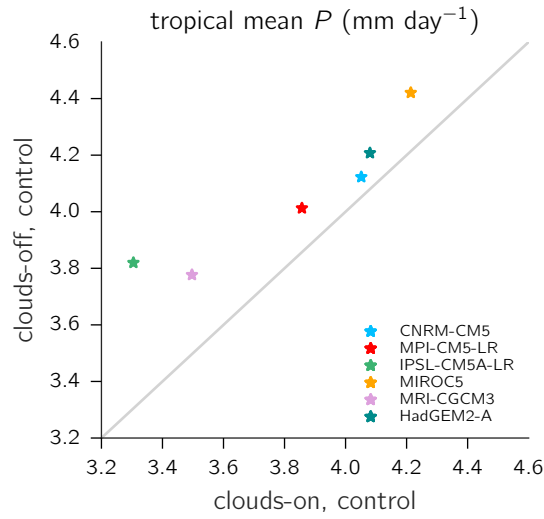


**Figure 3.4:** Comparison of tropical mean precipitation between the clouds-on and clouds-off simulations in the control state.

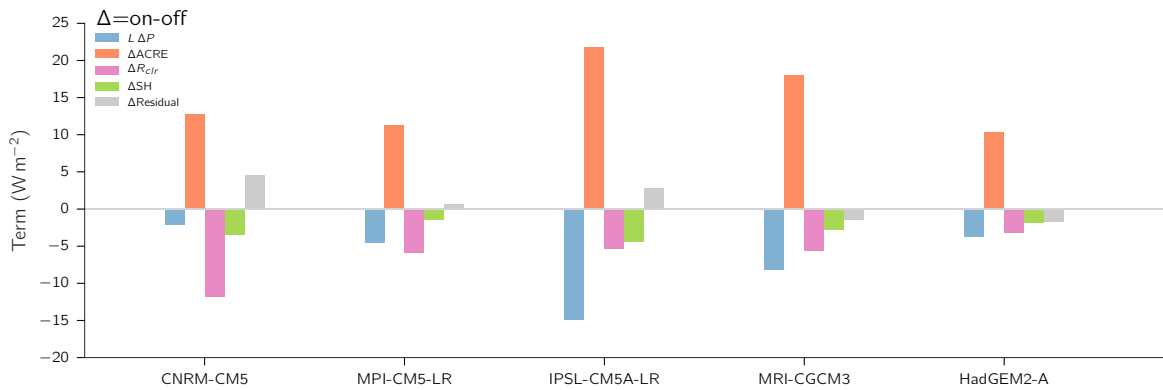


**Figure 3.5:** Change in the tropical atmospheric heat budget terms between the clouds-on and clouds-off simulations ( $\Delta = \text{on-off}$ ) in the control state. MIROC5 is not shown because of strong differences in the underlying SSTs in the clouds-on versus clouds-off simulations.

with reduced atmospheric temperatures and water vapor. The change in ACRE dominates over  $\Delta R_{\text{clr}}$ . This leads to the overall weaker atmospheric radiative cooling in the clouds-on simulations ( $\Delta R = 9.77 \pm 5.26 \text{ W m}^{-2}$ ), which is balanced by reductions in tropical mean precipitation ( $L_v \Delta P = -6.65 \pm 4.57 \text{ W m}^{-2}$ ) and the surface sensible heat flux ( $\Delta \text{SH} = -2.76 \pm 1.08 \text{ W m}^{-2}$ ). The residual change, associated with changes in heat export out of the tropics owing to inhibiting cloud-radiation interaction, is the smallest term in almost all models. Though energy is exported out of the tropics in all models and simulations (not shown), the residual change between the clouds-on and clouds-off simulations shows both signs, indicating a change in energy transport across the tropical border of  $\pm 30^\circ$  or that the change in the tropical border due to a widening or narrowing of the Hadley cell is not captured by our fixed definition of the tropics. The change in precipitation is uncorrelated with the change in residual ( $R^2 = 0.02$ ), but  $L_v \Delta P$  correlates strongly with  $\Delta R$  in both the control and 4K states ( $R^2 = 0.79$ ). The cloud radiative heating is thus the main contributor for weaker tropical mean precipitation in the clouds-on simulations.

Next we explore how the changes in atmospheric cloud radiative effects with warming influence the intermodel spread in the hydrological sensitivity parameter ( $\eta$ ) in the tropics, which is the rate of increase of tropical mean precipitation with tropical mean surface warming (see Section 2.1). Figure 3.6 indicates that the intermodel spread in  $\eta$  is larger in the absence of ACREs ( $1.9 \text{ W m}^{-2} \text{ K}^{-1}$  difference between MIROC5 and HadGEM2-A) than in the control clouds-on configuration ( $1.5 \text{ W m}^{-2} \text{ K}^{-1}$  between IPSL-CM5A-LR and HadGEM2-A). Though again the MIROC5 model strongly determines the intermodel spread and it is unclear whether the previous statement would hold true if the SST profile followed ‘Qobs’ in the clouds-on simulation. Nevertheless, for the remainder of the models, the change in ACREs with warming causes a weaker increase in precipitation with warming than when ACREs are disabled, with the exception of IPSL-CM5A-LR.

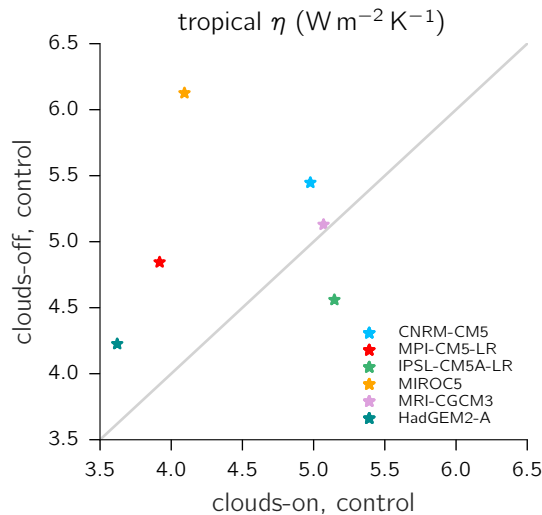


**Figure 3.6:** Comparison of the tropical hydrological sensitivity parameter ( $\eta$ ) between the clouds-on and clouds-off simulations.

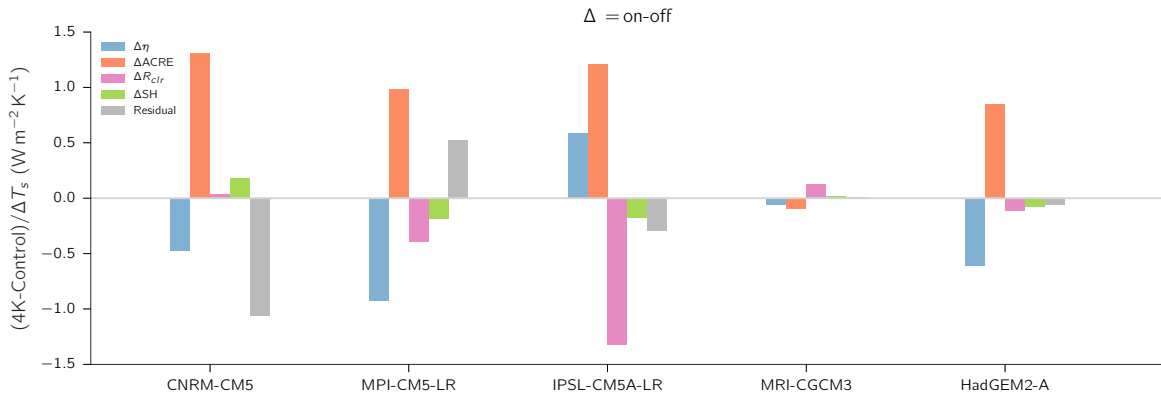


**Figure 3.7:** Comparison of the change in the tropical heat budget with warming between the clouds-on and clouds-off simulations. All terms are normalized by the tropical mean surface temperature change with warming.

Comparing how the different terms in the tropical energy budget change with warming between the clouds-on and clouds-off simulation will give insight into reasons for the generally weaker  $\eta$  in the clouds-on simulation (Figure 3.7). Besides the MRI-CGCM3 model, for which  $\eta$  does not change much between the on/off experiments, the atmospheric cloud radiative effect in the clouds-on simulation changes with tropical warming such that clouds heat the atmosphere more, thus reducing the precipitation increase. The change of the clear-sky radiative cooling with warming is more diverse among models between clouds-on/off simulations.  $\Delta R_{\text{clr}}$  barely differs in CNRM-CM5, MRI-CGCM3 and HadGEM2-A, and reduces in MPI-CM5-LR and IPSL-CM5A-LR when removing ACREs. In fact, for the IPSL model the clear-sky cooling increases more in the clouds-on simulation and even overcompensates the heating effect from the change in ACREs. Because of the greater clear-sky cooling, the hydrological sensitivity parameter can become greater in the clouds-on simulation in the IPSL model (Figure 3.6).

### 3.3.2 Spatial characterization of the tropical precipitation and circulation

Whereas the diabatic cooling by radiation gives a good indication of the latent heating by condensation due to precipitation at large spatial scales (Muller and O’Gorman, 2011), i.e. the entire tropics, at finer scales other processes determine the rate of precipitation and its spatial organization. The most notable feature of precipitation organization in the tropics is the intertropical convergence zone (ITCZ). To investigate how atmospheric cloud radiative effects influence the intermodel spread of tropical precipitation patterns we first focus on the position and strength of the ITCZ. To reduce the dependence on the model’s horizontal resolution, we fit a cubic spline to the zonal-mean precipitation with a latitudinal resolution of  $0.1^\circ$ . The position is defined as the latitude where the zonal-mean precipitation maximizes and the strength of the ITCZ as the precipitation rate at the ITCZ position.

For all models, turning off cloud radiative effects shifts the ITCZ polewards (Figure 3.8a). That cloud radiative effects lead to a more equatorward positioning of the ITCZ in the

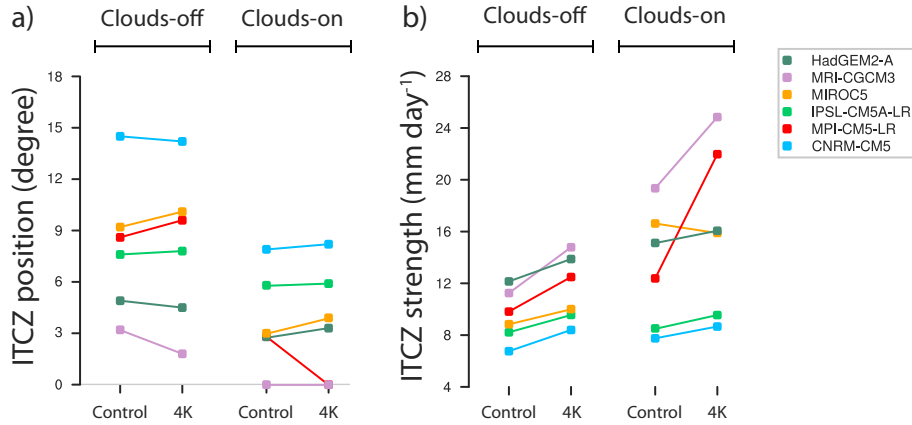


**Figure 3.8:** a) Position and b) strength of the ITCZ in the COOKIE simulations.

control experiment was also recently reported by Harrop and Hartmann (2016) who also analyze the COOKIE simulations. They hypothesize that changes in the atmospheric cloud radiative effects drive changes in the convective available potential energy (CAPE): clouds heat the upper tropical troposphere, thus increasing the tropospheric stability and weakening CAPE; on the other hand CAPE is strengthened by ACRE by increases in boundary layer moisture associated with an increased circulation strength. We will offer a different hypothesis in Section 4.4.2. Also in the 4K experiment, the ITCZ is consistently located more equatorward in the presence of ACREs.

The different positions of the ITCZ among models and between the clouds-on and clouds-off simulations entail a further implication: the temperature structure will differ. In the tropics, the free tropospheric temperature structure is set in the most convective areas, where convective heating makes the temperature profile follow the moist adiabat (Johnson and Xie, 2010). Temperature gradients between convective and subsiding areas are efficiently flattened out by gravity waves such that a weak temperature gradient is a good approximation for the tropics (Sobel et al., 2001). Due to the different ITCZ positions among models and experiments, the convective areas coincide with different surface temperatures, entailing different free tropospheric temperature profiles following the moist adiabat. The tropospheric temperature structure sets the static stability and influences the radiative cooling rate, which in turn affect the strength of subsidence motion and aggregation, as will be discussed later.

In general, the ITCZ positions are more diverse among models in the absence of ACREs (Figure 3.8a) and the ITCZ strength is more similar (Figure 3.8b). In the control clouds-off simulations, the ITCZ position ranges between  $3.2^\circ$  in the MRI model, which can almost be considered a single ITCZ (Möbis and Stevens, 2012), and  $14.5^\circ$  in CNRM-CM5, forming a double ITCZ with the widest extension between precipitation peaks in the northern and southern hemisphere; this extreme poleward position in CNRM-CM5 would correspond to a permanent rain band in the Sahel zone in a realistic geographic configuration. When clouds and radiation can interact, the range in the ITCZ position reduces to  $0^\circ$  also in MRI-CGCM3 and  $7.9^\circ$  in CNRM-CM5. In the IPSL model, ACREs shift the ITCZ equatorwards by  $1.8^\circ$ . Fermepin and Bony (2014, their Figure 5), who analyze COOKIE simulations of the IPSL-

CM5A-LR model where only the planetary boundary layer clouds are made transparent to the radiation scheme, do not find a shift in the ITCZ position. This comparison indicates that at least in the IPSL-CM5A-LR model heating of the upper troposphere by the deep clouds is the main reason for the ITCZ shift. Generally, the shift in the ITCZ position is not related to the strength of atmospheric cloud radiative effects or the ITCZ position in the clouds-on configuration (Harrop and Hartmann, 2016). Contrary to the assertion that ACREs lead to more diverse model behavior (Voigt and Shaw, 2015), the interaction of clouds and radiation leads to more consistent precipitation patterns across models in the case of the ITCZ position.

Changes of cloud radiative effects with warming have been identified as the main contributor for the spread in the tropical precipitation response to warming between the IPSL-CM5A-LR and the MPI model (Voigt and Shaw, 2015): here cloud radiative effects contract the ITCZ equatorwards in the MPI model and widen the ITCZ in the IPSL model. Indeed, the shift in the ITCZ position with warming is diverse among the models in the clouds-on simulations, with equatorwards movement in the MPI model ( $-2.7^\circ$ ) and weaker polewards movement in the remaining models up to  $0.4^\circ$  in HadGEM2-A ( $0.9^\circ$  in MIROC5), or no movement in MRI-CGCM3. With the exception of the MPI model, ACRE changes do not seem to strongly influence the ITCZ position. However, in the absence of ACRE changes with warming, the movement of the ITCZ differs among models. The ITCZ shifts equatorwards in MRI-CGCM3 ( $-1.5^\circ$ ), HadGEM2-A ( $-0.4^\circ$ ), and CNRM-CM5 ( $-0.3^\circ$ ); it shifts polewards in IPSL-CM5A-LR ( $0.2^\circ$ ), MIROC5 ( $0.2^\circ$ ) and in MPI-CM5-LR ( $1.0^\circ$ ). The comparison between the on/off simulations shows that changes in ACRE with warming are probably not the main reasons for intermodel differences in ITCZ shifts.

The peak precipitation at the ITCZ is generally stronger when clouds and radiation interact (Figure 3.8b), with the exception of the IPSL model where the precipitation amount is almost constant. The strength of the ITCZ and its position are anti-correlated in the clouds-on ( $R^2=0.86$ ) as well as clouds-off simulations ( $R^2=0.63$ ) across the control and 4K simulations. Though the intermodel spread in the ITCZ position is larger in the absence of ACREs, the spread in the ITCZ strength is smaller despite the correlation between position and strength. The ITCZ strength is strongly correlated with the upwards velocity, which in turn is related to the fractional organization of the tropical circulation into convecting and subsiding regions.

Because of mass conservation arguments, different ITCZ positions among models and in the presence or absence of ACREs imply that the fraction of areas with subsiding motion will also differ. Following a simple consideration of mass conservation (e.g. Bjerknes, 1938), the subsidence fraction ( $A_\downarrow$ ) is given by a relationship between mean upwards velocity ( $\omega_\uparrow$ ) and downwards velocity ( $\omega_\downarrow$ )

$$A_\downarrow = \frac{\omega_\uparrow}{\omega_\downarrow - \omega_\uparrow}. \quad (3.2)$$

Figure 3.9 shows the relation of the subsidence fraction with  $\omega_\uparrow$  and  $\omega_\downarrow$  estimated at 500 hPa, where the vertical motion strength at 500 hPa is a widely used proxy for the large-scale tropical circulation (Bony et al., 2004). As expected,  $A_\downarrow$  is fairly unrelated to the strength of the subsiding motion at 500 hPa ( $R^2=0.06$ ). The weak correlation makes sense because the subsiding motion is given by the ratio of the radiative cooling rate and the static stability

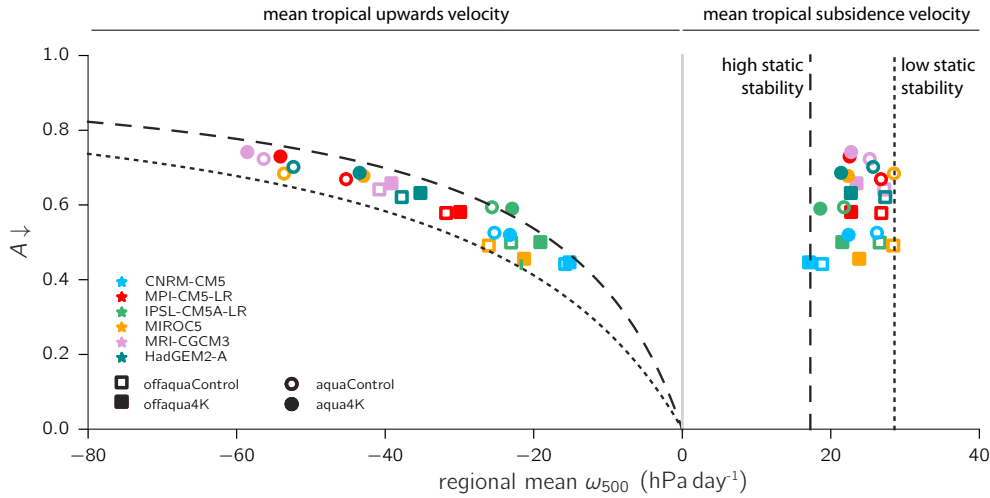


**Figure 3.9:** The relationship of mean tropical upwards and subsidence pressure velocity at 500 hPa ( $\omega_{500}$ ) with the subsidence fraction ( $A_{\downarrow}$ ) in the COOKIE simulations. The vertical gray line marks the border between convective (negative  $\omega_{500}$ ) and subsidence regime (positive  $\omega_{500}$ ). The vertical velocities according to a low static stability of  $0.035 \text{ K hPa}^{-1}$  and a high static stability of  $0.058 \text{ K hPa}^{-1}$  are marked by the dotted and dashed lines respectively when assuming a radiative cooling rate of  $1 \text{ K day}^{-1}$ .

in clear-sky regions. The vertical temperature structure, which is set by the moist adiabat in the convective regions (e.g. Johnson and Xie, 2010), determines both the static stability and, along with the distribution of water vapor, the cooling rate. The subsidence velocity is thus unrelated to the subsidence fraction.

The subsidence velocities vary between  $17.1$  and  $28.5 \text{ hPa day}^{-1}$ , with stronger subsidence motion in the control state and weaker subsidence when the surface is warmed by  $4 \text{ K}$  (Figure 3.9). Because the radiative cooling rates are not available from the model output, we assume a typical tropical clear-sky cooling rate of  $1 \text{ K day}^{-1}$  (e.g. Hartmann and Larson, 2002). Using this cooling rate, the static stability has to be weak ( $\approx 0.035 \text{ K hPa}^{-1}$ ) to support the maximum  $\omega_{\downarrow}$  and it has to be stronger ( $\approx 0.058 \text{ K hPa}^{-1}$ ) to support the minimum  $\omega_{\downarrow}$ . Higher static stabilities are expected when the surface temperature rises in association with the more stable moist adiabatic temperature lapse rate in a warmer climate (Bony et al., 2016, their Figure 4c). Though also the cooling rate depends on the temperature and moisture, its variation with temperature does not seem to account for the radiatively driven divergence in the upper tropical troposphere (Bony et al., 2016).

The independence of the mean subsidence velocity on the subsidence area fraction implies that the mean upwards velocity has to vary according to mass conservation arguments (Eq. 3.2). The mean upwards velocity is stronger if the subsidence fraction is large and decreases with decreasing subsidence fraction (Figure 3.9). In the models,  $\omega_{\uparrow}$  aligns well within the bounds of low and high static stability as a simple estimate of the minimum and maximum subsidence velocity. Because the subsidence velocity is greater in the control than in the  $4\text{K}$  state, convective motion must be stronger in the colder state for the given model and on/off experiment. Convection is generally weaker in the clouds-off experiments because of the more poleward ITCZ position and with that a smaller subsidence fraction.

Indications of the intermodel spread found in the ITCZ position extend to the intermodel spread in subsidence fraction because both are anti-correlated ( $R^2=0.88$ ).

From the above considerations it is unclear why the convective velocity, or alternatively the subsidence fraction, differs between the clouds-on and clouds-off simulations. We explore this issue by considering the probability density function of the vertical pressure velocity at 500 hPa ( $\text{PDF}_{\omega_{500}}$ ). In the clouds-on experiment, with the exception of CNRM-CM5 the models agree well on the negatively skewed shape of  $\text{PDF}_{\omega_{500}}$  (Figure 3.10), with the typical peak at subsidence velocities between 15 and 30  $\text{hPa day}^{-1}$  controlled by clear-sky radiative cooling and the static stability (e.g. Bony et al., 2004). It is unclear why CNRM-CM5 presents the exception to the common model behavior. In the clouds-off experiment, however, the statistics of the circulation differ more markedly among models. Three models (HadGEM2-A, MRI-CGCM and MPI-CM5-LR) still place the peak of  $\text{PDF}_{\omega_{500}}$  at subsidence velocities similar to the clouds-on experiment. The remaining models (IPSL-CM5A-LR, MIROC5 and CNRM-CM5) show weak convecting motion in the majority of the tropics with only secondary peaks in the subsidence regime. The absence of atmospheric cloud radiative effects thus increases the intermodel spread in the statistics of the large-scale circulation in the tropics.

What causes the difference between the circulation statistics in the clouds-on and clouds-off experiments? A look at  $\text{PDF}_{\omega_{500}}$  separately diagnosed only for areas poleward of the ITCZ position (Figure 3.10, middle column) and areas between the two ITCZs (Figure 3.10, right column) gives some indication that the differences in the tropical  $\text{PDF}_{\omega_{500}}$  stem from areas equatorward of the ITCZ – hereafter the inner-ITCZ zone. The PDFs in the clear-sky areas,

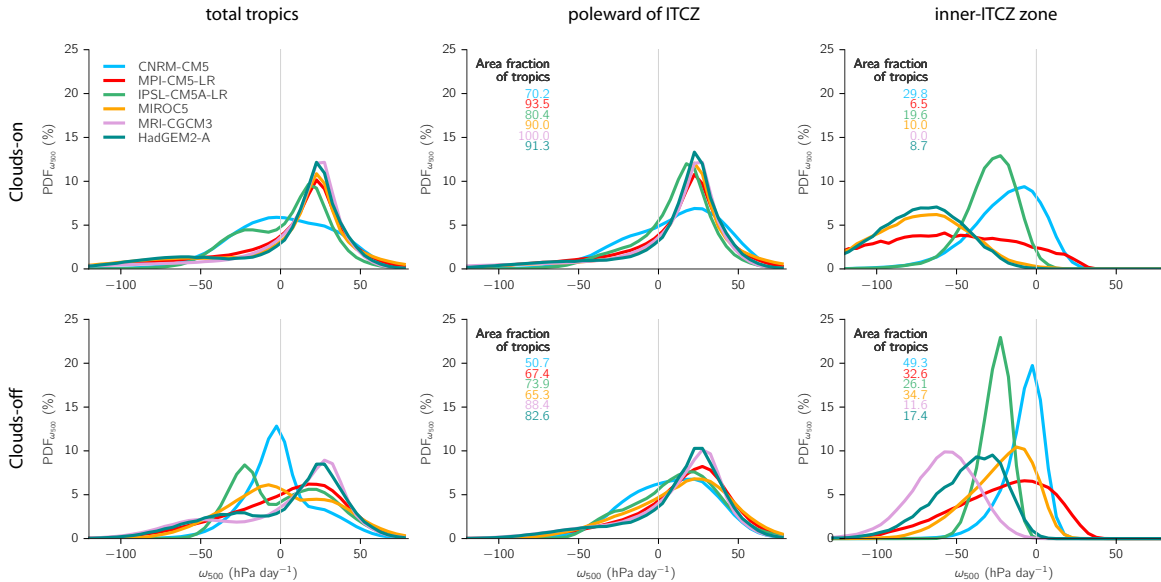


**Figure 3.10:** Probability density function of the vertical pressure velocity at 500 hPa ( $\text{PDF}_{\omega_{500}}$ ) in the control clouds-on (top row) and control clouds-off (bottom row) experiment. The total tropical  $\text{PDF}_{\omega_{500}}$  (left column) is separated into the  $\text{PDF}_{\omega_{500}}$  considering only tropical areas poleward of the ITCZ latitude (middle column) and equatorward of the ITCZ latitude (right column). The respective fractions of tropical areas is given in percent. The data is binned by  $5 \text{ hPa day}^{-1}$ .

which are expected in regions poleward of the ITCZ, show similar shapes among models as well as the clouds-on and clouds-off experiments. Inter-experiment differences between on/off simulations thus are rooted in the inner-ITCZ zone.

In the inner-ITCZ zone, which is characterized by upward motion, the peaks of  $\text{PDF}_{\omega_{500}}$  are located at negative vertical pressure velocities, though of different magnitudes among the models. The strength of the convective motion is similar between on/off simulations in IPSL-CM5A-LR and CNRCM-CM5, weakens in the absence of clouds for HadGEM2-A, MPI-CM5-LR and MIROC5, and cannot be compared in MRI-CGCM3 as it has a single ITCZ in the clouds-on experiment. For MIROC5 it is unclear whether the shift in mean convective velocity is merely due to cloud radiative effects or also due to a different SST profile. Because the area fraction of the inner-ITCZ zone is greater when clouds are transparent to radiation, the model inconsistencies imprint stronger on the total tropical  $\text{PDF}_{\omega_{500}}$ , leading to larger intermodel spread in the absence of clouds.

Next we explore a possible reason for the intermodel differences in upward motion strength within the inner-ITCZ zone that is related to the ITCZ position. The inner-ITCZ zone is characterized by high surface moist static energy owing to high surface temperature and boundary layer moisture content, and thus convection will frequently occur (Möbis and Stevens, 2012). If the ITCZ is located near the equator, the upward motion will lead to divergence in a poleward direction in the upper troposphere. However, the further away the ITCZ is located from the equator, the more the divergent motion can be directed into the inner-ITCZ zone as well, whereupon the dry air from aloft starts to subside. This mechanism may stabilize the upper troposphere and suppress convective motion in the inner-ITCZ zone. Indeed, the mean vertical velocity in the inner-ITCZ zone correlates strongly ( $R^2=0.81$ ) with the position of the ITCZ latitude (Figure 3.11).

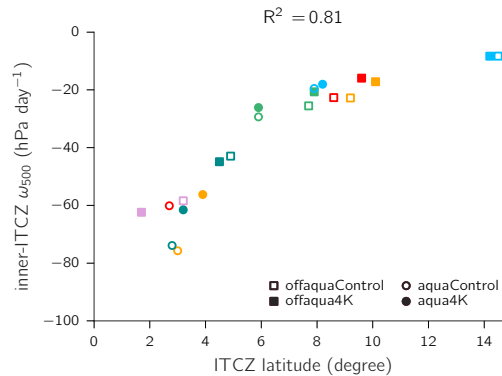


**Figure 3.11:** Relationship between the mean vertical velocity at 500 hPa ( $\omega_{500}$ ) averaged over the area between the double ITCZs and the ITCZ latitude.



### 3.4 Synthesis: Is the seed for intermodel spread present in the absence of cloud radiative effects?

In this chapter, we investigate the influence of atmospheric cloud radiative effects (ACREs) on different aspects of the tropical precipitation. For this we analyze aquaplanet simulations from six models participating in the Clouds On-Off Klimate Intercomparison Experiment (COOKIE, Stevens et al., 2012). In COOKIE the cloud-radiation interaction is either active (“clouds-on”) or inhibited (“clouds-off”), which allows inferences of how the diabatic heating by cloud radiative effects influences the tropical circulation and consequently the tropical precipitation patterns. Upon removing ACREs, the intertropical convergence zone (ITCZ) shifts polewards in all models. The degree to which the ITCZ shifts differs among models, however.

We first explore a hypothesis regarding the dominant source of intermodel spread in tropical precipitation changes. By investigating the precipitation response to warming in two aquaplanet models, Voigt and Shaw (2015) conclude that different responses of cloud radiative effects are the main contributor to the spread among the two models. However, upon closer inspection of their results, the question arises whether differences in the precipitation response originate already without cloud radiative changes, whereupon different responses in ACREs might merely exacerbate the initial differences.

We addressed our hypothesis – whether the seed for intermodel spread is present in the absence of cloud-radiation interaction – by exploring tropical mean as well as spatial aspects of precipitation and the tropical circulation. The arguments discussed above either directly support or do not support the hypothesis depending on the investigated parameter.

The hypothesis is supported by larger spread among models in the absence of cloud radiative effects in:

- how the tropical mean precipitation changes with warming, as given by the tropical hydrological sensitivity parameter ( $\eta$ ),
- the position of the intertropical convergence zone (ITCZ) which implies different vertical temperature structures,
- the statistics of the large-scale tropical circulation, as shown by  $\text{PDF}_{\omega_{500}}$ , where differences among models are determined by a different organization of the circulation in the inner-ITCZ zone.

However, we also identified parameters which do not support our hypothesis in that the intermodel spread is larger when cloud radiative effects are absent:

- the tropical mean precipitation rate both in the control and 4K state, and
- the peak precipitation rate at the position of the ITCZ.

All of the above considerations rely on a small model ensemble (six models) where in the case of clouds-on experiments the MIROC5 model results are difficult to interpret owing

to the different underlying SST profile. However, the COOKIE experiments are the largest available data set as of now that allows to investigate the impact of cloud radiative effects on the simulated climate. Although we identified parameters that do not support our hypothesis – that cloud radiative effects are not the primary reason for intermodel spread of tropical precipitation characteristics – we also identified a number of parameters that lead to strongly differing tropical circulation and precipitation patterns in the absence of cloud radiative effects, supporting our hypothesis. The question whether ACREs lead to larger or smaller intermodel spread thus has to be discussed in context of the parameter of interest. Overall our results show that contrary to the common assumption, where making a problem simpler by e.g. removing the cloud radiative effect would entail a more similar solution, simplifying a problem does not necessarily lead to convergence of the results to a more common answer.

---

## 4 Diagnosing the zonal-mean precipitation via an MSE framework

### 4.1 Introduction

The regional precipitation is strongly correlated with vertical velocity, as discussed in the introduction of this thesis (Section 1.2) and shown in Figure 3.3. Likewise, differences in how patterns of precipitation change with warming are primarily associated with differences in the circulation among models, rather than differences associated with the thermodynamics (e.g. Shepherd, 2014; Xie et al., 2015). In this chapter we develop a framework to diagnose the vertical velocity from the energetics. We employ this framework to understand the controls on the zonal-mean vertical velocity on aquaplanets as well as to explore why the intertropical convergence zone shifts polewards when the cloud-radiation interaction is inhibited.

The idealized configuration of aquaplanets, planets in which the surface is completely water-covered, presents a convenient testbed for the framework developed here. The sea surface temperatures (SSTs) are prescribed to follow the ‘Qobs’ profile as given by the AquaPlanet Experiment Project (Neale and Hoskins, 2001), which peak at the equator at 27°C, decline until they are held constant at 0° poleward of 60° latitude. Because of the eliminated land-sea distribution, orography, seasonality, and neglected sea-ice, the aquaplanets’ simulated mean climate is zonally symmetric. The dynamics and parameterizations of the full general circulation model (GCM) are retained; with that, the aquaplanet is a configuration to study intermodel differences in a simpler context. Despite their simple configuration, aquaplanets have been shown to capture the robust responses of the hydrological cycle and large-scale circulation to surface warming found in the Earth-like configuration (Medeiros et al., 2015). In this study, we employ our diagnostic framework to the aquaplanet simulations provided by the Clouds On-Off Climate Intercomparison Experiment (COOKIE, Stevens et al., 2012), in which simulations either include cloud-radiation interaction as in the standard aquaplanet configuration, or in which cloud-radiation interaction is inhibited.

On aquaplanets, tropical precipitation is organized in convective rainbands associated with the intertropical convergence zone (ITCZ). Aquaplanets have been widely used to study the double ITCZ problem. This problem refers to the persistent second ITCZ in coupled climate models, which is located south of the equator over the Atlantic and Pacific oceans for longer periods than observed (Mechoso et al., 1995; Dai, 2006; Oueslati and Bellon, 2015; Zhang et al., 2015). On aquaplanets, the position of the ITCZ can depend on various factors. The ITCZ shifts from a single to a double structure as tropical SST gradients flatten (e.g. Dahms et al., 2011; Williamson et al., 2013; Oueslati and Bellon, 2013b). Further factors

influencing the ITCZ position on aquaplanets are: the dynamical core and model resolution (Landu et al., 2014), the convection parameterization (Liu et al., 2010; Möbis and Stevens, 2012; Oueslati and Bellon, 2013a), the feedback between surface wind and evaporation (Numaguti, 1993; Chou and Neelin, 2004; Liu et al., 2010; Möbis and Stevens, 2012), and various boundary conditions such as solar constant specifications (Kirtman and Schneider, 2000; Barsugli et al., 2005).

The role of atmospheric cloud radiative effects on the ITCZ position in aquaplanets has received little attention. Chao and Chen (2004) found no influence on the ITCZ position upon inhibiting the cloud-radiation interaction. This result is contrary to our analysis (Chapter 3) and the recent findings in Harrop and Hartmann (2016) who also investigate the impact of ACREs on the ITCZ position in aquaplanet COOKIE simulations: inhibiting ACREs leads to a consistent poleward shift in all models. Harrop and Hartmann (2016) propose a mechanism based on the convective available potential energy (CAPE) to explain the equatorward contraction of the ITCZ in the presence of ACREs. They argue that cloud radiative heating exerted on the upper troposphere leads to a stabilization of the upper troposphere, which induces a contraction of high CAPE values towards the equator, thus contracting the ITCZ equatorwards. We offer another possible reason for the poleward shift when inhibiting ACREs, inferred from a simple diagnostic framework for the vertical velocity that we propose.

Our framework, which we derive from the moist static energy (MSE) budget, expresses the vertical mean vertical velocity as the ratio of a column-integrated heating term and the gross moist stability. The gross moist stability can be understood as a normalized vertical advection of a conserved moist quantity, such that it represents the efficiency of exporting energy from the atmospheric column. Originally, the concept was introduced by Neelin and Held (1987) as “a convenient way of summarizing our ignorance of the details of the convective and large scale transients”. Since then many different definitions for the gross moist stability have been used (for a review see Raymond et al., 2009). Roughly they can be grouped into theoretical and diagnostic definitions. The diagnostic definitions vary, but essentially the vertically integrated horizontal divergence of a quantity conserved in moist adiabatic processes is normalized by some measure of the strength of convective motion. Both this measure of strength as well as the divergence are directly estimated from observed or modeled fields of the conserved quantity and velocity.

The theoretical studies rely on assuming a structure of the vertical velocity. Based on an assumed moist adiabatic temperature stratification, this structure resembles a first baroclinic mode associated with deep convective motion (Yu et al., 1998; Neelin and Zeng, 2000; Zeng et al., 2000). By representing the vertical velocity as a deep convective mode (e.g. Figure 4.1c), gross moist stability values are found to be positive in the tropics (Yu et al., 1998; Chou et al., 2013). However, diagnostic approaches identify that the gross moist stability becomes negative in tropical areas where shallow convection predominates (e.g. Back and Bretherton, 2006), or in the early stages of the convective life cycle characterized by shallow convection (e.g. Inoue and Back, 2015b).

Shallow convection is characterized by low-level convergence and mid-level divergence (Figure 4.1b). Due to the vertical profile of MSE, with high surface values, a mid-tropospheric

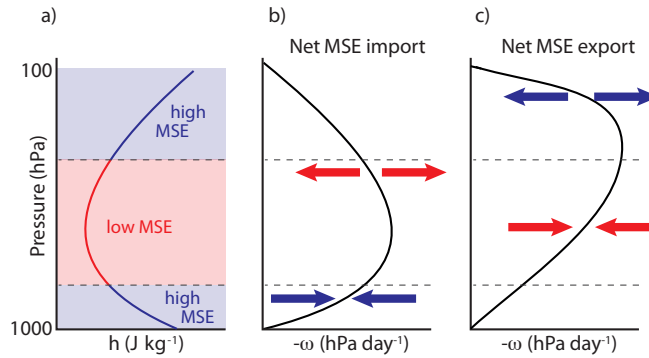


**Figure 4.1:** Illustration of the net column moist static energy (MSE) and vertical velocity ( $\omega$ , positive for descending motion) associated with shallow and deep convection. a) A typical tropical MSE profile is characterized by high values close to the surface owing to high temperature and humidity, a minimum of MSE in the mid-troposphere due to the rapid decrease of humidity, and increasing values in the upper troposphere because of the contribution from the geopotential. b) Shallow convection leads to a net import of MSE because of low-level convergence in areas of high MSE and mid-level divergence where MSE is low. c) Deep convection stabilizes the troposphere by net MSE export due to mid-level convergence in areas of low MSE and upper-level divergence where MSE is high.

minimum and increasing values in the upper troposphere, a low-level convergence and mid-level divergence lead to a net import of MSE into the tropospheric column, destabilizing the atmosphere by vertical motion. Back and Bretherton (2009) attempted to include shallow convection by a second mode to predict a precipitation climatology, but could not successfully constrain the deep-mode amplitude when using the MSE budget; their model thus had to be based on the dry static energy, neglecting horizontal variations in moisture. In Lintner et al. (2012), the addition of a second mode to a tropical model of intermediate complexity did not strongly improve the precipitation climatology with respect to the model based on a single deep-convective mode (Neelin and Zeng, 2000). Because of the success of the single-mode theoretical models in simulating tropical precipitation climatologies (Neelin and Held, 1987; Neelin and Zeng, 2000; Zeng et al., 2000), and the lack of evidence that adding a second mode has clearly greater explanatory power, in this study we base our diagnostic framework on a gross moist stability formulation with one vertical velocity structure related to deep convection (similar to Figure 4.1c). The import of MSE due to shallow convection is retained as a forcing in the framework.

In the remaining part of this chapter, we briefly describe the COOKIE experiments (Section 4.2). We introduce and discuss the diagnostic framework derived from the MSE budget (Section 4.3), and apply the framework to the COOKIE simulations (Section 4.4). Specifically we investigate whether the heating or the gross moist stability explain the zonal-mean shape of the vertical mean vertical velocity, and with that the precipitation (Section 4.4.1). Last we develop a theory for the poleward shift of the ITCZ upon inhibiting ACREs with the help of the diagnostic framework (Section 4.4.2). We summarize our findings in Section 4.5.

## 4.2 Simulations

We test the diagnostic MSE framework with the help of the aquaplanet simulations provided by the Clouds On-Off Klimate Intercomparison Experiment (COOKIE, Stevens et al., 2012). We refer to simulations with active cloud-radiation interaction as “clouds-on” and to those with inhibited cloud-radiation interaction as “clouds-off”. From the comparison between clouds-on and clouds off simulations the impact of atmospheric cloud radiative effects (ACREs) on the simulated circulation and spatial precipitation distribution can be assessed. Climate change can be investigated by comparing the control simulation with ‘Qobs’ SSTs to simulations where SSTs are uniformly raised by 4 K. Six models performed the control and 4 K COOKIE simulations: CNRM-CM5, MPI-CM5-LR, IPSL-CM5A-LR, MIROC5, MRI-CGCM3, HadGEM2-A. In MIROC5 the prescribed SSTs differ between the cloud-on and clouds-off simulations, where SSTs follow ‘Qobs’ in the cloud-off experiment, but tropical SST gradients are steeper in the clouds-off experiment. More information on the simulations and aquaplanet configuration is given in Section 3.2.

## 4.3 Diagnostic MSE framework for precipitation investigation

The moist static energy ( $h$ ) is given by the sum of thermal, latent and potential energy

$$h = c_p T + gz + L_v q, \quad (4.1)$$

where  $c_p$  is the specific heat of dry air at constant pressure,  $T$  the absolute temperature,  $q$  the specific humidity, and  $gz$  the geopotential. The moist static energy is a convenient variable to characterize the energy in an air parcel as its vertical integral is approximately conserved in moist adiabatic motions. A typical tropical MSE profile has large values at the surface associated with high specific humidity and temperature. With increasing height, the humidity content decreases rapidly, leading to a mid-tropospheric minimum in MSE. In the upper troposphere, where  $L_v q$  is low, MSE increases again owing to the contribution of the geopotential.

In stationarity, the column integrated moist static energy budget at any point is

$$0 = SH + LH + R - [\vec{v} \cdot \vec{\nabla} h] - \left[ \omega \frac{\partial h}{\partial p} \right], \quad (4.2)$$

where the terms from left to right correspond to the surface sensible and latent heat fluxes, the radiative flux divergence across the column, and the horizontal and vertical advection of moist static energy; square brackets denote the mass weighted vertical integral. Generally, the turbulent surface fluxes transport energy into the troposphere and represent a source of column MSE while the radiation cools the atmosphere through longwave radiation and represents a sink of column MSE. The horizontal and vertical advection can become both sinks and sources of column MSE depending on the vertical structure of MSE, horizontal winds, as well as the vertical velocity.

The vertical structure of vertical velocity in the tropics is thought to be represented by two baroclinic modes, one related to deep convection with low level convergence and upper level divergence, and one related to shallow circulations with middle level convergence/divergence (e.g. Yuan and Hartmann, 2008; Inoue and Back, 2015a). The deep mode explains most of the variance in tropical vertical velocity profiles. Our aim, to get an expression for the vertical velocity, can be achieved by separating the vertical advection term into the vertical advection related to an assumed vertical velocity structure, and vertical advection associated with the deviation from this structure

$$-\left[\omega \frac{\partial h}{\partial p}\right] = -\omega^* \left[\phi(p) \frac{\partial h}{\partial p}\right] - \left[(\omega(p) - \omega^* \phi(p)) \frac{\partial h}{\partial p}\right]. \quad (4.3)$$

We express the vertical velocity profile  $\omega(p)$  by one single mode of deep convection with the vertical mean vertical velocity  $\omega^*$  yielding the amplitude of the assumed structure  $\phi$  of deep convection.  $\phi$  is chosen to be positive, with more details on its specification presented in Section 4.3.1. The deviation vertical advection term,  $V_h^\alpha = -[(\omega(p) - \omega^* \phi(p)) \frac{\partial h}{\partial p}]$ , then retains the vertical advection associated with shallow circulations and further modes. Essentially, our approach follows the framework introduced by Bony et al. (2013).

The vertical MSE advection normalized by some quantity related to a mass flux, in our case  $\omega^*$ , is traditionally referred to as gross moist stability (Neelin and Held, 1987)

$$\Gamma_h = -\left[\phi(p) \frac{\partial h}{\partial p}\right]. \quad (4.4)$$

It is a convenient quantity to characterize the stability of the tropical troposphere related to moist convective processes in a column-integrated sense. The gross moist stability represents the export or import of moist static energy in the tropospheric column, where deep vertical motions typically export MSE and stabilize the troposphere, while shallow circulations tend to import MSE having a destabilizing effect (e.g. Back and Bretherton, 2006) as illustrated in Figure 4.1.

We rearrange the MSE budget (Eq. 4.2) using Eq. 4.4, such that the vertical mean vertical velocity is expressed as the ratio of a heating term  $Q = SH + LH + R + H + V_h^\alpha$  and the gross moist stability:

$$-\omega^* = \frac{Q}{\Gamma_h} = \beta Q, \quad (4.5)$$

with  $\beta$  denoting the inverse gross moist stability, and  $H$  the horizontal advection. With the help of Eq. 4.5 it is thus possible to test whether the models' spread in the heating or in the gross moist stability are more decisive in setting the zonal-mean structure of  $\omega^*$  in the individual models (Section 4.4). Note that technically  $V_h^\alpha$  is an additional vertical advection term, however, we consider it as part of the forcing by including it into the heating term. In doing so we follow the reasoning by Chou et al. (2013) in that the destabilizing effect of shallow circulations is responsible for the import of MSE and thus represents a forcing that deep vertical motion responds to. Because the diagnostic framework is based on one vertical mode, we will in particular explore the question how much of the vertical velocity can be explained by assuming one single mode associated with deep convection. Once the controls on the vertical mean vertical velocity are understood, precipitation patterns can

be reconstructed using the close relationship of precipitation as a function of the vertical velocity shown in Figure 3.3.

### 4.3.1 Choice of generic vertical velocity profile influences gross moist stability

By considering the definition of the gross moist stability (Eq. 4.4) it becomes imminently clear that the magnitude of  $\Gamma_h$  will depend on the choice of the assumed vertical velocity structure  $\phi$ . The profile of  $\phi$  determines how strongly the vertical gradient of  $h$ , shown in Figure 4.2a, is weighted at different heights. Because of the profile of  $h$  with high surface values, a mid-tropospheric minimum and increasing  $h$  in the upper troposphere (as illustrated in Figure 4.1a), the vertical gradient  $-\frac{\partial h}{\partial p}$  is negative in the lower troposphere and positive in the upper troposphere. If  $\phi$  is chosen to be more top-heavy,  $\Gamma_h$  will become more positive; if its maximum is placed in the mid-troposphere the sign of  $\Gamma_h$  strongly depends on the level of the mid-tropospheric minimum in  $h$ ; if  $\phi$  is bottom-heavy  $\Gamma_h$  will be negative. Optimally, the choice of  $\phi$  should be based on physical considerations.

One such consideration is that heating drives vertical motion more easily where the gross moist stability minimizes. According to Eq. 4.5, convection (negative  $\omega^*$ ) is associated with a heating (positive  $Q$ ) of the gridbox column when the gross moist stability is positive, which conforms to the physical view of deep convection heating and stabilizing the troposphere by releasing latent heat. Considering Eq. 4.5, in the case of negative gross moist stabilities, deep convection would have to be associated with a cooling of the column, which contradicts the above physical view. We thus will define  $\phi(p)$  such that  $\Gamma_h$  is positive in the considered COOKIE simulations (Section 4.2), which additionally ensures that the sign of  $\Gamma_h$  corresponds to export of MSE from the column as expected from deep vertical motion (Back and Bretherton, 2006). Furthermore, to allow the framework set by Eq. 4.5 to be

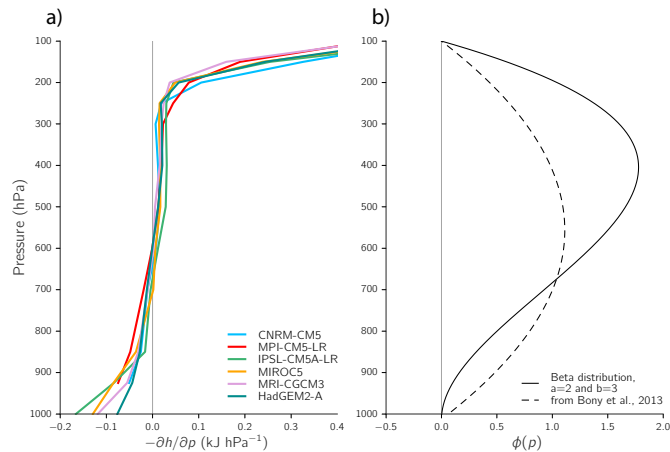


**Figure 4.2:** a) Vertical pressure gradient of the moist static energy with height in the clouds-off control experiment, horizontally averaged between the double ITCZs. b) Profiles of the vertical velocity profile ( $\phi$ ) assumed in the study of Bony et al. (2013) (dashed line) and in this study (solid line) with a surface and tropopause placed at 1013 hPa and 100 hPa respectively.



applicable,  $\Gamma_h$  has to remain unequal to zero, which is most easily achieved by requiring  $\Gamma_h$  to be positive.

To choose  $\phi$  such that  $\Gamma_h$  remains positive in all four experiments of the COOKIE aquaplanet suite, we started our tests with the profile of  $\phi$  used in Bony et al. (2013). This profile follows a cubic polynomial that vanishes below the surface and above the tropopause, and places the maximum in the mid-troposphere at 600 hPa (Figure 4.2b). However, using this profile, the near-equatorial minimum in time zonal-mean  $\Gamma_h$  did not fulfill our requirement to remain positive in all experiments. As discussed before,  $\phi$  with a mid-tropospheric maximum puts weight on vertical levels where  $-\frac{\partial h}{\partial p}$  is negative, thus resulting in a negative vertical integral. In order to be able to specify a bounded profile that can easily be modified from symmetric to skewed, we introduce a beta distribution; the profile of  $\phi$  can thus be changed via the shape parameters  $a$  and  $b$ . The requirement that  $\Gamma_h$  remains positive in all four experiments was met when  $a = 2$  and  $b = 3$  which yields a top-heavy profile of  $\phi$  with the maximum approximately at 400 hPa (Figure 4.2b). Various other choices of  $a$  and  $b$  that produce a top-heavy profile would have also given positive  $\Gamma_h$  but would have modified its magnitude.

Considering the steep gradients of MSE in the upper troposphere, it is clear that the integration depth set by the chosen level of the tropopause ( $p_t$ ) also modifies the magnitude of  $\Gamma_h$ . Most often in previous work a fixed tropopause height, e.g. 100 hPa is assumed. However, the tropopause height varies among models and with latitude. We estimate  $p_t$  at each time and gridcell using the WMO definition whereby the tropopause height is given by the level at which the temperature lapse rate is  $2 \text{ K km}^{-1}$  or less. Using a variable  $p_t$  especially reduces  $\Gamma_h$  for the CNRM model owing to its low tropical tropopause height of approximately 150 hPa. Taking into account the requirements for the profile, the integration borders and further that  $\int \phi(p) \frac{dp}{g} = 1$ , we define the generic vertical velocity profile as:

$$\phi(p) = \begin{cases} \frac{(p_s - p_t)(p - p_t)^{a-1}(p_s - p)^{b-1}}{B(p_s, p_t, a, b)}, & p_t \leq p \leq p_s \\ 0, & \text{otherwise} \end{cases}, \quad (4.6)$$

with  $B(p_s, p_t, a, b) = \frac{\Gamma(a)\Gamma(b)}{\Gamma(a+b)(p_s - p_t)^{a+b-1}}$ , and  $\Gamma$  the gamma function.

Figure 4.3 shows the resulting time zonal-mean gross moist stability in the control clouds-on and clouds-off experiments (left column) as well as the changes with warming (right column). The time zonal-mean  $\Gamma_h$  is characterized by the minimum values in areas which coincide roughly with the areas between the two ITCZs. This minimum of  $\Gamma_h$  is consistent with the physical expectation that where  $\Gamma_h$  is low, less heating is required to drive convective motion.  $\Gamma_h$  increases poleward of the ITCZs, indicating that the greater stability hinders convection. The polewards increase in  $\Gamma_h$  arises from a combination of increased stability in the upper troposphere as well as the reduced moisture in the lower troposphere of areas located polewards of the ITCZ, placing the minimum in MSE at lower vertical levels and thus increasing the weight of positive  $-\frac{\partial h}{\partial p}$ . The change in  $\Gamma_h$  with warming is inconsistent in sign among models and dependent on the latitude. The inconsistency applies to both the clouds-on and clouds-off experiments.

Though the regional variation in  $\Gamma_h$  is determined by the vertical gradient of MSE, the discussion above concerning the choice of  $\phi$  and the integration borders emphasizes that

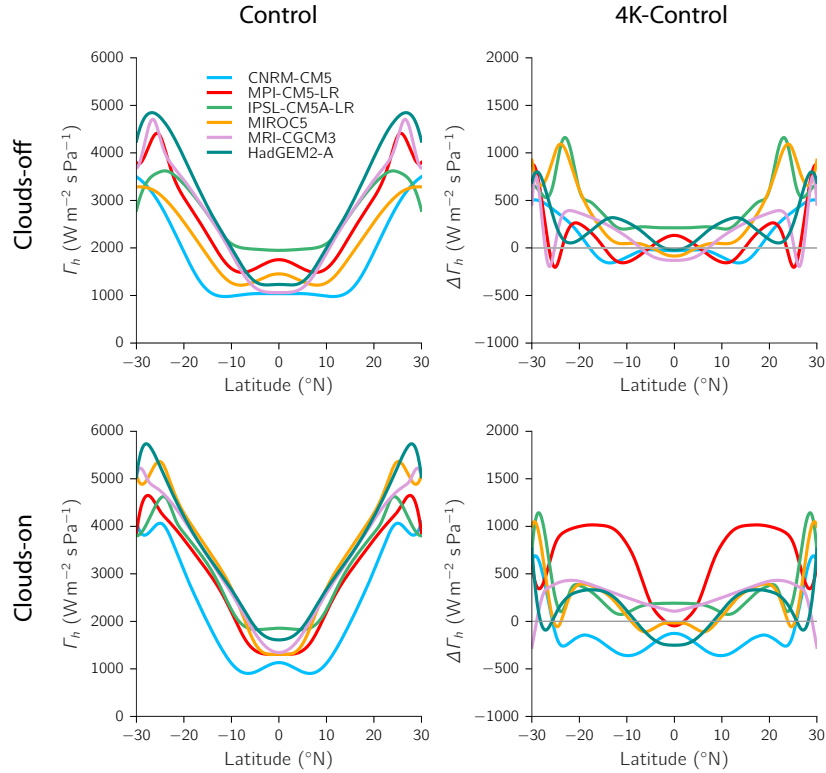


**Figure 4.3:** Gross moist stability ( $\Gamma_h$ ) of the control clouds-off and clouds-on experiments (left column) and its change with warming (right column). Clouds-off and clouds-on simulations are shown in the top and bottom row, respectively.

the magnitude of  $\Gamma_h$  is hardly comparable among studies. Climatologies of the gross moist stability (e.g. Yu et al., 1998; Chou et al., 2013) thus should be interpreted in terms of the chosen definition of gross moist stability and the generic vertical velocity profile.

### 4.3.2 Validity of the MSE framework

Before employing the framework given by Eq. 4.5 we test its validity in diagnosing the vertical mean vertical velocity from time zonal-mean  $Q$  and  $\Gamma_h$ . The atmospheric radiative flux is the divergence between TOA and surface radiative fluxes, and the surface turbulent fluxes are directly available from the model output. We calculated the horizontal advection, as well as the gross moist stability and deviation vertical advection from monthly mean fields of moist static energy, horizontal winds and vertical velocity. Originally the budget in Eq. 4.2 was not closed and the residual term was not substantially smaller than the other terms. However, we could only diagnose the horizontal advection from monthly mean values, whereas the total horizontal advection comprises a non-negligible eddy advection term in the tropics (Peters et al., 2008) in addition to the mean horizontal advection. By rerunning the MPI model with diagnostic transport output we reassured ourselves that the zonal-mean distribution and magnitude stem from the horizontal eddy advection to a first degree. The

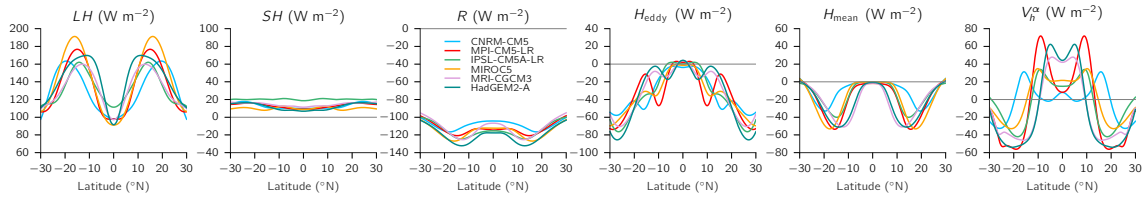


**Figure 4.4:** Time zonal-mean of the individual terms comprised in the heating term  $Q$  shown for the control clouds-off experiment. Note the different choice of value ranges for each term, but for all subplots a total range of  $140 \text{ W m}^{-2}$  is shown.

residual is thus regarded as eddy advection, such that the horizontal advection  $H$  is given as the sum of monthly mean and eddy horizontal advection ( $H_{\text{mean}}$  and  $H_{\text{eddy}}$ ).

The individual terms in  $Q$  differ quite strongly in their zonal-mean contribution to the heating as well as among models (Figure 4.4). The surface turbulent heat fluxes ( $SH$  and  $LH$ ) are sources to the column moist static energy throughout the tropics, while the sensible heat flux is small in magnitude compared to the latent heat flux. The atmospheric radiation and the horizontal time-mean advection represent a sink of column MSE, with the strongest cooling resulting from the radiation. Column MSE is also exported by the horizontal eddy advection throughout the tropics, with the exception of equatorial areas, where  $H_{\text{eddy}}$  is close to zero or slightly positive. Because horizontal temperature gradients in the tropics are small (e.g. Sobel et al., 2001), the column export of MSE by horizontal advection is dominated by horizontal moisture advection. The deviation vertical advection term  $V_h^\alpha$  both represents a sink and source term, where areas of MSE import roughly coincide with convective regions, and MSE is exported in subsidence areas. As elaborated in Section 4.3,  $V_h^\alpha$  represents the vertical advection of MSE associated with deviations from the assumed deep convective vertical velocity mode  $\phi$ . Per definition, the vertical advection owing to the deep mode exports MSE in convective regions and imports MSE in subsidence areas. That  $V_h^\alpha$  is positive in convective areas signifies the import of MSE due to shallow convective motion, and with that leads to a heating of the tropospheric column.

The zonal-mean  $-\omega^*$  diagnosed from other terms in the MSE budget, e.g. for the clouds-off control experiment, is shown in Figure 4.5a. The peak values associated with the ITCZ range from approximately 15 to  $44 \text{ hPa day}^{-1}$ , whereas subsidence velocities are quite consistent among models for reasons discussed in Section 3.3.2. The deviation between diagnosed and model  $-\omega^*$  is small compared to the magnitude of  $-\omega^*$  in all four experiments (Figure 4.5b). The framework given by Eq. 4.5 is thus applicable to investigate the controls on the zonal-mean  $-\omega^*$  by separating between the heating term  $Q$  and the gross moist stability  $\Gamma_h$ .

## 4.4 Employing the MSE framework

With the help of the MSE framework described in the previous section, we investigate how the different terms of the MSE budget balance the time zonal-mean, vertical mean vertical

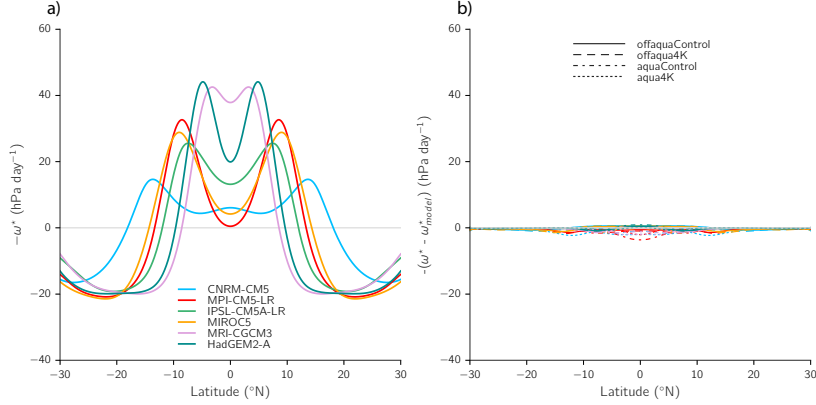


**Figure 4.5:** a) Vertical mean vertical velocity ( $-\omega^*$ ) diagnosed with Eq. 4.5 for the control clouds-off experiment and b) the difference between diagnosed and model  $-\omega^*$  for all four experiments.

velocity (hereafter simply referred to as ‘vertical velocity’). First, we examine the extent to which the vertical velocity can be understood by assuming that the spatial variability of the vertical velocity profile can be expressed by one dominant mode associated with deep convection (Section 4.4.1). Second, we investigate the shift of the ITCZ due to atmospheric cloud radiative effects (Section 4.4.2). In this section all analysis is performed on the control clouds-off experiment if not otherwise noted.

#### 4.4.1 Controls on the zonal-mean vertical velocity

To separate the impacts of zonal-mean variations in the heating term  $Q_i$  and inverse gross moist stability  $\beta_i$  of the model  $i$  on the zonal-mean vertical velocity  $-\omega_i^*$  (the asterisk is omitted in the following for simplicity), we decompose  $\omega_i = \bar{\omega} + \omega_i'$  into the multi-model mean zonal-mean (denoted by the overline) and the anomaly from the multi-model mean (denoted by a prime); we treat  $Q_i$  and  $\beta_i$  in the same way. Then the anomalous vertical velocity from Eq. 4.5 can be written as

$$-\omega_i' = \beta_i' \bar{Q} + \bar{\beta} Q_i' + \beta_i' Q_i' + \bar{\beta}_i' Q_i'. \quad (4.7)$$

The anomalous vertical velocity in relation to the four terms on the right side of Eq. 4.7 is shown in Figure 4.6. One term ( $\bar{\beta} Q_i'$ ), which comprises the anomalous heating, stands out from the others. For all models this term follows most closely the one-to-one line. That  $\beta_i' \bar{Q}$  is not related to  $-\omega_i'$  demonstrates that the stability is only secondary in explaining the zonal-mean variation in the vertical velocity. In fact, there is no notable relationship of the other three terms in Eq. 4.7 with  $\omega_i'$ , implying that most of the zonal-mean variation in  $\omega_i'$  is explained by the zonal-mean variation in the anomalous heating term in all models.

We further ask how much the sums of different combinations of the four terms in the decomposition explain the zonal-mean variation in  $\omega_i'$  (Figure 4.7). In total, fifteen possible combinations of terms are available. We estimate the root mean square error (RMSE)

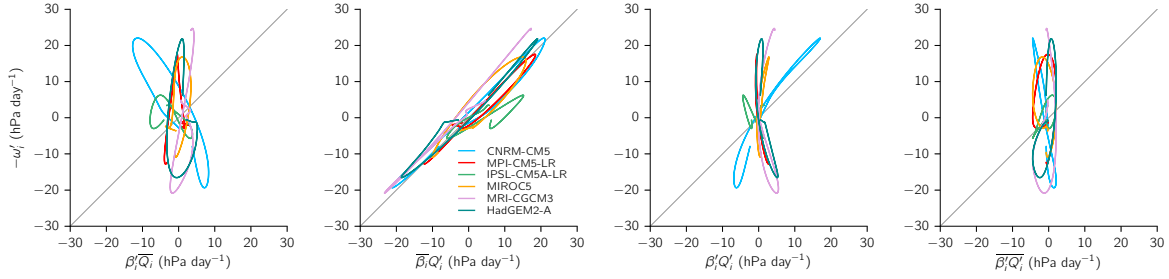


**Figure 4.6:** Anomalous vertical mean vertical velocity as a function of its decomposition into four terms given by Eq. 4.7 for the control clouds-off experiment.

between the actual model's  $-\omega'_i$  and each of these combinations of terms, e.g. the RMSE between  $-\omega'_i$  and  $\beta'_i \bar{Q}'_i + \bar{\beta}'_i Q'_i + \beta'_i Q'_i + \bar{\beta}'_i Q'_i$ . Further we normalize the RMSE of each combination by the RMSE of the 'no term'; 'no term' signifies the relationship of  $\omega'_i$  with  $\bar{\omega}$ . A separation between the combinations is apparent (Figure 4.7): all of the combinations of terms that contain  $\bar{\beta}'_i Q'_i$  have smaller normalized RMSE as measured by the multi-model median with values between about 0.1 and 0.2 than all other combinations (about 0.5 to 0.6). Variations in the anomalous heating term are thus fundamental in explaining variations in the vertical velocity, whereas variations in gross moist stability are of less importance.

Is there a dominant term contained in  $Q_i$  that is most responsible for the high correlation between  $\bar{\beta}'_i Q'_i$  and  $-\omega'_i$ ? To investigate this question, we estimate the normalized RMSE for the different combinations of source terms in  $Q_i$ : for the sum of surface latent and sensible

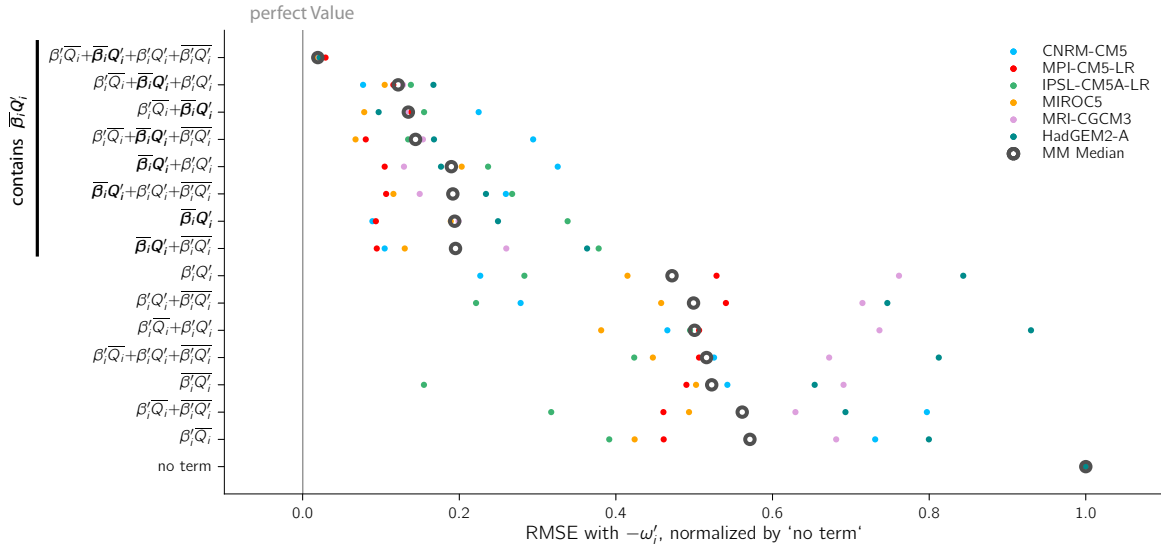


**Figure 4.7:** Normalized root mean square error (RMSE) between the zonal-mean of the expression given on the  $y$ -Axis and zonal-mean  $-\omega'_i$ . The RMSE is normalized by the 'no term' which is the RMSE between  $-\bar{\omega}$  and  $-\omega'_i$ . Small dots are individual models, the multi-model median of normalized RMSE is shown by dark gray circles. The terms are ordered by the multi-model median. The analysis is performed on the control clouds-off experiment.

heat flux ( $SF_i$ ), the atmospheric radiative heating rate ( $R_i$ ), the horizontal advection ( $H_i$ ), and the vertical advection due to second and higher baroclinic modes ( $V_h^\alpha$ ). This again results in fifteen possible combinations (Figure 4.8). Though a separation in the magnitude of multi-model median error is not as apparent as in the previous figure, one term again ranks among the smallest: the deviation vertical advection term  $V_h^\alpha$ . In fact, when only considering  $V_h^\alpha$  we obtain the smallest error. The other terms comprised by  $Q_i$ , however, do not seem to be important in shaping the zonal-mean vertical velocity structure. The single terms  $\bar{\beta}R_i'$ ,  $\bar{\beta}SF_i'$ , and  $\bar{\beta}H_i'$  rank at the tenth, twelfth and fifteenth place with respect to their multi-model median normalized RMSE. Though the normalized RMSEs are shown only for the control clouds-off experiment (Figures 4.7 and 4.8), the general conclusions are the same for the other experiments.

The small RMSEs of all terms associated with anomalous  $V_h^\alpha$  encourage us to explore the controls on  $V_h^\alpha$  in more detail (Figure 4.9). As expected from the good correlation with  $-\omega_i'$ ,  $V_h^\alpha$  is positive in convective areas and negative in subsidence regions (Figure 4.4, right-most plot). A positive sign implies that moist static energy is imported into the column via vertical circulations, providing energy to support convective motions. Import of MSE by vertical advection is associated with shallow circulations rather than differences in the vertical gradients of MSE (e.g. Back and Bretherton, 2006). Indeed,  $-\frac{\partial h}{\partial p}$  is similar among different vertical velocity regimes as well as among models (Figure 4.9, top row).

It is the deviation of the vertical velocity from the assumed deep mode ( $\omega(p) - \omega^*\phi(p)$ ) shown in the middle row of Figure 4.9, that varies between the velocity regimes, therefore setting the zonal-mean variation in  $-\omega_i'$ . Overall,  $\omega(p) - \omega^*\phi(p)$  has the greatest absolute values in the lower troposphere and is of the same sign as  $\omega^*$ . This underestimation of

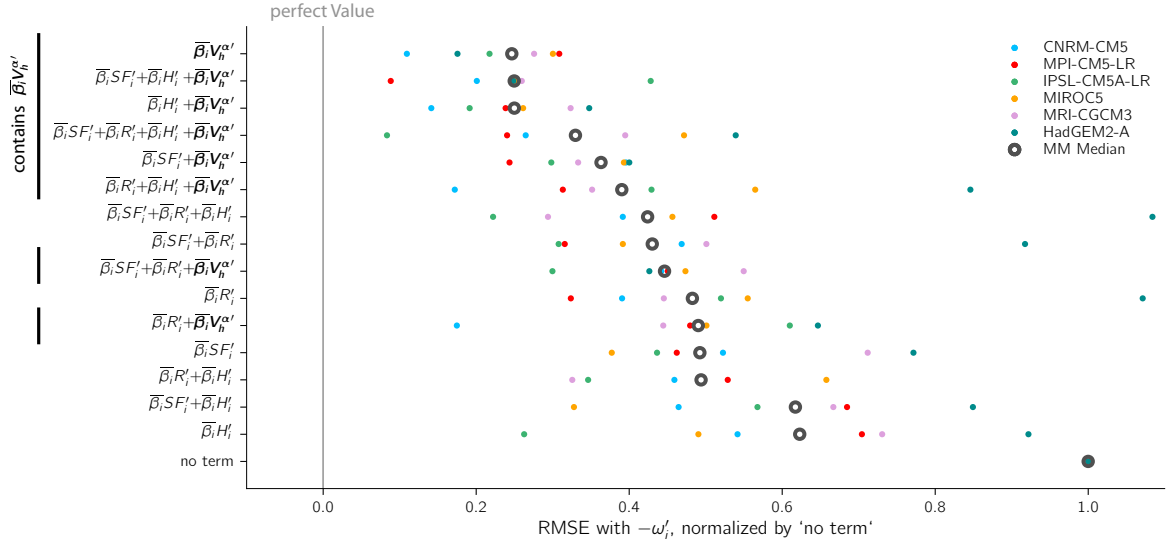


**Figure 4.8:** As in Figure 4.7 but for the sums of combinations of the individual terms in  $\bar{\beta}Q_i'$ .  $SF$  is the sum of surface sensible and latent heat flux,  $H$  the horizontal advection,  $R$  the atmospheric heating rate,  $V_h^\alpha$  the vertical advection of MSE owing to deviations from the assumed deep convective vertical velocity structure. The analysis is performed on the control clouds-off experiment.

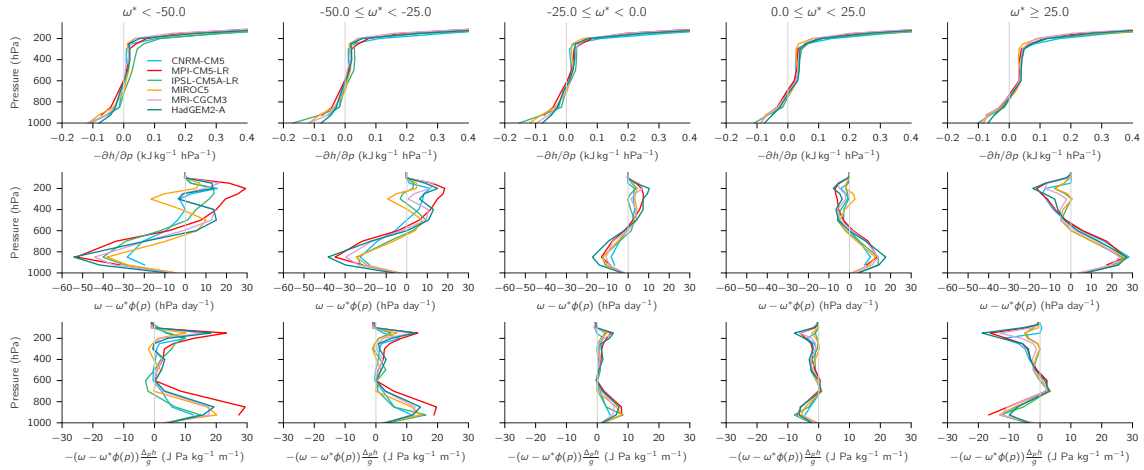


**Figure 4.9:** Vertical profiles averaged in different velocity regimes, from strong convective (left) to strong subsidence (right) of the vertical gradient of moist static energy (top row), the deviation vertical velocity from the assumed deep mode velocity (middle row), and the corresponding non-integrated  $V_h^\alpha$  term. The control clouds-off experiment was used for plotting.

vertical velocity by the assumed deep mode  $\phi$ , together with the negative lower tropospheric  $-\frac{\partial h}{\partial p}$ , results in the lower-tropospheric positive contribution to  $V_h^\alpha$  in convective areas and negative contribution in subsidence areas (Figure 4.9, bottom row). The assumed deep mode additionally overestimates the vertical velocity in the upper troposphere, enhancing the lower-tropospheric contribution to  $V_h^\alpha$ ; however the overestimation has a minor impact compared to the lower-tropospheric underestimation. Furthermore, the magnitude of  $\omega(p) - \omega^* \phi(p)$  is correlated with the magnitude of  $\omega^*$ , indicating that the velocity in the lower troposphere is systematically underestimated by the assumed top-heavy vertical velocity structure. Thus, the close relationship between the vertical velocity and  $V_h^\alpha$  arises from the deviation of the actual vertical velocity profile from the assumed generic vertical velocity structure associated with deep convection.

To understand the zonal-mean variation in the vertical velocity, understanding of the vertical advection due to secondary and higher modes of the vertical velocity profile is indispensable. However, the assumptions made in the choice of  $\phi$  (Section 4.3.1) required us to select a somewhat more top-heavy shape than what an empirical orthogonal function analysis has identified as the tropical deep mode (Yuan and Hartmann, 2008). Our assumptions may introduce deviations from the vertical velocity profile that are not necessarily related to a physical mode of spatial variability in  $\omega$ , e.g. from shallow circulations.

To test whether  $V_h^\alpha$  is still the dominant term in explaining the vertical mean vertical velocity, we repeat the previous analysis for the control clouds-off experiment, but estimate  $\phi$  with different parameters ( $a = 1.7, b = 1.8$ ) which yields a shape with a mid-tropospheric maximum, similar to the deep mode in Yuan and Hartmann (2008) or Bony et al. (2013). Due to the constraint of a positive gross moist stability (Section 4.3.1), the mid-heavy  $\phi$  could not be used for all experiments. Changing the assumed shape impacts the magnitude of the gross moist stability, and the anomalous vertical advection  $V_h^\alpha$ , which in turn impacts

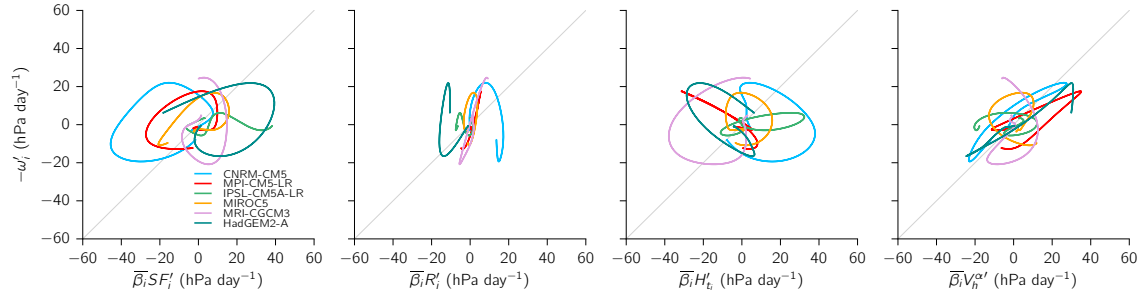


**Figure 4.10:** Anomalous vertical mean vertical velocity as a function of the decomposed four terms in  $\bar{\beta}Q'_i$ , shown for the control clouds-off experiment and calculated by using the mid-heavy  $\phi$  given by  $a = 1.7$  and  $b = 1.8$ .

not only the RMSEs of  $\bar{\beta}V_h^{\alpha'}$  but also the other terms in  $\bar{\beta}Q'_i$ . Likewise, with the mid-heavy shape the anomalous heating term  $\bar{\beta}Q'_i$  best explains the zonal-mean variations of  $-\omega'_i$ . But with the new shape, the signal of  $\bar{\beta}V_h^{\alpha'}$  becomes less clear (Figure 4.10); none of the terms systematically correlate well with  $-\omega'_i$ . Overall, the normalized RMSEs increase (not shown) compared to Figure 4.8. Also the ordering of the terms changes, with  $\bar{\beta}R'_i$  ranked as the second term of smallest normalized multi-median RMSEs, and  $\bar{\beta}V_h^{\alpha'}$  as the sixth term, whereas with the top-heavy  $\phi$  the  $\bar{\beta}V_h^{\alpha'}$  term ranked first and  $\bar{\beta}R'_i$  ranked as the tenth term. Apparently the success of the different terms comprised in  $\bar{\beta}Q'_i$  for explaining zonal-mean variations of  $\omega'_i$  partly hinges upon the assumed shape of the vertical velocity profile  $\phi$ .

The above results provide a limitation to the applicability of the framework by which the vertical mean vertical velocity is given as the ratio between a heating term and the gross moist stability (Eq. 4.5). By the constraint that the gross moist stability remains positive in all models and experiments, the export efficiency of MSE given by  $\Gamma_h$  can only be represented by a top-heavy generic vertical velocity structure in COOKIE. That the results depend sensitively on the specification of  $\phi$  in the lower troposphere, highlights the importance of column MSE import by bottom-heavy convective motion. Including bottom-heaviness of vertical motion, which is physically related to the impact of shallow convection, into the gross moist stability within our framework thus seems a next natural step. However, if the gross moist stability was expressed as the sum of a deep mode (subscript  $d$ ) and shallow mode (subscript  $s$ ), such that  $\Gamma_h = \Gamma_{h,d} + \Gamma_{h,s}$ , then  $\Gamma_h$  would become negative in parts of the tropics with shallow circulations. Then singularities in the ratio between heating and gross moist stability would exist and the framework would lose its diagnostic property.

The one-mode vertical velocity structure approach has previously been successfully applied in other models. A model of intermediate complexity, the Quasi-equilibrium Tropical Circulation Model (QTCM, Neelin and Zeng, 2000), is built upon the assumption to represent the vertical structure of temperature, humidity and the vertical velocity by one mode related to deep convection. In this one-mode configuration, the QTCM successfully predicted the gross features of the tropical convergence zones (Zeng et al., 2000). Including a second mode associated with a prognostic boundary layer only modestly improves the precipitation climatology with respect to the one-mode QTCM (Lintner et al., 2012). Back and Bretherton (2009) attempted to predict precipitation based on two modes of vertical velocity estimated



from reanalysis data also via the moist static energy budget. However, they were faced with problems in constraining the deep mode and had to revert to applying their framework to the dry static energy budget, effectively neglecting horizontal variations in moisture. We showed the diagnostic power of our one-mode framework. Despite being limited to one assumed top-heavy vertical velocity shape, the framework merits further investigation due to its simplicity.

#### 4.4.2 Influence of ACRE on the ITCZ shift

The diagnostic MSE framework presented in the previous section offers the opportunity to study the impact of atmospheric cloud radiative effects (ACREs) on the vertical velocity through the ACRE influence on the zonal-mean distribution of column MSE heating. In this section, we investigate how the ITCZ would shift if ACRE did not contribute to the MSE column heating in the control clouds-on experiment. We define  $Q_{clr}$  as the clear-sky column MSE heating, where  $Q_{clr} = Q - \text{ACRE}$  is obtained by subtracting zonal-mean ACREs from the zonal-mean  $Q$  of the control clouds-on experiment.

In all models,  $Q_{clr}$  is weaker than the total column MSE heating  $Q$  (Figure 4.11) because deep clouds heat the atmospheric column by their ACRE. Similarly to Harrop and Hartmann (2016) we find no correlation between the integrated ACRE heating and the ITCZ shift between the clouds-on and clouds-off experiment. Neither does the original ITCZ location correlate with the strength of the ITCZ shift upon inhibiting ACRE. Instead we find that the heterogeneous zonal-mean shape of ACRE has a great influence on the zonal-mean shape of the clear-sky column heating,  $Q_{clr}$ .  $Q_{clr}$  peaks at lower latitudes than  $Q$  as indicated by the dashed and solid vertical lines in Figure 4.11 (top row) in the CNRM, MPI and HadGEM models. In the IPSL model, the peak shifts equatorwards although almost non-negligibly. No shift is evident in the MRI model which has a single ITCZ. Why is the ACRE influencing the zonal-mean distribution of  $Q$ ? In the two models with the greatest ITCZ shifts (CNRM-CM5 and MPI-CM5-LR), the peak in  $Q$  is dislocated polewards from the peak in ACRE (not shown), such that removing ACREs can impact the location of the peak in  $Q_{clr}$ . In the other models, the peak in ACRE aligns with the peak in  $Q$ , implying that removing ACRE can only reduce the magnitude to smaller  $Q_{clr}$  but not the location of the peak. We compare the model zonal-mean vertical velocity  $\omega^*$  with the estimated  $\omega_{clr}^*$  (Figure 4.11, bottom row), which is diagnosed via Eq. 4.5 by using  $Q_{clr}$ . A poleward shifting peak in the heating upon removal of ACREs is indicative of a shift in the ITCZ position.

Finally we test whether the poleward shift in the ITCZ position just by considering clear-sky instead of all-sky heating is related to the observed ITCZ shift between the clouds-on and clouds-off experiment (Figure 4.12). Generally, the diagnosed shift from simply removing ACRE from the heating term is smaller than the total shift related to inhibiting cloud-radiation interaction in the models. This is not surprising, as the models can adjust to the removed heating in the atmosphere and feedbacks between the environment and the convection scheme may enhance an initial signal. With the exception of the MRI model, models that have a small diagnosed shift also tend to exhibit a small ITCZ shift between the clouds-on/off experiments and respectively for models with a greater shift. Whether there

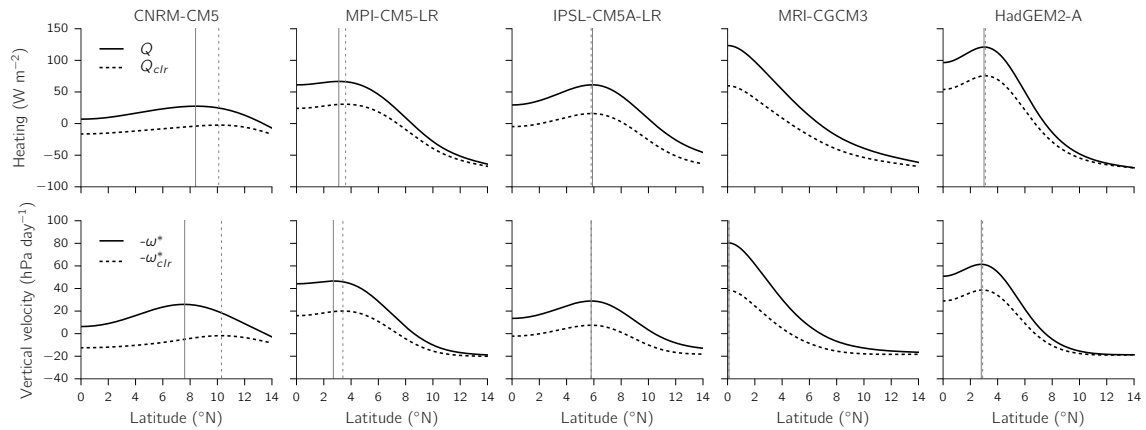


**Figure 4.11:** Comparison between the zonal-mean clear-sky heating  $Q_{clr}$  and the total heating  $Q$  for five COOKIE models in the top row, and in the bottom row between the corresponding clear-sky and total vertical mean vertical velocity ( $\omega_{clr}^*$  and  $\omega^*$ ). The analysis is shown for the control clouds-on experiment. MIROC5 is excluded because of the differing underlying SST profile from the other models. Latitudes are only shown for the northern hemisphere. The vertical lines indicate the latitude where either the clear-sky or total zonal-mean variable maximizes.

is indeed a relationship between the diagnosed and actual shift in the ITCZ is difficult to infer from just five models, of which four models show the expected behavior. However, we propose a reason for the models to initially relocate the ITCZ polewards – by subtle changes in the distribution of the column heating, it becomes easier for the models to convect more poleward if ACREs are switched off. Upon this initial ITCZ shift, the feedbacks between convection and the large-scale environment seem to shift the ITCZ even further polewards.

Recently, Harrop and Hartmann (2016) also proposed a mechanism to explain the equatorward shift of the ITCZ due to atmospheric radiative effects in the COOKIE models. Their mechanism is based on a diagnostic convective available potential energy (CAPE) approach introduced by Landu et al. (2014). Both studies estimate CAPE, which can be considered as a measure for atmospheric stability, from the monthly-mean temperature and moisture fields in COOKIE. Harrop and Hartmann (2016) find, that the cloud radiative effect of deep tropical clouds heats the upper troposphere, leading to an overall increase in atmospheric stability in the clouds-on case. The increased stability reduces CAPE. Higher specific humidity, especially in the boundary layer, increases CAPE in the clouds-on experiment. Because the temperature effect dominates over the humidity effect in contracting the ITCZ equatorwards in the clouds-on experiment, Harrop and Hartmann (2016) conclude that the ITCZ is contracted equatorwards because the upper-tropospheric temperature increases due to cloud radiative heating. However, the temperature structure of the tropics is also determined by the moist adiabat in the areas of stronger convection (e.g. Johnson and Xie, 2010). As the ITCZ is located further equatorward because of cloud radiative effects, upper-tropospheric temperatures will follow a warmer moist adiabat and consequently be more stable. The estimated CAPE is simply a result of the temperature and humidity structure, which in turn are set by the circulation. The hypothesized temperature effect on

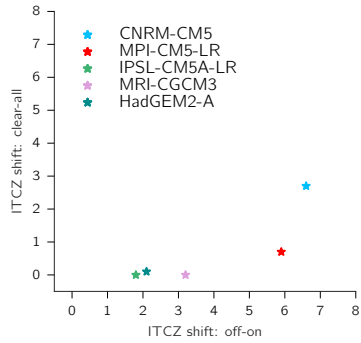


**Figure 4.12:** Comparison of the ITCZ shift as found by the difference in ITCZ location between the clouds-off and clouds-on experiment, and the ITCZ shift as diagnosed by considering  $Q_{clr}$  and  $Q$ . The comparison is shown for the control experiment.

CAPE may therefore partly be a result of the ITCZ shift itself and the argument is circular to some degree.

Because of the design of COOKIE it was possible to show that the interaction between radiation and clouds shifts the ITCZ equatorwards by Harrop and Hartmann (2016) and the current study. While their argument is based on a zonally homogeneous increase in atmospheric stability owing to cloud radiative effects leading to a contraction of high CAPE values towards the equator, our argument is based on the heterogeneous effect that clouds have in heating the atmosphere. Both approaches are based on a diagnostic analysis and cannot disentangle the feedbacks between the circulation and the environment, which have been shown to strongly impact the ITCZ position (e.g. Möbis and Stevens, 2012).

## 4.5 Summary

We introduce a framework derived from the moist static energy (MSE) budget with which the vertical mean vertical velocity can be diagnosed as the ratio of a column-integrated heating term and the gross moist stability. The heating term contains the diabatic heating from the surface turbulent heat fluxes, the radiative heating, and the import or export of moist static energy from horizontal advection as well as a vertical advection term associated with the import of MSE from deviations in the vertical velocity profile from the assumed deep-mode vertical velocity structure. This assumed vertical velocity structure is used in the estimation of the normalized vertical advection related to deep convection, as expressed by the gross moist stability. For the applicability of the framework, the vertical velocity structure is defined such that the gross moist stability remains positive in all COOKIE simulations. For that, a top-heavy vertical velocity structure had to be chosen. With the help of the framework, the zonal-mean vertical mean vertical velocity can be diagnosed with only a negligible residual.

In applying the framework, we find that the zonal-mean variation in the vertical advection associated with the deviation from the assumed shape ( $V_h^\alpha$ ) is the best predictor of the ver-

tical mean vertical velocity consistently among models and experiments. As  $V_h^\alpha$  represents the import or export of column MSE due to deviations of the assumed from the actual vertical velocity profile, this term highlights the importance of shallow convection for importing MSE into the column, and thus destabilizing the troposphere, such that deep convection can occur. Unfortunately, the degree to which  $V_h^\alpha$  explains the vertical mean vertical velocity depends on the choice of the vertical velocity structure.

Nevertheless, we also find that the other source terms, the sensible and latent heat flux as well as the horizontal advection of MSE, are less successful in explaining the zonal-mean vertical mean vertical velocity from a diagnostic point of view. Variations in the gross moist stability are less important in explaining the vertical velocity than variations in the heating term. This implies that for understanding what drives the tropical circulation it is fundamental to understand the controls on the diabatic heating.

Finally, we attempt to explain why inhibiting cloud-radiation interaction leads to a poleward shift of the ITCZ with the help of the diagnostic framework. In addition to the diagnosed vertical velocity estimated using the total heating term, we can estimate the vertical velocity when the ACRE is subtracted from the total heating. In four of five models, for which this analysis was possible, the estimated ITCZ shift owing to the missing ACRE is related to the ITCZ shift between the clouds-on to the clouds-off experiment. In these models, the diagnosed peak in the vertical mean vertical velocity shifts because the peak in ACRE does not coincide with the peak in the total heating term. In the MRI model, we diagnose a zero shift in the ITCZ position. As it has a single ITCZ, the peak in ACRE is aligned with the peak in the heating term. However, upon turning off cloud-radiation interaction the ITCZ still shifts polewards in the MRI model.

As our analysis is based on a diagnostic framework we cannot expect to be able to explain the full behavior of the ITCZ. The location of the ITCZ is strongly determined by subtleties in the representation of moist convective processes and how convection interacts with the large-scale environment. However, our results point out that the heterogeneous distribution of ACRE with respect to the column heating by surface turbulent heat fluxes, clear-sky radiative cooling, and MSE import by horizontal and anomalous vertical advection may be important for explaining the shift of the ITCZ once cloud-radiation interaction is inhibited.

## 5 Conclusions

The present thesis investigates the intermodel spread in state-of-the-art general circulation model simulations of precipitation and its change with warming. Previous work has highlighted the large spread in both the simulation of global-mean precipitation with warming as well as the spatial pattern change of tropical precipitation (Hawkins and Sutton, 2011; Knutti and Sedláček, 2013; Xie et al., 2015) compared to, for example, the simulation of temperature and temperature change.

A careful reading of the literature suggests that part of the discrepancy in reported global-mean precipitation rate of increase with surface warming, often termed “hydrological sensitivity”, is due to an ambiguous use of the term. For one, the term has been used to refer to the total rate of global-mean precipitation increase with surface warming. And second, only the temperature-mediated global-mean precipitation rate of increase with surface warming was considered. The latter definition explicitly separates between the temperature-mediated precipitation response and the direct precipitation changes to e.g. changing atmospheric CO<sub>2</sub> occurring on fast time scales without changes in the surface temperature. The direct precipitation response is called “adjustment” ( $A$ ). To help distinguish the different definitions in the present thesis as well as in future work, a consistent terminology is proposed. We refer to the temperature-mediated precipitation rate of increase with warming as “hydrological sensitivity parameter” ( $\eta$ ) and to the other definition as “apparent hydrological sensitivity parameter” ( $\eta_a$ ). When estimating  $\eta$ , we find a small spread with a factor of 1.5 difference between models, which increases by 35% when estimating  $\eta_a$  in the same experiment. The spread is greater for  $\eta_a$ , because the spread in the adjustments is intermingled with that of the temperature-mediated precipitation response. The conundrum of large versus small global-mean precipitation rate increase in the literature can be resolved with a consistent terminology. The terminology proposed in the present thesis has begun to be adopted in other work (Samset et al., 2016; Myhre et al., submitted).

Further, we make use of the atmospheric energetic constraint on global-mean precipitation to understand how climate feedbacks drive the intermodel spread in  $\eta$  and  $A$ . Typical climate feedbacks on the surface temperature are: the surface albedo, the cloud, the water vapor, and the temperature feedback (separated into lapse-rate changes and uniform warming). Because changes in these variables modify the atmospheric radiation budget, they also impact both  $\eta$  and  $A$ . To investigate impacts of climate feedbacks on the intermodel spread in  $\eta$  and  $A$ , we apply the radiative kernel technique (Soden et al., 2008) to the atmospheric heat budget changes. Of all climate feedbacks, the intermodel spread is largest in the hydrological sensitivity parameter of clouds and the combined effect of lapse-rate plus water vapor. In particular, the intermodel spread in the latter can be traced to model disagreement in how the lower-tropospheric tropical temperature and humidity structure changes with warming. A non-negligible residual in the decomposition of  $A$  hinders conclusions about the causes

for intermodel spread. Nevertheless, our analysis suggests that the spread in fast global-mean precipitation response to lapse-rate and cloud changes may be important also for the intermodel spread in  $A$ .

The adjustment, and consequently the hydrological sensitivity parameter, can only be estimated from idealized step-like forcing experiments, as for example abruptly quadrupling the atmospheric  $\text{CO}_2$  concentration. With a simple linear model, we show that estimates of  $A$  and  $\eta$  from the  $4\times\text{CO}_2$  experiment serve to predict global-mean precipitation changes also in a transient  $\text{CO}_2$  increase experiment. The small spread found in  $\eta$  raises confidence that it is a characteristic quantity to describe temperature-mediated precipitation changes. Recently, the Precipitation Driver Response Model Intercomparison Project (PDRMIP, Samset et al., 2016) provides idealized simulations with step-like forcing changes of black carbon, the solar constant, sulfur, methane and  $\text{CO}_2$ , in a multi-model context. Initial results (Appendix B) from PDRMIP suggest that the magnitude of  $\eta$  is indeed independent of the individual forcing. This independence of  $\eta$  supports our general argument of Chapter 2 – the precipitation response to a forcing should be separately viewed in the context of the hydrological sensitivity parameter and the precipitation adjustment. So doing indicates that to disentangle the twentieth century global-mean precipitation trend in models it is important to understand and quantify the precipitation adjustments to forcings such as aerosols, the solar constant and greenhouse gases.

The spatial distribution of tropical precipitation patterns and their changes with warming is less well constrained than the global-mean precipitation. The large intermodel spread in regional precipitation has been related to the dynamical precipitation response in the tropics (Xie et al., 2015) which is determined by changes in the vertical velocity. Going one step further, Voigt and Shaw (2015) focus on the impact of cloud radiative effect (CRE) changes on the tropical circulation in two models with very different precipitation responses to warming in a very idealized aquaplanet setup. Their results suggest that diverse CRE changes constitute the root cause for the difference in the tropical circulation response between the two models. We explore the impact of CRE on tropical precipitation and circulation quantities in a larger model ensemble provided by the Clouds On-Off Klimate Intercomparison Experiment (COOKIE, Stevens et al., 2012). For a few quantities removing CREs reduces the model spread, for instance in the tropical mean precipitation or in the magnitude of peak precipitation at the intertropical convergence zone (ITCZ). However, we find a larger intermodel spread in the tropical circulation organization, which contradicts the expectation from Voigt and Shaw (2015) that model results would become more similar in the absence of cloud-radiation interaction. In particular, for the experiments where the cloud-radiation interaction is inhibited we find: a greater spread in tropical-mean  $\eta$ ; a greater spread in the simulated position of the ITCZ; and an overall more diverse organization of the tropical circulation especially in the inter-ITCZ region at and near the equator. It becomes clear that different representations of atmospheric CRE are not the root cause for intermodel differences in the tropical precipitation and circulation. Our analysis suggests that the seed for intermodel differences in spatial precipitation patterns is present in the absence of cloud-radiation interaction.

We develop a simple diagnostic framework to investigate the diverse model response in how the ITCZ shifts polewards upon inhibiting cloud-radiation interaction. Because we

---

find that precipitation and vertical velocity are strongly related, it suffices to understand the vertical velocity. Our framework is derived from the column-integrated moist static energy budget, which represents the coupling between radiation, surface turbulent fluxes and the circulation. The framework diagnoses the vertical mean vertical velocity as the ratio between column heating terms and the gross moist stability. The gross moist stability (e.g. Neelin and Held, 1987) can be defined by assuming that the tropical vertical velocity can be expressed by a generic vertical velocity structure associated with deep convection. The vertical velocity's amplitude is given by the vertical mean vertical velocity. The gross moist stability represents the efficiency with which large-scale motion exports moist static energy (MSE) from the column. The residual between the model and diagnosed vertical velocity is small, such that the framework can be applied to separately understand the influence of column heating and the gross moist stability. To avoid singularities in the framework, the assumed mode of vertical velocity has to be specified such that the gross moist stability is positive everywhere. The framework then yields the behavior expected from physical reasoning, namely that to support convective motion, less heating is needed when the gross moist stability is low. Building upon the longstanding success of conceptual models of the tropical dynamics based on the MSE budget, in this thesis we develop a framework that directly diagnoses the vertical velocity from known fields of heating and stability. With that, a new diagnostic tool to explore the controls on the tropical vertical velocity is available that ranges in complexity between the two-layer model by Neelin and Held (1987) and the more sophisticated models for tropical dynamics that are coupled to radiation, cloud and land surface schemes (e.g. Neelin and Zeng, 2000).

From applying the framework to the COOKIE aquaplanet simulations, several findings emerge. The zonal-mean vertical velocity on the aquaplanets is controlled by zonal-mean variations in the heating term rather than the gross moist stability. This opposes the common conception that the gross moist stability represents a decisive quantity to understand how the large-scale flow controls convection (Raymond et al., 2009). While indeed the gross moist stability is low in regions with convective motion, it is nevertheless the heterogeneous distribution of column heating that best explains the distribution of the vertical velocity in the COOKIE simulations. The heating term is comprised of surface turbulent fluxes, the atmospheric cooling, the horizontal advection, and an anomalous vertical advection term associated with the deviation vertical velocity from the assumed deep-mode velocity structure. Of the various heating terms, the anomalous vertical advection term individually explains most of the tropical vertical velocity distribution. However, the choice of the assumed vertical velocity structure somewhat influences the importance of the anomalous vertical advection. This dependence on the assumed structure represents a caveat to the framework proposed in this study. Nevertheless, that neither the gross moist stability, nor the distribution of surface latent or sensible heat flux strongly determine the vertical velocity distribution emerges as a finding independent of the specified vertical velocity structure.

With the help of the framework we propose a possible explanation for why the ITCZ shifts polewards when the cloud-radiation interaction is inhibited in the COOKIE aquaplanet simulations. The atmospheric radiation consists of a clear-sky and a cloudy-sky component in the simulations where clouds are active. By merely considering the clear-sky radiative contribution to the column heating, the cloud radiative effect can be extracted from the total

heating. With that, the vertical velocity due to clear-sky components can be diagnosed. We find that the heterogeneous atmospheric cloud radiative heating by deep clouds with respect to the remaining clear-sky heating terms is key to explain the shift in the ITCZ. If the peak of the cloud radiative heating aligns with the peak of the clear-sky heating terms, the ITCZ will not shift in the experiment where cloud radiative effects are inhibited. When, however, the peak clear-sky heating is situated more poleward than the peak cloud radiative heating, then the peak in the diagnosed vertical velocity shifts polewards; and with it the ITCZ. This explanation holds true in four of five investigated models. Understanding the heterogeneous nature of cloud radiative heating by deep clouds with respect to the other heating terms of the MSE budget is the key to understand the shifting ITCZ upon inhibiting cloud radiative effects in aquaplanet simulations.

In summary, this thesis explored the intermodel spread in precipitation and its change with warming in many different aspects. From the investigation of global-mean spread, a new terminology emerged that helped reconcile the varying estimates in the literature concerning the rate of precipitation increase with warming. By emphasizing the need to explicitly separate between the hydrological sensitivity parameter and the adjustment, the importance of adjustments was highlighted. There is as of yet little understanding on how the global-mean precipitation adjustment responds to changes in the temperature, humidity, and clouds induced by modifications of the atmospheric composition. In terms of the intermodel spread in the tropical precipitation patterns and circulation, focus was placed on the importance of clouds. Contrary to the expectation that simplifying the problem by inhibiting cloud-radiation interaction, we found that a considerable intermodel spread persists, especially in the organization of the tropical circulation and location of the ITCZ position. To answer the exciting question, which physical process may constitute the key cause for intermodel differences in the tropical precipitation distribution, remains a challenge.



## A Supplementary material to Chapter 2

### A.1 Temperature and water vapor kernels

Any interpretation of radiative decomposition of precipitation changes using the radiative kernel method depends on the applied kernel. The temperature kernel used in this study (Figure A1, left column) compares well with the one in Previdi (2010, their Figure 1) in terms of magnitude and structure. However, differences are found in the longwave water vapor kernel (Previdi (2010, their Figure 2) vs. Figure A1, middle column). In Previdi

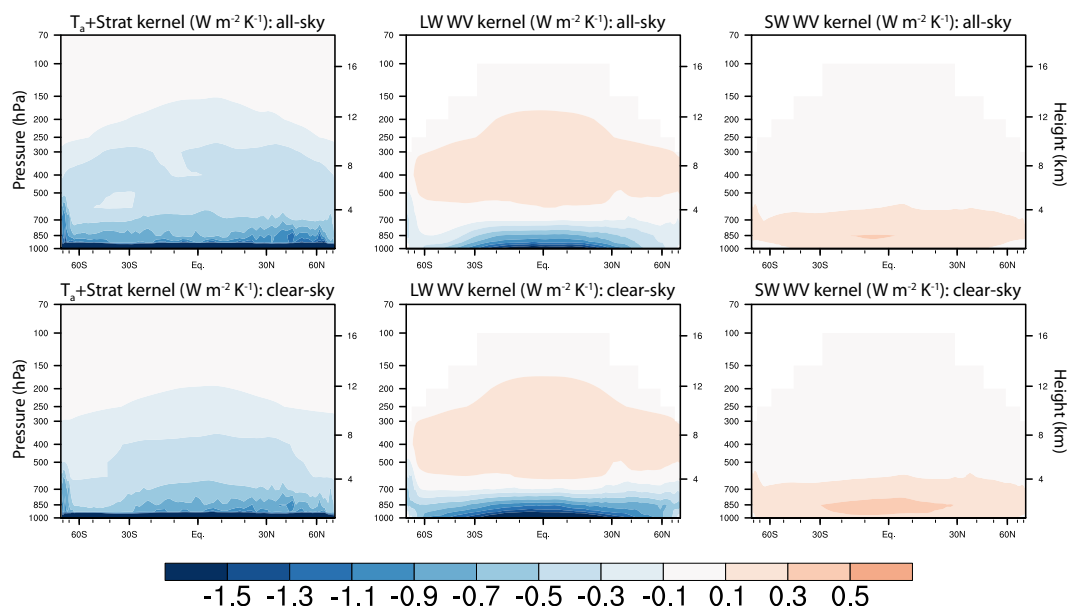


**Figure A1:** Annual zonal mean temperature and water vapor kernels used for the radiative decomposition of precipitation change with warming in Section 5a. Atmospheric heating due to a uniform raise of atmospheric temperatures by 1 K (left), the heating of water vapor change due to a 1 K warming at constant relative humidity is separated into the longwave (middle) and shortwave (right) components. The all-sky (top) and clear-sky (bottom) are shown. Data is weighted by the depth of the corresponding pressure level.

(2010), the longwave cooling due to water vapor increases from a 1 K warming at constant relative humidity is of similar magnitude in the lower troposphere as the longwave warming in the middle and upper troposphere. In the water vapor kernel used here, the lower-tropospheric cooling is larger than the warming by more than a factor of three. Here, the longwave (LW) component of  $\eta_{WV}$  enhances precipitation increase ( $\eta_{WV, LW} = -0.66 \pm 0.07 \text{ W m}^{-2} \text{ K}^{-1}$ ). The negative sign might arise because changes in water vapor in the

lower troposphere are weighted more strongly and thus dominate the sign of the vertically integrated  $\eta_{\text{WV, LW}}$  contrary to Previdi (2010) who finds  $\eta_{\text{WV, LW}} = 0.29 \text{ W m}^{-2} \text{ K}^{-1}$ . The values of the shortwave (SW) component of  $\eta_{\text{WV}}$  ( $\eta_{\text{WV, SW}} = 0.87 \pm 0.07 \text{ W m}^{-2} \text{ K}^{-1}$  here and  $0.98 \text{ W m}^{-2} \text{ K}^{-1}$  in Previdi (2010)) are commensurate.

## A.2 Testing for influences on the adjustment residual

### A.2.1 Non-linearity of $\Delta R_x$ with $\Delta T_s$

The employed regression method assumes linear changes of  $\Delta R_x$  with  $\Delta T_s$ . The evolution of  $\Delta R_x$  with  $\Delta T_s$  is quasi-linear for most of the models and for all  $x$  besides  $\Delta R_{\text{LR}}$  and  $\Delta R_{\text{WV}}$  (not shown). The strongest non-linear behavior is found for the GFDL models in the lapse-rate and water vapor response, where the slope changes at approximately  $\Delta T_s = 2.5 \text{ K}$  (or after approximately 5 years). This issue extends to the estimates of the  $\eta$  decomposition. Nevertheless, the adjustment estimates are affected more strongly than the  $\eta$  decomposition as it relies on a good estimate of the slope during the beginning years of an abrupt forcing experiment; the estimate of the hydrological sensitivity parameter, however, is dominated by the weight of the remaining years. In fact, the GFDL models yield the lowest estimates of the lapse-rate adjustment (not shown) and thus represent the models with the greatest residual. The median of the adjustment residual does not strongly reduce when  $A_x$  are calculated from the regression over the first 10 years ( $2.29 \text{ W m}^{-2}$  vs.  $2.50 \text{ W m}^{-2}$ ). Even when excluding the GFDL models from the decomposition, the residual remains at  $1.95 \text{ W m}^{-2} \text{ K}^{-1}$ . The non-linearity does not appear to explain the offset of the residual.

### A.2.2 Internal variability

To test whether the residual in the adjustment radiative decomposition arises because the regression method does not account for internal variability, we estimate the adjustment of the radiative atmospheric heat budget from CMIP5 fixed SST experiments, where sea surface temperatures are held fixed for a subset of piControl years (sstClim), and  $\text{CO}_2$  concentrations are quadrupled (sstClim4xCO2). The change of the equilibrium mean radiative atmospheric fluxes gives the fast adjustment of precipitation (Hansen et al., 2005; Bala et al., 2010), which is then decomposed as described in Section 5a. Among other difficulties, this method features the disadvantage, that global mean  $\Delta T_s \neq 0$  due to land surface warming (Sherwood et al., 2015). We account for this additional warming by comparing the adjustments of the regression and fixed SST methods at the global mean  $\Delta T_s$  found for the given model from the fixed SST experiment. The comparison is performed for the intersection of 12 available fixed SST and abrupt4xCO2 models (BNU-ESM is excluded as it provides an unreasonably low global mean longwave surface emittance of  $271.35 \text{ W m}^{-2} \text{ K}^{-1}$  for a mean surface temperature of  $286.95 \text{ K}$ ).

Although the comparison of methods points out some differences for the decomposed adjustment, the offset in the residual is only slightly reduced (Figure A2). Differences in

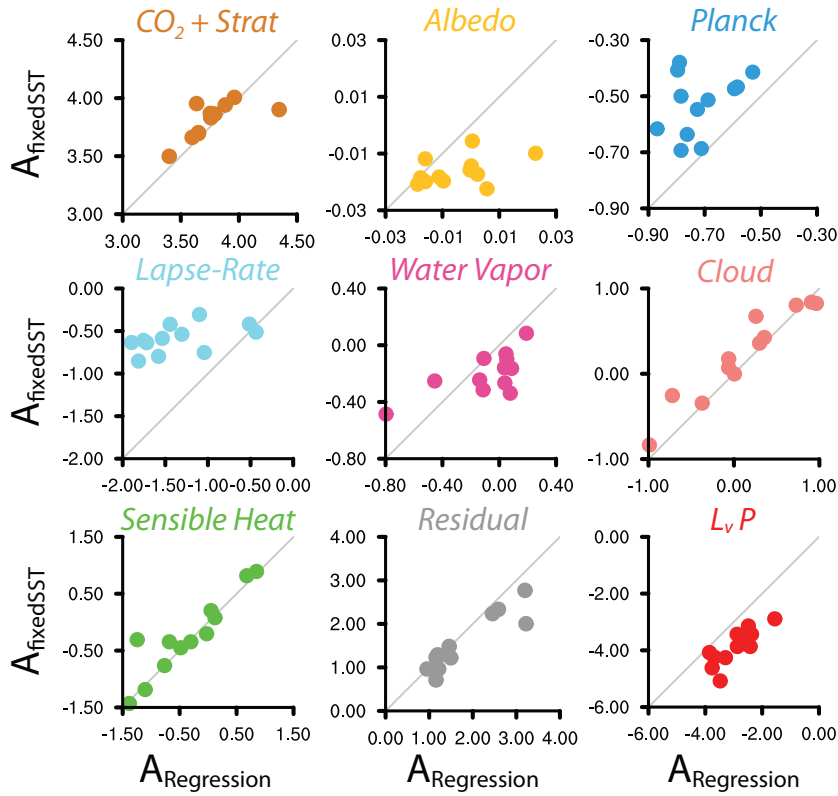


**Figure A2:** Comparison of adjustment estimates with two calculation methods: regression method for abrupt4xCO<sub>2</sub> experiment and fixed-SST method for sstClim4xCO<sub>2</sub> experiment. Dots represent individual models. The line with a slope of one is shown in gray.

the surface albedo, Planck and water vapor adjustment will not appreciably modify the residual, because their values are small compared to the residual. The CO<sub>2</sub>+Stratospheric temperature, cloud and sensible heat flux adjustment agree well among both methods. The lapse-rate adjustment is less negative in the fixed SST method, probably due to different land temperature changes in the fixed SST experiment. The less negative lapse-rate adjustment in the fixed SST method leads to a greater  $\sum_x \Delta R_x$ , and with that, contributes to the slightly reduced offset in the residual (medians of fixed SST and regression method are  $1.27 \text{ W m}^{-2}$  vs.  $1.34 \text{ W m}^{-2}$  for the subset of 12 models). It remains open, though, whether the different lapse-rate adjustment estimate is an indication that the regression method overestimates fast lapse-rate changes, or whether the actual fast lapse-rate changes are underestimated because the coupling between SST and the atmosphere is disabled in the sstClim experiments.



## B Hydrological sensitivity parameter estimates from PDRMIP

During the course of this thesis I performed simulations with the coupled MPI-ESM1.1-LR model (revision 7931) for the Precipitation Driver and Response Model Intercomparison Project (PDRMIP, Samset et al., 2016). This project aims at investigating the separate precipitation responses to idealized step-like forcing changes in black carbon, the solar constant, sulfur, methane and CO<sub>2</sub> with respect to present-day concentrations. Specifically, the concentrations are increased tenfold for black carbon (BC×10), twofold for CO<sub>2</sub> (CO<sub>2</sub>×2), threefold for methane (CH<sub>4</sub>×3), fivefold for sulfur (SO<sub>4</sub>×5), and the solar constant is increased by 2%. Nine models participated in this initiative: CanESM2, GISS-E2, HadGEM2, HadGEM3-GA4, MPI-ESM1.1, NCAR CESM1 CAM4, NCAR CESM1 CAM5, NorESM1, and MIROC-SPRINTARS. All models performed all forcing simulations, with the exception of our model for which the BC×10 experiment was not possible.

Some studies have pointed out that the rate of temperature-mediated precipitation increase with warming – “hydrological sensitivity parameter” ( $\eta$ ) in our terminology – is more similar for different forcing agents, than the total precipitation increase with warming termed “apparent hydrological sensitivity parameter” ( $\eta_a$ ), e.g. Andrews et al. (2009); Andrews et al. (2010); Kvalevåg et al. (2013). However, these studies were based on individual model results which raised the question whether  $\eta$  is indeed independent of the forcing in other models as well. The PDRMIP framework yields the first opportunity to explore the dependence of  $\eta$  on idealized forcing changes in a multi-model context.

Indeed, the multi-model mean  $\eta$  is independent of the forcing agent (Figure B1a), ranging from  $2.14 \text{ W m}^{-2} \text{ K}^{-1}$  to  $2.53 \text{ W m}^{-2} \text{ K}^{-1}$ . These values correspond well to  $\eta = 2.24 \text{ W m}^{-2} \text{ K}^{-1}$  as estimated from the abrupt4xCO<sub>2</sub> experiment of the CMIP5 model ensemble. Not only is the magnitude of the multi-model mean similar among the forcing agents, but also the intermodel spread of  $\eta$ . Figure B1b shows the dispersion, given as the ratio between intermodel standard deviation and the multi-model mean, to again allow a better comparison to the spread in the CMIP5 ensemble. The dispersion in PDRMIP is commensurate to that in the CMIP5 ensemble. The precipitation response to increases in black carbon concentration presents the only exception. For this forcing agent, the models’ precipitation response is very diverse. The diverse model response to black carbon changes may be due to the different ways through which black carbon can interact with the atmospheric heat budget; it can both directly absorb and scatter solar radiation, through heating it can modify the stability, and it can change the cloud microphysical properties. Nevertheless, we could show from the analysis of PDRMIP, that the hydrological sensitivity parameter is a characteristic quantity to express precipitation changes in response to surface temperature changes. The hydrological sensitivity parameter is more meaningful than the apparent hydrological sensitivity

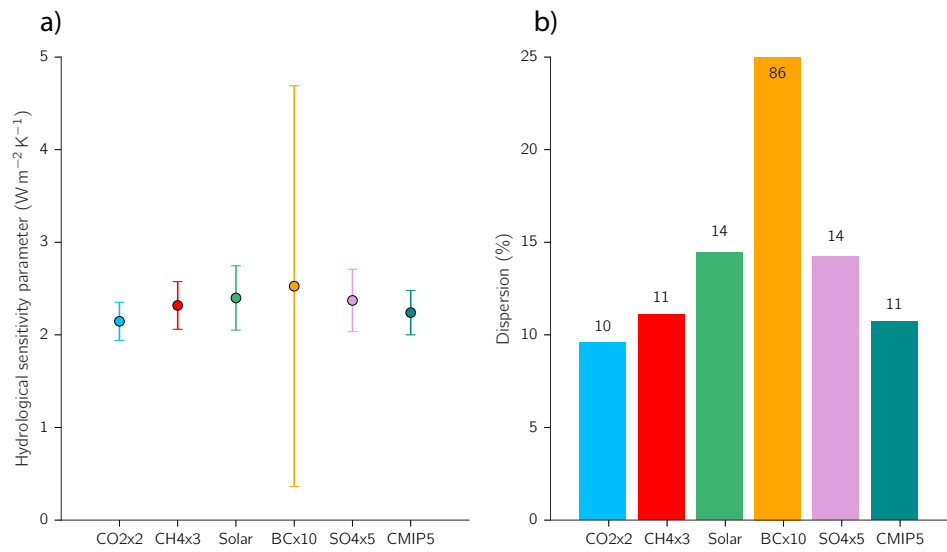


**Figure B1:** a) Hydrological sensitivity parameter estimated for the PDRMIP experiments and *abrupt4xCO2* from the CMIP5 model ensemble. Dots represent the multi-model mean, and error bars show one intermodel standard deviation. b) The dispersion for the experiments in a) given by the multi-model standard deviation normalized by the mean.

parameter for which temperature-independent precipitation adjustments are intermingled with the temperature-mediated precipitation response.

## List of Figures

- 1.1 Illustration of the processes that influence the atmospheric heat budget. The net atmospheric radiation is given by the difference of top-of-atmosphere (TOA) and surface radiative fluxes. Longwave and shortwave radiative fluxes are abbreviated by LW and SW, respectively. Blue arrows denote the latent and sensible heat fluxes (LH and SH). Well-mixed greenhouse gases ( $\text{GHG}_{\text{wm}}$ ) are for example carbon dioxide or methane. . . . . 4
- 1.2 Illustration of how the cloud-radiation interaction is manipulated in the Clouds On-Off Klimate Intercomparison Experiment. Longwave and shortwave radiative fluxes are abbreviated by LW and SW, respectively. . . . . 8
- 1.3 Illustration of the constraints on the tropical precipitation. The radiation and circulation are strongly coupled in that they both depend on and influence the temperature ( $T$ ) and humidity ( $q$ ) structure, the clouds, and the atmospheric composition (e.g. by transporting chemical species). The radiation and surface turbulent fluxes both influence and depend on the near-surface vertical temperature and humidity gradients. The circulation and surface fluxes are coupled by the wind-induced surface heat exchange (WISHE), which constitutes a positive feedback. A stronger circulation enhances the transport of heat from the surface to the atmosphere through stronger surface winds. A stronger heat input from the surface in turn enhances convection and strengthens the circulation. Because the vertical velocity determines the precipitation, understanding the coupling between radiation, surface turbulent fluxes and the circulation is a prerequisite to advance understanding of the tropical precipitation distribution. . . . . 9
- 2.1 Illustration of the terminology for precipitation change with surface temperature change adopted in this work, by the example of abrupt4xCO2 data from IPSL-CM5A-LR. The “hydrological sensitivity parameter” ( $\eta$ ) is the slope of the global-mean precipitation response with respect to surface temperature change when explicitly taking into account the rapid “Adjustment” of precipitation due to forcing agents. The “apparent hydrological sensitivity parameter” ( $\eta_a$ ) is given by the slope of global time-mean responses without accounting for rapid precipitation adjustments. The equilibrium precipitation change due to a quadrupling of  $\text{CO}_2$  is denoted as “equilibrium hydrological sensitivity” at  $4\times\text{CO}_2$  ( $\text{EHS}_{4\times}$ ). Small circles signify annual global-means, and large circles the endpoint and equilibrium mean. . . . . 14
- 2.2 Comparison of the slope of precipitation change with respect to surface temperature change for different definitions of the slope and different CMIP5 experiments. a) The spread is shown as Gaussian curves, as given by the ensemble mean and standard deviation of the hydrological sensitivity parameter ( $\eta$ ) and the apparent hydrological sensitivity parameter ( $\eta_a$ ). b) The ensemble standard deviation is scaled by the ensemble mean to yield the dispersion. Table 2.2 lists the parameter values for all models. . . . . 17

- 2.3 a) Evolution of annual mean precipitation change ( $\Delta P$ ) with corresponding surface temperature change ( $\Delta T_s$ ) in the 1pctCO2 experiment, with respect to the climatological mean in piControl. Gray thin lines show actual model results, and colored thick lines the predicted precipitation change following Eq. 2.2. b) Absolute deviation of predicted and model  $\Delta P$ . All colored lines are smoothed by a 5-year running average. The gray shading ranges from  $-0.80$  to  $0.86 \text{ W m}^{-2}$ . All 1pctCO2 experiments from Table 2.2 are shown, except GFDL-ESM2M and GFDL-ESM2G as our analysis suggests that their CO<sub>2</sub> increase stopped after 70 years. . . . . 21
- 2.4 a) Adjustment ( $A$ ), hydrological sensitivity parameter ( $\eta$ ), and Equilibrium Climate Sensitivity for a quadrupling of CO<sub>2</sub> ( $ECS_{4\times}$ ) in the 28 abrupt4xCO2 models. Dots denote the Equilibrium Hydrological Sensitivity for a quadrupling of CO<sub>2</sub> ( $EHS_{4\times}$ ), where dot size increases for larger  $EHS_{4\times}$ . Colors darken for increasing  $ECS_{4\times}$ . b) Contributions to spread in  $EHS_{4\times}$  from  $A$ ,  $\eta$  and  $ECS_{4\times}$ ; estimated via Eq. 2.1, by setting 2 of the three factors to their corresponding ensemble-mean values. The standard deviations of  $\Delta P$  due to variation of the free factors are normalized by the actual standard deviation in equilibrium  $\Delta P$ . Note that normalized standard deviations do not add to unity. . . . . 22
- 2.5 Contributions of surface warming, hydrological sensitivity parameter, adjustment and residual to the sum of their respective normalized standard deviation ( $\hat{\sigma}_i$ ) as a function of years after the  $4\times\text{CO}_2$  forcing. Note the logarithmic timescale. The  $\hat{\sigma}_i$  are estimated as in Figure 2.4b but for annual mean standard deviations of  $\Delta P$ . The residual contribution is given by the portion of normalized standard deviation of differences between model and calculated  $\Delta P$  following Eq. 2.1. . . . . 23
- 2.6 a) Decomposition of the hydrological sensitivity parameter ( $\eta$ ) for 26 abrupt4xCO2 models. Box-whisker-plots show the minimum and maximum as the whiskers; the box shows the 1st quartile, the median and the 3rd quartile as horizontal lines. The residual is the difference between model  $\Delta R/\Delta T_s$  and  $\sum_x \eta_x$ . b) Vertical separation of  $\eta_{\text{LR+WV}}$  into the lower (pressure  $p > 700 \text{ hPa}$ ), middle ( $700 \text{ hPa} \geq p > 400 \text{ hPa}$ ) and upper ( $400 \text{ hPa} \geq p \geq 100 \text{ hPa}$ ) troposphere. The lower tropospheric  $\eta_{\text{LR+WV}}$  is further separated into regions and shown here for the tropics (equatorward of  $\pm 30^\circ$ ), the mid-latitudes ( $\pm 30^\circ$  to  $\pm 60^\circ$ ) and the poles (poleward of  $\pm 60^\circ$ ). For any separation, first  $\Delta R_x$  is vertically integrated at each grid point and month, then if applicable, regionally averaged and last regressed against global annual-mean  $\Delta T_s$ . . . . . 26
- 2.7 Decomposition of the atmospheric heat budget adjustment derived from 26 models performing the abrupt4xCO2 experiment. More details are provided in the caption of Figure 2.6. . . . . 28
- 2.8 Comparison of the decomposed hydrological sensitivity parameter ( $\eta$ ) between coupled (abrupt4xCO2) and noncoupled (amip4K & amipFuture) experiments. Analysis is performed analogously to Figure 2.6a, but for a common set of 8 available coupled and noncoupled models. . . . . 31



3.1	Precipitation change ( $\Delta P$ ) in response to a 4 K uniform warming for the MPI-CM5-LR and IPSL-CM5A-LR models (left and right column). The response is shown for the clouds-on and clouds-off simulations (top and bottom row). . . . .	34
3.2	Sea surface temperature in the control clouds-off simulation in the tropics. The thick dashed line corresponds to the ‘Qobs’ profile. . . . .	37
3.3	Relationship of tropical precipitation with the vertical mean vertical velocity ( $\omega^*$ ). The precipitation is averaged in bins of $\omega^*$ of 5 hPa day <sup>-1</sup> . Negative $\omega^*$ denote convective regimes, and positive $\omega^*$ denote subsidence regimes. . . . .	38
3.4	Comparison of tropical mean precipitation between the clouds-on and clouds-off simulations in the control state. . . . .	39
3.5	Change in the tropical atmospheric heat budget terms between the clouds-on and clouds-off simulations ( $\Delta =\text{on-off}$ ) in the control state. MIROC5 is not shown because of strong differences in the underlying SSTs in the clouds-on versus clouds-off simulations. . . . .	39
3.6	Comparison of the tropical hydrological sensitivity parameter ( $\eta$ ) between the clouds-on and clouds-off simulations. . . . .	40
3.7	Comparison of the change in the tropical heat budget with warming between the clouds-on and clouds-off simulations. All terms are normalized by the tropical mean surface temperature change with warming. . . . .	41
3.8	a) Position and b) strength of the ITCZ in the COOKIE simulations. . . . .	42
3.9	The relationship of mean tropical upwards and subsidence pressure velocity at 500 hPa ( $\omega_{500}$ ) with the subsidence fraction ( $A\downarrow$ ) in the COOKIE simulations. The vertical gray line marks the border between convective (negative $\omega_{500}$ ) and subsidence regime (positive $\omega_{500}$ ). The vertical velocities according to a low static stability of 0.035 K hPa <sup>-1</sup> and a high static stability of 0.058 K hPa <sup>-1</sup> are marked by the dotted and dashed lines respectively when assuming a radiative cooling rate of 1 K day <sup>-1</sup> . . . . .	44
3.10	Probability density function of the vertical pressure velocity at 500 hPa ( $\text{PDF}_{\omega_{500}}$ ) in the control clouds-on (top row) and control clouds-off (bottom row) experiment. The total tropical $\text{PDF}_{\omega_{500}}$ (left column) is separated into the $\text{PDF}_{\omega_{500}}$ considering only tropical areas poleward of the ITCZ latitude (middle column) and equatorward of the ITCZ latitude (right column). The respective fractions of tropical areas is given in percent. The data is binned by 5 hPa day <sup>-1</sup> . . . . .	45
3.11	Relationship between the mean vertical velocity at 500 hPa ( $\omega_{500}$ ) averaged over the area between the double ITCZs and the ITCZ latitude. . . . .	46
4.1	Illustration of the net column moist static energy and vertical velocity associated with shallow and deep convection. . . . .	51
4.2	a) Vertical pressure gradient of the moist static energy with height in the clouds-off control experiment, horizontally averaged between the double ITCZs. b) Profiles of the vertical velocity profile ( $\phi$ ) assumed in the study of Bony et al. (2013) (dashed line) and in this study (solid line) with a surface and tropopause placed at 1013 hPa and 100 hPa respectively. . . . .	54
4.3	Gross moist stability ( $\Gamma_h$ ) of the control clouds-off and clouds-on experiments (left column) and its change with warming (right column). Clouds-off and clouds-on simulations are shown in the top and bottom row, respectively. . . . .	56

- 4.4 Time zonal-mean of the individual terms comprised in the heating term  $Q$  shown for the control clouds-off experiment. Note the different choice of value ranges for each term, but for all subplots a total range of  $140 \text{ W m}^{-2}$  is shown. 57
- 4.5 a) Vertical mean vertical velocity ( $-\omega^*$ ) diagnosed with Eq. 4.5 for the control clouds-off experiment and b) the difference between diagnosed and model  $-\omega^*$  for all four experiments. . . . . 58
- 4.6 Anomalous vertical mean vertical velocity as a function of its decomposition into four terms given by Eq. 4.7 for the control clouds-off experiment. . . . . 59
- 4.7 Normalized root mean square error (RMSE) between the zonal-mean of the expression given on the  $y$ -Axis and zonal-mean  $-\omega'_i$ . The RMSE is normalized by the ‘no term’ which is the RMSE between  $-\bar{\omega}$  and  $-\omega'_i$ . Small dots are individual models, the multi-model median of normalized RMSE is shown by dark gray circles. The terms are ordered by the multi-model median. The analysis is performed on the control clouds-off experiment. . . . . 59
- 4.8 As in Figure 4.7 but for the sums of combinations of the individual terms in  $\bar{\beta}Q'_i$ .  $SF$  is the sum of surface sensible and latent heat flux,  $H$  the horizontal advection,  $R$  the atmospheric heating rate,  $V_h^\alpha$  the vertical advection of MSE owing to deviations from the assumed deep convective vertical velocity structure. The analysis is performed on the control clouds-off experiment. . . 60
- 4.9 Vertical profiles averaged in different velocity regimes, from strong convective (left) to strong subsidence (right) of the vertical gradient of moist static energy (top row), the deviation vertical velocity from the assumed deep mode velocity (middle row), and the corresponding non-integrated  $V_h^\alpha$  term. The control clouds-off experiment was used for plotting. . . . . 61
- 4.10 Anomalous vertical mean vertical velocity as a function of the decomposed four terms in  $\bar{\beta}Q'_i$ , shown for the control clouds-off experiment and calculated by using the mid-heavy  $\phi$  given by  $a = 1.7$  and  $b = 1.8$ . . . . . 62
- 4.11 Comparison between the zonal-mean clear-sky heating  $Q_{clr}$  and the total heating  $Q$  for five COOKIE models in the top row, and in the bottom row between the corresponding clear-sky and total vertical mean vertical velocity ( $\omega_{clr}^*$  and  $\omega^*$ ). The analysis is shown for the control clouds-on experiment. MIROC5 is excluded because of the differing underlying SST profile from the other models. Latitudes are only shown for the northern hemisphere. The vertical lines indicate the latitude where either the clear-sky or total zonal-mean variable maximizes. . . . . 64
- 4.12 Comparison of the ITCZ shift as found by the difference in ITCZ location between the clouds-off and clouds-on experiment, and the ITCZ shift as diagnosed by considering  $Q_{clr}$  and  $Q$ . The comparison is shown for the control experiment. . . . . 65

- 
- A1 Annual zonal mean temperature and water vapor kernels used for the radiative decomposition of precipitation change with warming in Section 5a. Atmospheric heating due to a uniform raise of atmospheric temperatures by 1 K (left), the heating of water vapor change due to a 1 K warming at constant relative humidity is separated into the longwave (middle) and shortwave (right) components. The all-sky (top) and clear-sky (bottom) are shown. Data is weighted by the depth of the corresponding pressure level. . . . . 71
- A2 Comparison of adjustment estimates with two calculation methods: regression method for abrupt4xCO<sub>2</sub> experiment and fixed-SST method for sst-Clim4xCO<sub>2</sub> experiment. Dots represent individual models. The line with a slope of one is shown in gray. . . . . 73
- B1 a) Hydrological sensitivity parameter estimated for the PDRMIP experiments and *abrupt4xCO<sub>2</sub>* from the CMIP5 model ensemble. Dots represent the multi-model mean, and error bars show one intermodel standard deviation. b) The dispersion for the experiments in a) given by the multi-model standard deviation normalized by the mean. . . . . 76



## List of Tables

2.1	Comparison between the literature and this study for estimates of the slope of precipitation change with respect to surface temperature change. $\eta$ denotes the hydrological sensitivity parameter and $\eta_a$ the apparent hydrological sensitivity parameter. The absolute spread shows the lowest and highest model estimate ( $\text{W m}^{-2} \text{K}^{-1}$ , values in parantheses have the unit $\% \text{K}^{-1}$ ). The factor of spread is the approximate ratio between the lowest and highest model estimate. The dispersion ( $\%$ ) is the ensemble standard deviation divided by the ensemble mean. . . . .	12
2.2	Values of the hydrological sensitivity parameter ( $\eta$ ) and the apparent hydrological sensitivity parameter ( $\eta_a$ ) from different CMIP5 experiments. All values are in $\text{W m}^{-2} \text{K}^{-1}$ or for abrupt4xCO2 additionally in parantheses in $\% \text{K}^{-1}$ . Error estimates are given as plus or minus one standard error from the ordinary least squares regression. Ensemble error is plus or minus one ensemble standard deviation. The models are ordered such that their $\eta$ value in the abrupt4xCO2 simulation increases. Data has been horizontally interpolated to a common Gaussian T63 grid prior to analysis. . . . .	18
2.3	Comparison of the regression and the endpoint method. The regression method applied to abrupt4xCO2 yields $\eta$ , all other estimates yield $\eta_a$ . Values shown are the ensemble mean plus or minus one ensemble standard deviation and in parantheses are the minimum-maximum range of model values. Units are $\text{W m}^{-2} \text{K}^{-1}$ . . . . .	19
3.1	Aquaplanet COOKIE models used in this study. . . . .	36



## Bibliography

- Abe, M., H. Shiogama, T. Yokohata, S. Emori, and T. Nozawa (2015). “Asymmetric impact of the physiological effect of carbon dioxide on hydrological responses to instantaneous negative and positive CO<sub>2</sub> forcing”. *Climate Dynamics*, pp. 1–12.
- Allen, M. R. and W. J. Ingram (2002). “Constraints on future changes in climate and the hydrologic cycle”. *Nature*, **419**, pp. 224–232.
- Andrews, T., P. Forster, and J. M. Gregory (2009). “A Surface Energy Perspective on Climate Change”. *Journal of Climate*, **22**, pp. 2557–2570.
- Andrews, T., M. Doutriaux-Boucher, O. Boucher, and P. Forster (2011). “A regional and global analysis of carbon dioxide physiological forcing and its impact on climate”. *Climate Dynamics*, **36**, no. 3-4, pp. 783–792.
- Andrews, T., P. Forster, O. Boucher, N. Bellouin, and A. Jones (2010). “Precipitation, radiative forcing and global temperature change”. *Geophysical Research Letters*, **37**, no. 14, n/a–n/a.
- Arora, V. K., J. F. Scinocca, G. J. Boer, J. R. Christian, K. L. Denman, G. M. Flato, V. V. Kharin, W. G. Lee, and W. J. Merryfield (2011). “Carbon emission limits required to satisfy future representative concentration pathways of greenhouse gases”. *Geophysical Research Letters*, **38**, no. 5, p. L05805.
- Back, L. E. and C. S. Bretherton (2006). “Geographic variability in the export of moist static energy and vertical motion profiles in the tropical Pacific”. *Geophysical Research Letters*, **33**, no. 17. L17810, n/a–n/a.
- Back, L. E. and C. S. Bretherton (2009). “A Simple Model of Climatological Rainfall and Vertical Motion Patterns over the Tropical Oceans”. *Journal of Climate*, **22**, no. 23, pp. 6477–6497.
- Bala, G., K. Caldeira, and R. Nemani (2010). “Fast versus slow response in climate change: implications for the global hydrological cycle”. *Climate Dynamics*, **35**, no. 2-3, pp. 423–434.
- Bala, G., P. B. Duffy, and K. E. Taylor (2008). “Impact of geoengineering schemes on the global hydrological cycle”. *Proceedings of the National Academy of Sciences*, **105**, no. 22, pp. 7664–7669.

- Bao, Q., P. Lin, T. Zhou, Y. Liu, Y. Yu, G. Wu, B. He, J. He, L. Li, et al. (2013). “The Flexible Global Ocean-Atmosphere-Land system model, Spectral Version 2: FGOALS-s2”. *Advances in Atmospheric Sciences*, **30**, no. 3, pp. 561–576.
- Barnes, E. A. and R. J. Barnes (2015). “Estimating Linear Trends: Simple Linear Regression versus Epoch Differences”. *J. Climate*, **28**, no. 24, pp. 9969–9976.
- Barrios, S., L. Bertinelli, and E. Strobl (2010). “Trends in Rainfall and Economic Growth in Africa: A Neglected Cause of the African Growth Tragedy”. *Review of Economics and Statistics*, **92**, no. 2, pp. 350–366.
- Barsugli, J., S.-I. Shin, and P. D. Sardeshmukh (2005). “Tropical Climate Regimes and Global Climate Sensitivity in a Simple Setting”. *Journal of the Atmospheric Sciences*, **62**, no. 4, pp. 1226–1240.
- Bentsen, M., I. Bethke, J. B. Debernard, T. Iversen, A. Kirkevåg, Ø. Seland, H. Drange, C. Roelandt, I. A. Seierstad, et al. (2013). “The Norwegian Earth System Model, NorESM1-M – Part 1: Description and basic evaluation of the physical climate”. *Geosci. Model Dev.* **6**, no. 3, pp. 687–720.
- Bergman, J. W. and H. H. Hendon (2000). “Cloud Radiative Forcing of the Low-Latitude Tropospheric Circulation: Linear Calculations”. *J. Atmos. Sci.* **57**, no. 14, pp. 2225–2245.
- Bi, D., M. Dix, S. J. Marsland, S. O’Farrell, H. A. Rashid, P. Uotila, A. C. Hirst, E. Kowalczyk, M. Golebiewski, et al. (Mar. 2013). “The ACCESS coupled model: description, control climate and evaluation”. *Australian Meteorological and Oceanographic Journal*, **63**, no. 1, pp. 41–64.
- Bjerknes, J. (1938). “Saturated-adiabatic ascent of air through dry-adiabatically descending environment”. *Quarterly Journal of the Royal Meteorological Society*, **64**, pp. 325–330.
- Block, K. and T. Mauritsen (2013). “Forcing and feedback in the MPI-ESM-LR coupled model under abruptly quadrupled CO<sub>2</sub>”. *Journal of Advances in Modeling Earth Systems*, **5**, no. 4, pp. 676–691.
- Boer, G. J. (1993). “Climate change and the regulation of the surface moisture and energy budgets”. *Climate Dynamics*, **8**, pp. 225–239.
- Bony, S., G. Bellon, D. Klocke, S. Sherwood, S. Fermepin, and S. Denvil (2013). “Robust direct effect of carbon dioxide on tropical circulation and regional precipitation”. *Nature Geosciences*, **6**, no. 6, pp. 447–451.
- Bony, S., R. Colman, V. Kattsov, R. Allan, C. Bretherton, J.-L. Dufresne, A. Hall, S. Hallegatte, M. Holland, et al. (2006). “How Well Do We Understand and Evaluate Climate Change Feedback Processes?” *Journal of Climate*, **19**, 3445–3482.



- Bony, S., J.-L. Dufresne, H. Le Treut, J.-J. Morcrette, and C. Senior (2004). “On dynamic and thermodynamic components of cloud changes”. *Climate Dynamics*, **22**, no. 2-3, pp. 71–86.
- Bony, S., B. Stevens, D. Coppin, T. Becker, K. Reed, A. Voigt, and B. Medeiros (2016). “Thermodynamic control of anvil-cloud amount”. *Proceedings of the National Academy of Sciences of the United States of America*, **submitted**, pages.
- Bony, S. and J.-L. Dufresne (2005). “Marine boundary layer clouds at the heart of tropical cloud feedback uncertainties in climate models”. *Geophysical Research Letters*, **32**, no. 20, n/a–n/a.
- Bony, S., M. J. Webb, C. Bretherton, S. Klein, P. Siebesma, G. Tselioudis, and M. Zhang (2011). “CFMIP: Towards a better evaluation and understanding of clouds and cloud feedbacks in CMIP5 models”. *CLIVAR Exchanges*, **16**, no. 56, pp. 20–24.
- Boucher, O., D. Randall, P. Artaxo, C. Bretherton, G. Feingold, P. Forster, V.-M. Kerminen, Y. Kondo, H. Liao, et al. (2013). “Clouds and Aerosols”. *Climate Change 2013: The Physical Science Basis. Contribution of Working Group I to the Fifth Assessment Report of the Intergovernmental Panel on Climate Change*. Ed. by T. Stocker, D. Qin, G.-K. Plattner, M. Tignor, S. Allen, J. Boschung, A. Nauels, Y. Xia, V. Bex, and P. Midgley. Cambridge, United Kingdom and New York, NY, USA: Cambridge University Press. Chap. 7, 571–658.
- Cess, R. D., G. L. Potter, J. P. Blanchet, G. J. Boer, A. D. Del Genio, M. Deque, V. Dymnikov, V. Galin, W. L. Gates, et al. (1990). “Intercomparison and interpretation of climate feedback processes in 19 atmospheric general circulation models”. *Journal of Geophysical Research: Atmospheres*, **95**, no. D10, pp. 16601–16615.
- Chadwick, R., I. Boutle, and G. Martin (2013). “Spatial Patterns of Precipitation Change in CMIP5: Why the Rich Do Not Get Richer in the Tropics”. *Journal of Climate*, **26**, no. 11, pp. 3803–3822.
- Chadwick, R., P. Good, T. Andrews, and G. Martin (2014). “Surface warming patterns drive tropical rainfall pattern responses to CO<sub>2</sub> forcing on all timescales”. *Geophysical Research Letters*, **41**, no. 2, pp. 610–615.
- Chao, W. C. and B. Chen (2004). “Single and double ITCZ in an aqua-planet model with constant sea surface temperature and solar angle”. *Climate Dynamics*, **22**, no. 4, pp. 447–459.
- Charney, J. G., A. Arakawa, D. J. Baker, B. Bolin, R. E. Dickinson, R. M. Goody, C. E. Leith, H. M. Stommel, and C. I. Wunch (1979). *Carbon dioxide and climate: A scientific assessment*. Tech. rep.
- Chou, C. and J. D. Neelin (2004). “Mechanisms of Global Warming Impacts on Regional Tropical Precipitation”. *J. Climate*, **17**, no. 13, pp. 2688–2701.

- Chou, C., J. D. Neelin, C.-A. Chen, and J.-Y. Tu (2009). “Evaluating the “Rich-Get-Richer” Mechanism in Tropical Precipitation Change under Global Warming”. *Journal of Climate*, **22**, no. 8, pp. 1982–2005.
- Chou, C., J. D. Neelin, J.-Y. Tu, and C.-T. Chen (2006). “Regional Tropical Precipitation Change Mechanisms in ECHAM4/OPYC3 under Global Warming”. *Journal of Climate*, **19**, no. 17, pp. 4207–4223.
- Chou, C., T.-C. Wu, and P.-H. Tan (2013). “Changes in gross moist stability in the tropics under global warming”. *Climate Dynamics*, **41**, no. 9, pp. 2481–2496.
- Collins, M., R. Knutti, J. Arblaster, J.-L. Dufresne, T. Fichefet, P. Friedlingstein, X. Gao, W. Gutowski, T. Johns, et al. (2013). “Long-term Climate Change: Projections, Commitments and Irreversibility”. *Climate Change 2013: The Physical Science Basis. Contribution of Working Group I to the Fifth Assessment Report of the Intergovernmental Panel on Climate Change*. Ed. by T. Stocker, D. Qin, G.-K. Plattner, M. Tignor, S. Allen, J. Boschung, A. Nauels, Y. Xia, V. Bex, and P. Midgley. Cambridge, United Kingdom and New York, NY, USA: Cambridge University Press. Chap. 12, 1029–1136.
- Collins, W. J., N. Bellouin, M. Doutriaux-Boucher, N. Gedney, P. Halloran, T. Hinton, J. Hughes, C. D. Jones, M. Joshi, et al. (2011). “Development and evaluation of an Earth-System model – HadGEM2”. *Geosci. Model Dev.* **4**, no. 4, pp. 1051–1075.
- Dahms, E., H. Borth, F. Lunkeit, and K. Fraedrich (2011). “ITCZ Splitting and the Influence of Large-Scale Eddy Fields on the Tropical Mean State”. *Journal of the Meteorological Society of Japan. Ser. II*, **89**, no. 5, pp. 399–411.
- Dai, A. (2006). “Precipitation Characteristics in Eighteen Coupled Climate Models”. *Journal of Climate*, **19**, no. 18, pp. 4605–4630.
- Dai, A. (2013). “Increasing drought under global warming in observations and models”. *Nature Clim. Change*, **3**, no. 1, pp. 52–58.
- deMenocal, P. B. and J. E. Tierney (2012). “Green Sahara: African Humid Periods Paced by Earth’s Orbital Changes”. *Nature Education Knowledge*, **3(10):12**.
- Donner, L. J., B. L. Wyman, R. S. Hemler, L. W. Horowitz, Y. Ming, M. Zhao, J.-C. Golaz, P. Ginoux, S. J. Lin, et al. (2011). “The Dynamical Core, Physical Parameterizations, and Basic Simulation Characteristics of the Atmospheric Component AM3 of the GFDL Global Coupled Model CM3”. *J. Climate*, **24**, no. 13, pp. 3484–3519.
- Dufresne, J.-L. and S. Bony (2008). “An assessment of the primary sources of spread of global warming estimates from coupled atmosphere-ocean models”. *Journal of Climate*, **21**, 5135–5144.
- Dufresne, J.-L., M. A. Foujols, S. Denvil, A. Caubel, O. Marti, O. Aumont, Y. Balkanski, S. Bekki, H. Bellenger, et al. (2013). “Climate change projections using the IPSL-CM5 Earth System Model: from CMIP3 to CMIP5”. *Climate Dynamics*, **40**, no. 9-10, pp. 2123–2165.

- Dunne, J. P., J. G. John, A. J. Adcroft, S. M. Griffies, R. W. Hallberg, E. Shevliakova, R. J. Stouffer, W. Cooke, K. A. Dunne, et al. (2012). “GFDL’s ESM2 Global Coupled Climate–Carbon Earth System Models. Part I: Physical Formulation and Baseline Simulation Characteristics”. *J. Climate*, **25**, no. 19, pp. 6646–6665.
- Durack, P. J., S. E. Wijffels, and R. J. Matear (2012). “Ocean Salinities Reveal Strong Global Water Cycle Intensification During 1950 to 2000”. *Science*, **336**, no. 6080, pp. 455–458.
- Fermepin, S. and S. Bony (2014). “Influence of low-cloud radiative effects on tropical circulation and precipitation”. *Journal of Advances in Modeling Earth Systems*, **6**, no. 3, pp. 513–526.
- Frieler, K., M. Meinshausen, T. Schneider von Deimling, T. Andrews, and P. Forster (2011). “Changes in global-mean precipitation in response to warming, greenhouse gas forcing and black carbon”. *Geophys. Res. Lett.* **38**, no. 4, n/a–n/a.
- Giorgetta, M. A., J. Jungclaus, C. H. Reick, S. Legutke, J. Bader, M. Böttinger, V. Brovkin, T. Crueger, M. Esch, et al. (2013). “Climate and carbon cycle changes from 1850 to 2100 in MPI-ESM simulations for the Coupled Model Intercomparison Project phase 5”. *Journal of Advances in Modeling Earth Systems*, **5**, no. 3, pp. 572–597.
- Good, P., W. Ingram, F. H. Lambert, J. A. Lowe, J. M. Gregory, M. J. Webb, M. A. Ringer, and P. Wu (2012). “A step-response approach for predicting and understanding non-linear precipitation changes”. *Climate Dynamics*, **39**, no. 12, pp. 2789–2803.
- Graham, N. E. and T. P. Barnett (1987). “Sea Surface Temperature, Surface Wind Divergence, and Convection over Tropical Oceans”. *Science*, **238**, no. 4827, pp. 657–659.
- Gregory, J. M., W. J. Ingram, M. A. Palmer, G. S. Jones, P. A. Stott, R. B. Thorpe, J. A. Lowe, T. C. Johns, and K. D. Williams (2004). “A new method for diagnosing radiative forcing and climate sensitivity”. *Geophysical Research Letters*, **31**, no. 3, n/a–n/a.
- Hansen, J., M. Sato, R. Ruedy, L. Nazarenko, A. Lacis, G. A. Schmidt, G. Russell, I. Aleinov, M. Bauer, et al. (2005). “Efficacy of climate forcings”. *Journal of Geophysical Research: Atmospheres*, **110**, no. D18, n/a–n/a.
- Harrop, B. E. and D. L. Hartmann (2016). “The role of cloud radiative heating in determining the location of the ITCZ in aqua planet simulations”. *J. Climate*, pages.
- Hartmann, D. L., A. Klein Tank, M. Rusticucci, L. Alexander, S. Brönnimann, Y. Charabi, F. Dentener, E. Dlugokencky, D. Easterling, et al. (2013). “Observations: Atmosphere and Surface”. *Climate Change 2013: The Physical Science Basis. Contribution of Working Group I to the Fifth Assessment Report of the Intergovernmental Panel on Climate Change*. Ed. by T. Stocker, D. Qin, G.-K. Plattner, M. Tignor, S. Allen, J. Boschung, A. Nauels, Y. Xia, V. Bex, and P. Midgley. Cambridge, United Kingdom and New York, NY, USA: Cambridge University Press. Chap. 2, 159–254.

- Hartmann, D. L. and K. Larson (2002). “An important constraint on tropical cloud – climate feedback”. *Geophysical Research Letters*, **29**, no. 20, 4 pp.
- Hawkins, E. and R. Sutton (2009). “The Potential to Narrow Uncertainty in Regional Climate Predictions”. *Bull. Amer. Meteor. Soc.* **90**, no. 8, pp. 1095–1107.
- Hawkins, E. and R. Sutton (2011). “The potential to narrow uncertainty in projections of regional precipitation change”. *Climate Dynamics*, **37**, no. 1, pp. 407–418.
- Hegerl, G. C., E. Black, R. P. Allan, W. J. Ingram, D. Polson, K. E. Trenberth, R. S. Chadwick, P. A. Arkin, B. B. Sarojini, et al. (2015). “Challenges in Quantifying Changes in the Global Water Cycle”. *Bull. Amer. Meteor. Soc.* **96**, no. 7, pp. 1097–1115.
- Held, I. M. and B. J. Soden (2006). “Robust Responses of the Hydrological cycle to Global Warming”. *Journal of Climate*, **19**, pp. 5686–5698.
- Hourdin, F., J.-Y. Grandpeix, C. Rio, S. Bony, A. Jam, F. Cheruy, N. Rochetin, L. Fairhead, A. Idelkadi, et al. (Apr. 2013). “LMDZ5B: the atmospheric component of the IPSL climate model with revisited parameterizations for clouds and convection”. *Climate Dynamics*, **40**, no. 9-10, pp. 2193–2222.
- Inoue, K. and L. E. Back (2015a). “Column-Integrated Moist Static Energy Budget Analysis on Various Time Scales during TOGA COARE”. *J. Atmos. Sci.* **72**, no. 5, pp. 1856–1871.
- Inoue, K. and L. E. Back (2015b). “Gross Moist Stability Assessment during TOGA COARE: Various Interpretations of Gross Moist Stability”. *Journal of the Atmospheric Sciences*, **72**, no. 11, pp. 4148–4166.
- Ji, D., L. Wang, J. Feng, Q. Wu, H. Cheng, Q. Zhang, J. Yang, W. Dong, Y. Dai, et al. (2014). “Description and basic evaluation of BNU-ESM version 1”. *Geosci. Model Dev. Discuss.* **7**, no. 2, pp. 1601–1647.
- Jiménez Cisneros, B. E., T. Oki, N. W. Arnell, G. Benito, J. G. Cogley, P. Döll, T. Jiang, and S. S. Mwakalila (2014). “Freshwater resources”. *Climate Change 2014: Impacts, Adaptation, and Vulnerability. Part A: Global and Sectoral Aspects. Contribution of Working Group II to the Fifth Assessment Report of the Intergovernmental Panel of Climate Change*. Ed. by C. B. Field, V. R. Barros, D. J. Dokken, K. J. Mach, M. D. Mastrandrea, T. E. Bilir, M. Chatterjee, K. L. Ebi, Y. O. Estrada, et al. Cambridge, United Kingdom and New York, NY, USA: Cambridge University Press, pages.
- Johnson, N. C. and S.-P. Xie (2010). “Changes in the sea surface temperature threshold for tropical convection”. *Nature Geosci.* **3**, no. 12, pp. 842–845.
- Kamae, Y., M. Watanabe, T. Ogura, M. Yoshimori, and H. Shiogama (2015). “Rapid Adjustments of Cloud and Hydrological Cycle to Increasing CO<sub>2</sub>: A Review”. *Current Climate Change Reports*, **1**, no. 2, pp. 103–113.

- Kharin, V. V., F. W. Zwiers, X. Zhang, and M. Wehner (2013). “Changes in temperature and precipitation extremes in the CMIP5 ensemble”. *Climatic Change*, **119**, no. 2, pp. 345–357.
- Kirtman, B. P. and E. K. Schneider (2000). “A Spontaneously Generated Tropical Atmospheric General Circulation”. *Journal of the Atmospheric Sciences*, **57**, no. 13, pp. 2080–2093.
- Knutti, R., D. Masson, and A. Gettelman (2013). “Climate model genealogy: Generation CMIP5 and how we got there”. *Geophysical Research Letters*, **40**, no. 6, pp. 1194–1199.
- Knutti, R. and J. Sedláček (Apr. 2013). “Robustness and uncertainties in the new CMIP5 climate model projections”. *Nature Clim. Change*, **3**, no. 4, pp. 369–373.
- Kuper, R. and S. Kröpelin (2006). “Climate-Controlled Holocene Occupation in the Sahara: Motor of Africa’s Evolution”. *Science*, **313**, no. 5788, pp. 803–807.
- Kvalevåg M. M.ag, M. M., B. H. Samset, and G. Myhre (2013). “Hydrological sensitivity to greenhouse gases and aerosols in a global climate model”. *Geophysical Research Letters*, **40**, no. 7, pp. 1432–1438.
- Lambert, F. H. and M. R. Allen (2009). “Are Changes in Global Precipitation Constrained by the Tropospheric Energy Budget?” *J. Climate*, **22**, no. 3, pp. 499–517.
- Lambert, F. H. and M. J. Webb (2008). “Dependency of global mean precipitation on surface temperature”. *Geophysical Research Letters*, **35**, no. 16, n/a–n/a.
- Landu, K., L. R. Leung, S. Hagos, V. Vinoj, S. A. Rauscher, T. Ringler, and M. Taylor (Dec. 2014). “The Dependence of ITCZ Structure on Model Resolution and Dynamical Core in Aquaplanet Simulations”. *J. Climate*, **27**, no. 6, pp. 2375–2385.
- Li, G., S. P. Harrison, P. J. Bartlein, K. Izumi, and I. Colin Prentice (2013). “Precipitation scaling with temperature in warm and cold climates: An analysis of CMIP5 simulations”. *Geophysical Research Letters*, **40**, no. 15, pp. 4018–4024.
- Li, Y., D. W. J. Thompson, and S. Bony (2015). “The Influence of Atmospheric Cloud Radiative Effects on the Large-Scale Atmospheric Circulation”. *Journal of Climate*, **28**, no. 18, pp. 7263–7278.
- Liepert, B. G. and M. Previdi (2009). “Do Models and Observations Disagree on the Rainfall Response to Global Warming?” *Journal of Climate*, **22**, no. 11, pp. 3156–3166.
- Lintner, B. R., G. Bellon, A. H. Sobel, D. Kim, and J. D. Neelin (2012). “Implementation of the Quasi-equilibrium Tropical Circulation Model 2 (QTCM2): Global simulations and convection sensitivity to free tropospheric moisture”. *Journal of Advances in Modeling Earth Systems*, **4**, no. 4. M12002, n/a–n/a.

- Liu, Y., L. Guo, G. Wu, and Z. Wang (2010). “Sensitivity of ITCZ configuration to cumulus convective parameterizations on an aqua planet”. *Climate Dynamics*, **34**, no. 2, pp. 223–240.
- Ma, J. and S.-P. Xie (2013). “Regional Patterns of Sea Surface Temperature Change: A Source of Uncertainty in Future Projections of Precipitation and Atmospheric Circulation”. *Journal of Climate*, **26**, no. 8, pp. 2482–2501.
- MacDonald, G. M. (2010). “Water, climate change, and sustainability in the southwest”. *Proceedings of the National Academy of Sciences*, **107**, no. 50, pp. 21256–21262.
- Mauritsen, T., R. Graversen, D. Klocke, P. Langen, B. Stevens, and L. Tomassini (2013). “Climate feedback efficiency and synergy”. *Climate Dynamics*, **41**, no. 9-10, pp. 2539–2554.
- Mauritsen, T., B. Stevens, E. Roeckner, T. Crueger, M. Esch, M. Giorgetta, H. Haak, J. H. Jungclaus, D. Klocke, et al. (2012). “Tuning the climate of a global model”. *Journal of Advances in Modeling Earth Systems*, **4**, M00A01.
- Mechoso, C., A. Robertson, N. Barth, M. Davey, P. Delecluse, P. Gent, S. Ineson, B. Kirtman, M. Latif, et al. (1995). “The Seasonal Cycle over the Tropical Pacific in Coupled Ocean–Atmosphere General Circulation Models”. *Monthly Weather Review*, **123**, no. 9, pp. 2825–2838.
- Medeiros, B., B. Stevens, and S. Bony (2015). “Using aquaplanets to understand the robust responses of comprehensive climate models to forcing”. *Climate Dynamics*, **44**, no. 7, pp. 1957–1977.
- Meehl, G. A., W. M. Washington, J. M. Arblaster, A. Hu, H. Teng, C. Tebaldi, B. N. Sanderson, J.-F. Lamarque, A. Conley, et al. (Dec. 2011). “Climate System Response to External Forcings and Climate Change Projections in CCSM4”. *J. Climate*, **25**, no. 11, pp. 3661–3683.
- Mitchell, J., C. Wilson, and W. Cunningham (1987). “On CO<sub>2</sub> climate sensitivity and model dependence of results”. *Quarterly Journal of the Royal Meteorological Society*, **113**, pp. 293–322.
- Möbis, B. and B. Stevens (2012). “Factors controlling the position of the Intertropical Convergence Zone on an aquaplanet”. *Journal of Advances in Modeling Earth Systems*, **4**, no. 4, n/a–n/a.
- Muller, C. J. and P. A. O’Gorman (2011). “An energetic perspective on the regional response of precipitation to climate change”. *Nature Clim. Change*, **1**, no. 5, pp. 266–271.
- Myhre, G., P. Forster, B. Samset, Ø. Hodnebrog, J. Sillmann, T. Andrews, O. Boucher, G. Faluvegi, D. Fläschner, et al. (submitted). “PDRMIP: A Precipitation Driver and Response Model Intercomparison Project, Protocol and preliminary results”. *Bulletin of the American Meteorological Society*, -, pages.

- Neale, R. B. and B. J. Hoskins (2001). “A standard test for AGCMs including their physical parametrizations: I: the proposal”. *Atmospheric Science Letters*, **1**, no. 2, pp. 101–107.
- Neelin, J. D. and I. M. Held (1987). “Modeling Tropical Convergence Based on the Moist Static Energy Budget”. *Monthly Weather Review*, **115**, no. 1, pp. 3–12.
- Neelin, J. D. and N. Zeng (2000). “A Quasi-Equilibrium Tropical Circulation Model—Formulation”. *Journal of the Atmospheric Sciences*, **57**, no. 11, pp. 1741–1766.
- Newell, R. E., G. F. Herman, S. Gould-Stewart, and M. Tanaka (1975). “Decreased global rainfall during the past Ice Age”. *Nature*, **253**, no. 5486, pp. 33–34.
- Numaguti, A. (1993). “Dynamics and Energy Balance of the Hadley Circulation and the Tropical Precipitation Zones: Significance of the Distribution of Evaporation”. *Journal of the Atmospheric Sciences*, **50**, no. 13, pp. 1874–1887.
- O’Gorman, P. A., R. P. Allan, M. P. Byrne, and M. Previdi (2012). “Energetic Constraints on Precipitation Under Climate Change”. *Surveys in Geophysics*, **33**, pp. 585–608.
- Oueslati, B. and G. Bellon (2013a). “Convective Entrainment and Large-Scale Organization of Tropical Precipitation: Sensitivity of the CNRM-CM5 Hierarchy of Models”. *Journal of Climate*, **26**, no. 9, pp. 2931–2946.
- Oueslati, B. and G. Bellon (2013b). “Tropical precipitation regimes and mechanisms of regime transitions: contrasting two aquaplanet general circulation models”. *Climate Dynamics*, **40**, no. 9, pp. 2345–2358.
- Oueslati, B. and G. Bellon (2015). “The double ITCZ bias in CMIP5 models: interaction between SST, large-scale circulation and precipitation”. *Climate Dynamics*, **44**, no. 3, pp. 585–607.
- Pendergrass, A. G. and D. L. Hartmann (2012). “Global-mean precipitation and black carbon in AR4 simulations”. *Geophysical Research Letters*, **39**, no. 1, n/a–n/a.
- Pendergrass, A. G. and D. L. Hartmann (2014). “The Atmospheric Energy Constraint on Global-Mean Precipitation Change”. *J. Climate*, **27**, no. 2, pp. 757–768.
- Peters, M. E., Z. Kuang, and C. C. Walker (2008). “Analysis of Atmospheric Energy Transport in ERA-40 and Implications for Simple Models of the Mean Tropical Circulation”. *J. Climate*, **21**, no. 20, pp. 5229–5241.
- Previdi, M. (2010). “Radiative feedbacks on global precipitation”. *Environmental Research Letters*, **5**, no. 2, p. 025211.
- Previdi, M. and B. G. Liepert (2008). “Interdecadal Variability of Rainfall on a Warming Planet”. *Eos, Transactions American Geophysical Union*, **89**, no. 21, pp. 193–195.

- Ramanathan, V. (1981). “The Role of Ocean-Atmosphere Interactions in the CO<sub>2</sub> Climate Problem”. *Journal of the Atmospheric Sciences*, **38**, pp. 918–930.
- Ramanathan, V. (1987). “The role of earth radiation budget studies in climate and general circulation research”. *Journal of Geophysical Research*, **92 (D4)**, pp. 4075–4095.
- Randall, D. A., Harshvardhan, D. A. Dazlich, and T. G. Corsetti (1989). “Interactions among Radiation, Convection, and Large-Scale Dynamics in a General Circulation Model”. *Journal of the Atmospheric Sciences*, **46**, no. 13, pp. 1943–1970.
- Raymond, D. J., S. L. Sessions, A. H. Sobel, and Å. Fuchs (2009). “The Mechanics of Gross Moist Stability”. *J. Adv. Model. Earth Syst.* **1**, no. 3, n/a–n/a.
- Richardson, T. B., P. M. Forster, T. Andrews, and D. J. Parker (2016). “Understanding the Rapid Precipitation Response to CO<sub>2</sub> and Aerosol Forcing on a Regional Scale”. *Journal of Climate*, **29**, no. 2, pp. 583–594.
- Rotstayn, L. D., S. J. Jeffrey, M. A. Collier, S. M. Dravitzki, A. C. Hirst, J. I. Syktus, and K. K. Wong (2012). “Aerosol- and greenhouse gas-induced changes in summer rainfall and circulation in the Australasian region: a study using single-forcing climate simulations”. *Atmos. Chem. Phys.* **12**, no. 14, pp. 6377–6404.
- Salzen, K. von, J. F. Scinocca, N. A. McFarlane, J. Li, J. N. S. Cole, D. Plummer, D. Verseghy, M. C. Reader, X. Ma, et al. (2013). “The Canadian Fourth Generation Atmospheric Global Climate Model (CanAM4). Part I: Representation of Physical Processes”. *Atmosphere-Ocean*, **51**, no. 1, pp. 104–125.
- Samset, B. H., G. Myhre, P. M. Forster, Ø. Hodnebrog, T. Andrews, G. Faluvegi, D. Fläschner, M. Kasoar, V. Kharin, et al. (2016). “Fast and slow precipitation responses to individual climate forcings: A PDRMIP multimodel study”. *Geophysical Research Letters*, **43**. 2016GL068064, n/a–n/a.
- Schmidt, G. A., M. Kelley, L. Nazarenko, R. Ruedy, G. L. Russell, I. Aleinov, M. Bauer, S. E. Bauer, M. K. Bhat, et al. (2014). “Configuration and assessment of the GISS ModelE2 contributions to the CMIP5 archive”. *J. Adv. Model. Earth Syst.* **6**, no. 1, pp. 141–184.
- Shepherd, T. G. (2014). “Atmospheric circulation as a source of uncertainty in climate change projections”. *Nature Geosci.* **7**, no. 10, pp. 703–708.
- Sherwood, S. C., S. Bony, O. Boucher, C. Bretherton, P. M. Forster, J. M. Gregory, and B. Stevens (2015). “Adjustments in the Forcing-Feedback Framework for Understanding Climate Change”. *Bull. Amer. Meteor. Soc.* **96**, no. 2, pp. 217–228.
- Sherwood, S. C., V. Ramanathan, T. P. Barnett, M. K. Tyree, and E. Roeckner (1994). “Response of an atmospheric general circulation model to radiative forcing of tropical clouds”. *Journal of Geophysical Research: Atmospheres*, **99**, no. D10, pp. 20829–20845.



- Siongco, A. C., C. Hohenegger, and B. Stevens (2015). “The Atlantic ITCZ bias in CMIP5 models”. *Climate Dynamics*, **45**, no. 5, pp. 1169–1180.
- Slingo, A. and J. M. Slingo (1988). “The response of a general circulation model to cloud longwave radiative forcing. I: Introduction and initial experiments”. *Quarterly Journal of the Royal Meteorological Society*, **114**, no. 482, pp. 1027–1062.
- Slingo, J. M. and A. Slingo (1991). “The response of a general circulation model to cloud longwave radiative forcing. II: Further studies”. *Quarterly Journal of the Royal Meteorological Society*, **117**, no. 498, pp. 333–364.
- Sobel, A. H., J. Nilsson, and L. M. Polvani (2001). “The Weak Temperature Gradient Approximation and Balanced Tropical Moisture Waves”. *Journal of the Atmospheric Sciences*, **58**, no. 23, pp. 3650–3665.
- Soden, B. J., I. M. Held, R. Colman, K. M. Shell, J. T. Kiehl, and C. A. Shields (2008). “Quantifying Climate Feedbacks Using Radiative Kernels”. *J. Climate*, **21**, no. 14, pp. 3504–3520.
- Stephens, G. L., T. L’Ecuyer, R. Forbes, A. Gettleman, J.-C. Golaz, A. Bodas-Salcedo, K. Suzuki, P. Gabriel, and J. Haynes (2010). “Dreary state of precipitation in global models”. *Journal of Geophysical Research: Atmospheres*, **115**, no. D24, D24211, n/a–n/a.
- Stevens, B., S. Bony, and M. J. Webb (2012). *Clouds On-Off Klimate Intercomparison Experiment (COOKIE)*. Tech. rep.
- Stevens, B. (2015). “Rethinking the Lower Bound on Aerosol Radiative Forcing”. *J. Climate*, **28**, no. 12, pp. 4794–4819.
- Stevens, B. and S. Bony (2013). “What Are Climate Models Missing?” *Science*, **340**, no. 6136, pp. 1053–1054.
- Stevens, B., M. Giorgetta, M. Esch, T. Mauritsen, T. Crueger, S. Rast, M. Salzmann, H. Schmidt, J. Bader, et al. (2013). “Atmospheric component of the MPI-M Earth System Model: ECHAM6”. *Journal of Advances in Modeling Earth Systems*, **5**, no. 2, pp. 146–172.
- Sulochana Gadgil, S. G. (2006). “The Indian Monsoon, GDP and Agriculture”. *Economic and Political Weekly*, **41**, no. 47, pp. 4887–4895.
- Takahashi, K. (2009). “The Global Hydrological Cycle and Atmospheric Shortwave Absorption in Climate Models under CO<sub>2</sub> Forcing”. *J. Climate*, **22**, no. 21, pp. 5667–5675.
- Taylor, K. E., R. J. Stouffer, and G. A. Meehl (2012). “An Overview of CMIP5 and the Experiment Design”. *Bulletin of the American Meteorological Society*, **93**, pp. 485–498.
- Thorpe, L. and T. Andrews (2014). “The physical drivers of historical and 21st century global precipitation changes”. *Environmental Research Letters*, **9**, no. 6, p. 064024.

- Tian, B. and V. Ramanathan (2002). “Role of Tropical Clouds in Surface and Atmospheric Energy Budget”. *Journal of Climate*, **15**, no. 3, pp. 296–305.
- Trenberth, K., J. Fasullo, and L. Smith (2005). “Trends and variability in column-integrated atmospheric water vapor”. *Climate Dynamics*, **24**, no. 7-8, pp. 741–758.
- Vecchi, G. A. and B. J. Soden (2007). “Global Warming and the Weakening of the Tropical Circulation”. *Journal of Climate*, **20**, no. 17, pp. 4316–4340.
- Vial, J., J.-L. Dufresne, and S. Bony (2013). “On the interpretation of inter-model spread in CMIP5 climate sensitivity estimates”. *Climate Dynamics*, **41**, no. 11-12, pp. 3339–3362.
- Voigt, A., S. Bony, J.-L. Dufresne, and B. Stevens (2014). “The radiative impact of clouds on the shift of the Intertropical Convergence Zone”. *Geophysical Research Letters*, **41**, no. 12, pp. 4308–4315.
- Voigt, A. and T. A. Shaw (2015). “Circulation response to warming shaped by radiative changes of clouds and water vapour”. *Nature Geosci*, **8**, no. 2, pp. 102–106.
- Voldoire, A., E. Sanchez-Gomez, D. Salas y Méliá, B. Decharme, C. Cassou, S. Sénési, S. Valcke, I. Beau, A. Alias, et al. (2012). “The CNRM-CM5.1 global climate model: description and basic evaluation”. *Climate Dynamics*, **40**, no. 9-10, pp. 2091–2121.
- Volodin, E. M., N. A. Dianskii, and A. V. Gusev (2010). “Simulating present-day climate with the INMCM4.0 coupled model of the atmospheric and oceanic general circulations”. *Izv. Atmos. Ocean. Phys.* **46**, no. 4, pp. 414–431.
- Watanabe, M., T. Suzuki, R. O’ishi, Y. Komuro, S. Watanabe, S. Emori, T. Takemura, M. Chikira, T. Ogura, et al. (2010). “Improved Climate Simulation by MIROC5: Mean States, Variability, and Climate Sensitivity”. *J. Climate*, **23**, no. 23, pp. 6312–6335.
- Watanabe, S., T. Hajima, K. Sudo, T. Nagashima, T. Takemura, H. Okajima, T. Nozawa, H. Kawase, M. Abe, et al. (2011). “MIROC-ESM 2010: model description and basic results of CMIP5-20c3m experiments”. *Geosci. Model Dev.* **4**, no. 4, pp. 845–872.
- Wentz, F. J., L. Ricciardulli, K. Hilburn, and C. Mears (2007). “How Much More Rain Will Global Warming Bring?” *Science*, **317**, no. 5835, pp. 233–235.
- Williamson, D. L., M. Blackburn, K. Nakajima, W. Ohfuchi, Y. O. Takahashi, Y.-Y. Hayashi, H. Nakamura, M. ISHIWATARI, J. L. McGREGOR, et al. (2013). “The Aqua-Planet Experiment (APE): Response to Changed Meridional SST Profile”. *Journal of the Meteorological Society of Japan. Ser. II*, **91A**, pp. 57–89.
- Wu, T., L. Song, W. Li, Z. Wang, H. Zhang, X. Xin, Y. Zhang, L. Zhang, J. Li, et al. (2014). “An overview of BCC climate system model development and application for climate change studies”. *Journal of Meteorological Research*, **28**, no. 1, pp. 34–56.

- Xie, S.-P., C. Deser, G. A. Vecchi, M. Collins, T. L. Delworth, A. Hall, E. Hawkins, N. C. Johnson, C. Cassou, et al. (2015). “Towards predictive understanding of regional climate change”. *Nature Clim. Change*, **5**, no. 10, pp. 921–930.
- Xie, S.-P., C. Deser, G. A. Vecchi, J. Ma, H. Teng, and A. T. Wittenberg (2010). “Global Warming Pattern Formation: Sea Surface Temperature and Rainfall”. *Journal of Climate*, **23**, no. 4, pp. 966–986.
- Yu, J.-Y., C. Chou, and J. D. Neelin (1998). “Estimating the Gross Moist Stability of the Tropical Atmosphere”. *Journal of the Atmospheric Sciences*, **55**, no. 8, pp. 1354–1372.
- Yuan, J. and D. L. Hartmann (2008). “Spatial and temporal dependence of clouds and their radiative impacts on the large-scale vertical velocity profile”. *J. Geophys. Res.* **113**, no. D19, n/a–n/a.
- Yukimoto, S., Y. Adachi, M. Hosaka, T. Sakami, H. Yoshimura, M. Hirabara, T. Y. Tanaka, E. Shindo, H. Tujino, et al. (2012). “A New Global Climate Model of the Meteorological Research Institute: MRI-CGCM3 – Model Description and Basic Performance”. *Journal of the Meteorological Society of Japan*, **90A**, pp. 23–64.
- Zelinka, M. D., S. A. Klein, and D. L. Hartmann (2012). “Computing and Partitioning Cloud Feedbacks Using Cloud Property Histograms. Part I: Cloud Radiative Kernels”. *J. Climate*, **25**, no. 11, pp. 3715–3735.
- Zeng, N., J. D. Neelin, and C. Chou (2000). “A Quasi-Equilibrium Tropical Circulation Model—Implementation and Simulation”. *Journal of the Atmospheric Sciences*, **57**, no. 11, pp. 1767–1796.
- Zhang, X., H. Liu, and M. Zhang (2015). “Double ITCZ in Coupled Ocean-Atmosphere Models: From CMIP3 to CMIP5”. *Geophysical Research Letters*, **42**, no. 20. 2015GL065973, pp. 8651–8659.



# Acknowledgements

First and foremost, I would like to express my gratitude to Bjorn Stevens and Thorsten Mauritsen who have been the best PhD advisors that I could have hoped for. During the course of my PhD, I had the great privilege to closely discuss and share ideas with both of them. I not only profited from their immense knowledge about anything from physical processes in the Earth System to fine details in model code, but also from their helpful advice regarding skills like presentation style, improving figures, and writing. Further, I am very grateful to Sandrine Bony who warmly welcomed me for three months to the Laboratoire de Météorologie Dynamique. It was a pleasure to work with Sandrine and her ideas inspired large parts of this PhD thesis, namely the MSE framework.

My special thanks goes to Stefan Bühler who accepted to become an evaluator of this thesis on very short notice. I thank Verena Grützun, Eva-Maria Pfeiffer, Gerhard Schmiedl and Jürgen Böhner for their willingness to take part in the thesis evaluation. I further thank Jochem Marotzke for leading efficient and fruitful panel meetings.

Thanks to all members of the Climate Dynamics group for creating such an amiable atmosphere for discussion. In particular, I thank Traute and Tobi who have answered my numerous questions. I would like to further express my thanks to Angela Gruber, Antje Weitz, Wiebke Böhm and Connie Kampmann, who always had an open ear for questions or suggestions, and supported me throughout the course of my PhD with administrative advice.

I especially thank Stefan Kinne for giving me the opportunity to experience climate science from an observational point of view. Spending five weeks on the Atlantic ocean during a research cruise on the Polarstern allowed me to marvel at tropical clouds in all their variety.

Cheska, I thank you for being such a great office mate! I have loved sharing an office with you, sharing uncountable anti-social lunch breaks in our office with always interesting and fun conversations, coffee breaks, trips to the supermarket to stock up on bread, work during the week-end... And thank you very much for your advice, encouragement, support and motivation during the final phase of my PhD!

My thanks goes to Nick, Kylie, Cheska, Kathi, and Christine Auer for helping to proofread the final manuscript.

Ich möchte auch meinen Eltern danken, die mich in den langen Jahren meiner Ausbildung unterstützt haben. Ich danke auch meinen Schwiegereltern, die mir schon lange vor der Hochzeit zu einer Familie geworden sind. Und schlussendlich, vielen vielen Dank, Nick, für deine Liebe, bedingungslosen Rückhalt und deine Unterstützung vor und während der Doktorarbeit.

Thanks to everybody who has supported or influenced me during my research in the past three years!



# Aus dieser Dissertation hervorgegangene Veröffentlichungen

*List of Publications*

Fläschner, D., T. Mauritsen, and B. Stevens (2016). “Understanding the Intermodel Spread in Global-Mean Hydrological Sensitivity”. *Journal of Climate*, 29, no. 2, pp. 801–817, doi:10.1175/JCLI-D-15-0351.1.





# Eidesstattliche Versicherung

*Declaration of oath*

Hiermit erkläre ich an Eides statt, dass ich die vorliegende Dissertationsschrift selbst verfasst und keine anderen als die angegebenen Quellen und Hilfsmittel benutzt habe.

*I hereby declare, on oath, that I have written the present dissertation by myself and have not used other than the acknowledged resources and aids.*

Hamburg, den 26.04.2016

---

Dagmar Fläschner (geb. Popke)

## Hinweis / Reference

Die gesamten Veröffentlichungen in der Publikationsreihe des MPI-M  
„Berichte zur Erdsystemforschung / Reports on Earth System Science“,  
ISSN 1614-1199

sind über die Internetseiten des Max-Planck-Instituts für Meteorologie erhältlich:  
**<http://www.mpimet.mpg.de/wissenschaft/publikationen.html>**

*All the publications in the series of the MPI -M  
„Berichte zur Erdsystemforschung / Reports on Earth System Science“,  
ISSN 1614-1199*

*are available on the website of the Max Planck Institute for Meteorology:  
**<http://www.mpimet.mpg.de/wissenschaft/publikationen.html>***



